Department of Electrical Engineering and Automation

Real-time thermal state and component loading estimation in active distribution networks

Merkebu Zenebe Degefa

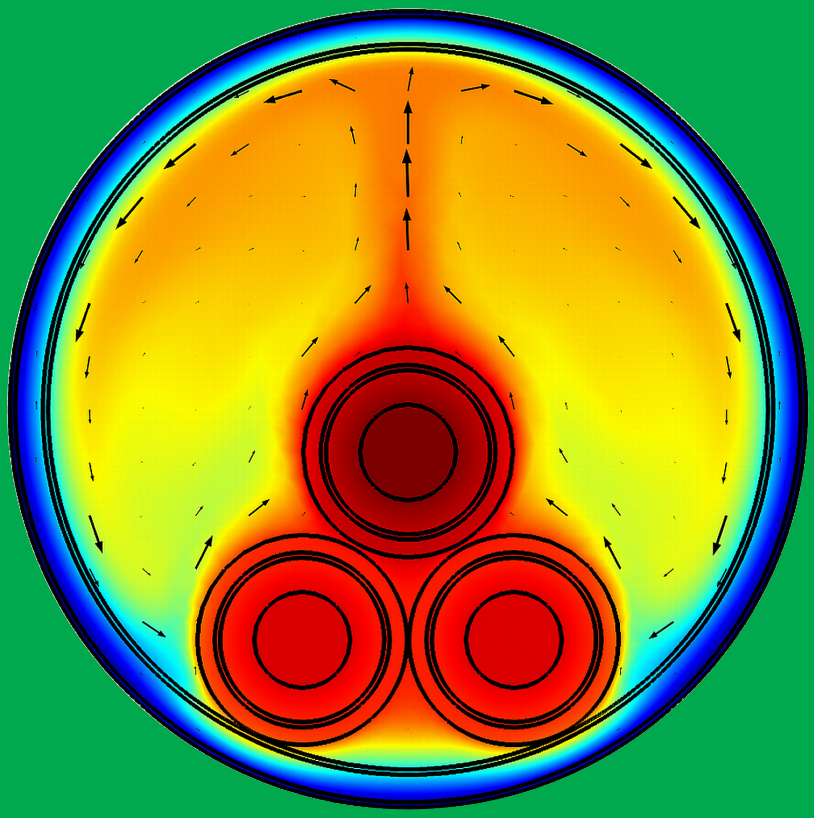

Aalto University

DOCTORAL DISSERTATIONS

Aalto University publication series
DOCTORAL DISSERTATIONS 104/2015

Real-time thermal state and component loading estimation in active distribution networks

Merkebu Zenebe Degefa

A doctoral dissertation completed for the degree of Doctor of Science (Technology) to be defended, with the permission of the Aalto University School of Electrical Engineering, at a public examination held at the lecture hall S4 of the school on the 7th of September 2015 at 12:00.

Aalto University
School of Electrical Engineering
Department of Electrical Engineering and Automation
Power Systems and High Voltage Engineering

Supervising professor
Professor Matti Lehtonen

Thesis advisor
Professor Matti Lehtonen

Preliminary examiners
Assoc. Prof. Sami Repo, Tampere University, Finland
Dr. Sasa Djokic, The University of Edinburgh, UK

Opponents
Prof. George J. Anders, Lodz University of Technology, Poland
Dr. Sasa Djokic, The University of Edinburgh, UK

Aalto University publication series
DOCTORAL DISSERTATIONS 104/2015

ISBN 978-952-60-6307-2 (printed)
ISBN 978-952-60-6308-9 (pdf)
ISSN-L 1799-4934
ISSN 1799-4934 (printed)
ISSN 1799-4942 (pdf)
http://urn.fi/URN:ISBN:978-952-60-6308-9

Unigrafia Oy
Helsinki 2015

Finland

441 697
Printed matter

Aalto University

Abstract

Aalto University, P.O. Box 11000, FI-00076 Aalto www.aalto.fi

Author
Merkebu Zenebe Degefa

Name of the doctoral dissertation
Real-time thermal state and component loading estimation in active distribution networks

Publisher School of Electrical Engineering

Unit Department of Electrical Engineering and Automation

Series Aalto University publication series DOCTORAL DISSERTATIONS 104/2015

Field of research Power Systems and High Voltage Engineering

Manuscript submitted 7 April 2015 **Date of the defence** 7 September 2015

Permission to publish granted (date) 22 July 2015 **Language** English

☐ **Monograph** ☒ **Article dissertation (summary + original articles)**

Abstract

Highly stochastic loading and distributed generation in the emerging active distribution networks means that electric utilities need to deploy intelligent network management tools in order to use their assets to the fullest. Real-Time Thermal Rating (RTTR) provides the possibility for short term and even real-time active distribution network management, enabling the network to run closer to an overload state without damage. In this dissertation, pertinent developments and proposals are presented in three stages on the path towards the development of a real-time monitoring and operation system for active distribution networks.

The first stage is the development of distribution network component thermal models for real time implementation. In this dissertation, a numerical model of the air-gap convective heat transfer for underground cable installations inside unfilled conduit is developed. In addition, a dynamic thermal model is developed for prefabricated secondary substation cabins. The most dominant but difficult to solve heat transfer mechanism, natural convection, is modelled by introducing the stack effect principle into the problem. Measurements from a scaled model of prefabricated substations, measurements from actual cabins and 3D Finite Element Method (FEM) simulations are used to validate the numerical model.

In the second stage, this dissertation explores the usability of customer level automatic meter reading (AMR) measurements for distribution network state estimation and for load forecasting applications. A method to forecast substation level loads with their respective confidence intervals using hourly AMR metered customer level consumptions is presented. The forecasting and monitoring of a distribution network in real-time can be met with the modeling of classified type load classes. However, it requires careful incorporation of the necessary factors, such as within-group and between-group correlations of customer classes.

Binding the aforementioned findings, in the third stage, a framework for day-ahead hour-by-hour thermal state forecasting and thermal ratings of distribution network components is proposed and studied. This work has demonstrated that up to three hours ahead thermal state forecasting of an active distribution network can be achieved with an acceptable level of accuracy. In this dissertation, the benefits and practical implications of the real-time thermal rating are investigated. The introduction of real-time thermal rating in an active distribution network management system enhances the loading capacity significantly compared to static rating. This has been revealed through an increased utilization of installed DGs and through better integration potential of additional DGs.

Keywords Active Network Management, Demand Response, Distributed Generation, Load Forecasting, Natural Convection, Prefabricated Substation, Real-time Thermal Rating, State Estimation, Smart Meters

ISBN (printed) 978-952-60-6307-2 **ISBN (pdf)** 978-952-60-6308-9

ISSN-L 1799-4934 **ISSN (printed)** 1799-4934 **ISSN (pdf)** 1799-4942

Location of publisher Helsinki **Location of printing** Helsinki **Year** 2015

Pages 190 **urn** http://urn.fi/URN:ISBN:978-952-60-6308-9

Acknowledgements

First and foremost, I thank God, he who knows the worthy in life and he who led me beside the still waters.

My supervisor, Prof. Matti Lehtonen, has been guiding me academically and consulting me as dear friend throughout the major developments in life, which in my case coincided with the doctoral study period. He believed in me perhaps more than the doubts I have in myself. He gave me the opportunities to flourish professionally. Simply, he is a good person I shall thank dearly.

I would like to thank the diligent and enthusiastic pre-examiners, Prof. Sami Repo from Tampere University and Dr. Sasa Djokic from The University of Edinburgh, for giving insightful, honest and constructive feedback on my doctoral thesis.

During my doctoral study at Aalto University's power systems and high voltage engineering laboratory, I was privileged to get to know and work with esteemed colleagues. Dr. John Millar is a person to whom I am greatly indebted for. I would especially like to thank Dr. John for proofreading most of my publications and the doctoral thesis. Professionally, he has been co-author in most of my publications in which he generously passed the torch of 'dynamic thermal modelling of cables'. As a friend, he taught me the wisdom in humility through the candid discussions on issues ranging from 'climate change' to the question 'why is the British Parliament always so rowdy?'

My collogue, Matti Koivisto, used to whip my forecasting and estimation figures and methods to get them in line with standard statistical principles. I am benefited from the discussions we had on the smart meter data as we were among the first who laid hand on hourly metered consumption data. I am grateful to work with Humayun Muhammed (former officemate and friend), Dr. Amir Safdarian and Ali Mubbashir with whom I had quality technical discussions in the coffee room. I would like also to thank my current officemate Antti Alahäivälä for the nice discussions we had on social and technical issues.

I owe a debt of gratitude to the former and current members of High Voltage Engineering Laboratory at Aalto University. Dr. Petri Hyvönen, Tatu Nieminen, Veli-Matti Niiranen, Jouni Mäkinen and Ari Haavisto are the colleagues I am hugely indebted for. Especially, Tatu Nieminen, took my experiment plan as his own and helped me to build the scale down model of prefabricated secondary substations.

My stay at power systems and high voltage engineering laboratory was made memorable with current and former members. I would not pass this opportunity without mentioning some of their names. Dr. Shafiq Muhammad, Dr. Muzamir Isa, Dr. Michael Omidiora, Dr. Eero Saarijarvi, Dr. Rafi Adzman, Dr. Zoko Ble, Dr. Kutt Lauri, Dr. Kluss Joni, Hussain Amjad, Bruno Sousa, Mahmood Farhan and Malik Farhan have been integral part of my professional and private life.

We humans are highly dependent and positively influenced by our families. One cannot just thank his parents and settle, one has to love and care them back. Nevertheless, the only way one can declare what he owes his families on paper is by writing about it. I would like to thank my diligent and big hearted mother, Tsige Demese and principled

father, Zenebe Degefa. I would like to extend appreciations to my big brother Aynalem Zenebe and two little sisters Beza Zenebe and Meron Zenebe.

Most importantly, the gracious God have blessed me with a kind hearted wife, Yordanos Tibebu, without whom my life would have been complicated and less bearable. With me, she have been equally ridding through the stresses with paper submission deadlines and pre-examination processes. Yordiye, I love you and I shall not stop admiring your persistence, forgiving heart and sheer purity. The merciful God filled my life with joy when he gave us our son, Noah Merkebu. Noah, you are my joy and you made me love life itself more. Grow up in wisdom and stature and in favour with God and men!

Merkebu Zenebe Degefa

Espoo, Finland
August, 2015

This work is dedicated to the soul of my grandmother Yeshihareg Birke Woldemeskel (Emaye).

Contents

List of Publications

This thesis consists of an overview of the following seven publications, which from here on are referred to as Roman numerals in the text:

I **Degefa, M. Z.**, Lehtonen, M. and Millar, R. (2012). Comparison of Air-Gap Thermal Models for MV Power Cables Inside Unfilled Conduit. *IEEE Trans. Power Delivery,* 27(3), pp.1662-1669.

II **Degefa, M. Z.**, Millar, R., Lehtonen, M. and Hyvonen, P. (2014). Dynamic Thermal Modeling of MV/LV Prefabricated Substations. *IEEE Trans. Power Delivery*, 29(2), pp.786-793.

III **Degefa, M. Z.**, Millar, R., Koivisto, M., Humayun, M. and Lehtonen, M. (2013). Load Flow Analysis Framework for Active Distribution Networks Based on Smart Meter Reading System. *Engineering,* 05(10), pp.1-8.

IV **Degefa, M. Z.**, & Lehtonen, M. (2013). Stochastic Characteristics of Load Profiling in Distribution Systems Based on AMR Measurements. *International Review of Electrical Engineering*, 8(6), pp.1833-1842

V **Degefa, M. Z.,** Koivisto, M., Millar, R. J. and Lehtonen, M. (2014). Dynamic thermal state forecasting of distribution network components: For enhanced active distribution network capacity, *13th International Conference on Probabilistic Methods Applied to Power* Systems (PMAPS 2014), Durham, UK, 7 - 10 July, 2014.

VI **Degefa, M. Z.,** Humayun, M., Safdarian, A., Koivisto, M., Millar, R. J., and Lehtonen, M. (2014). Unlocking distribution network capacity through real-time thermal rating for high penetration of DGs, Electric Power Systems Research, 117(C), pp. 36-46.

VII **Degefa, M. Z.**, Lehtonen, M., Millar, R. J., Alahäivälä A., and Saarijärvi, E. (2015) Optimal Voltage Control Strategies for Day-Ahead Active Distribution Network Operation, Electric Power Systems Research, 127, pp. 41-52.

Author's Contribution

I The author Merkebu Degefa had the main responsibility for planning the work, interpretation of the results and writing the publication under the supervision of Prof. Matti Lehtonen and D. Sc. (Tech.) John Millar.

II The author Merkebu Degefa had the main responsibility for planning the work, interpretation of the results and writing the publication under the supervision of Prof. Matti Lehtonen and D. Sc. (Tech.) John Millar. The laboratory measurement was planned together with D. Sc. (Tech.) Petri Hyvonen and he has also assisted in the interpretation of the IEC standards.

III The author Merkebu Degefa had the main responsibility for planning the work, interpretation of the results and writing the publication under the supervision of Prof. Matti Lehtonen. D. Sc. (Tech.) John Millar provided the Greenfield test distribution network utilized in the paper and Matti Koivisto assisted in the autoregressive model for load forecasting. Muhammad Humayun has contributed through discussions and comments throughout the analysis.

IV The main idea is developed by Merkebu Degefa and Prof. Matti Lehtonen. Merkebu Degefa had the main responsibility for writing the publication under the supervision of Prof. Matti Lehtonen.

V Merkebu Degefa had the main responsibility for planning the work, interpretation of the results and writing the publication. D. Sc. (Tech.) John Millar has provided the Greenfield network plan and also contributed through comments and discussions throughout the study. Matti Koivisto developed the statistical method for wind speed, solar irradiation, ambient temperature and soil temperature forecasting using the ARIMA model. Prof. Matti Lehtonen has supervised the work and contributed through comments and suggestions.

VI The author Merkebu Degefa had the main responsibility for planning the work, interpretation of the results and writing the publication under the supervision of Prof. Matti Lehtonen. Dr. Amir Safdarian has contributed with the development of the Optimal Power Flow formulation. Dr. Amir Safdarian and Muhammad Humayun have strongly contributed through discussions and comments during the work. Matti Koivisto has contributed in the wind turbine and solar panel models. D. Sc. (Tech.) John Millar provided the Greenfield test active distribution network and has also contributed through discussions, comments and proof reading of the final draft paper.

VII The main idea is developed by Merkebu Degefa and Prof. Matti Lehtonen. The author Merkebu Degefa had the main responsibility for planning the work, interpretation of the results and writing the publication under the supervision of Prof. Matti Lehtonen. D. Sc. (Tech.) John Millar and Eero Saarijärvi developed a typical active distribution network utilizing a network planning algorithm and GIS interface. Anti Alahäivälä has contributed through comments and discussions during the analysis.

List of Abbreviations

ACF	autocorrelation function
AMR	automatic meter reading
ARIMAX	auto regressive moving average with exogenous variable
CDA	conditional demand analysis
CDF	cumulative distribution function
CVC	coordinated voltage control
DE	direct electric heating system
DG	distributed generation
DIST	district heating system
DMS	distribution management system
DR	demand response
DTR	dynamic thermal rating
EMS	energy management system
FEM	finite element method
GAMS	general algebraic modeling system
GSHP	ground source heat pump heating system
HDPE	high-density polyethylene
LDPE	low-density polyethylene
LV	low voltage
MACT	maximum allowable conductor temperature
MAPE	mean absolute percentage error
MAS	multi-agent system
MV	medium voltage
NAE	normal absolute error
OLTC	on-load-tap-changer
OPF	optimal power flow
PV	photovoltaic
RMSE	root mean squared error

RRMSE	relative root mean squared error
RTTR	real-time thermal rating
STORE	electric storage heating system
SVC	static VAR compensator
VAR	volt ampere reactive
XLPE	cross-linked polyethylene

List of Symbols

Symbols	Description
A_f	Conduit cross-section area (m^2)
Cd	Discharge coefficient
c_{fluid}	Specific heat of the fluid ($J/kg.K$)
C_{pf}	Specific heat of air per unit volume ($J/m^3.K$)
De	Effective outer diameter of cables (m)
F_{amb}	Ambient view factor
FF	Filling factor
$\hat{F}_t$	Cumulative distribution function (CDF)
g	Gravitational constant (m/s^2)
G	Irradiance (W/m^2)
G_m	Mutual irradiation going to other boundaries
G_r	Grashof number
G_{ref}	Standard irradiance (W/m^2)
h_{conv}	Convection heat transfer coefficient (W/m^2K)
h_o	Heat transfer coefficient on cable surface
h_r	Radiation heat transfer coefficient
h_w	Heat transfer coefficient on conduit wall
I_{sc}	Short circuit current (A)
k	Fluid thermal conductivity ($W/m.K$)
k_f	Thermal conductivity of air
L	Characteristic dimension, length, width or diameter (m)
Nu	Nusselt number
Nu_{COND}	Nusselt number conduction flow regimes
N_{C_q}	Set of all SVCs connected at bus i
N_{DG_q}	Set of all DGs connected at bus i
N_{OLTC}	Set of all OLTCs connected at bus i
Nu_l	Nusselt number laminar flow regimes
Nu_T	Average 'thin-layer-solution' Nusselt number for laminar flow

Symbols	Description
$P_g^{it}(Q_g^{it})$	Generation active (reactive) powers
$P_l^{it}(Q_l^{it})$	Load active (reactive) powers
$P_s^{it}(Q_s^{it})$	Injected active (reactive) powers
P_r	Prandtle number
Q_{stack}	Ventilation rate (m^3/s)
Ra	Rayleigh number
S	Insolation (mW/cm^2)
T_{air}	Air temperature (^oC)
T_j	PV cell temperature (K)
T_{jref}	Reference cell temperature (K)
V	Mean air velocity
v	Kinematic viscosity
V_i^t	Voltage magnitude at bus i and time t
V_{oc}	Open circuit voltage (V)
α	Thermal diffusivity
β	Fluid thermal expansion coefficient $(1/K)$
δ_t^i	Voltage angle
θ	Temperature rise
ϑ	Kinematic viscosity
θ_f^{ij}	Power flow angle
μ	Dynamic fluid viscosity
ρ_{fluid}	Fluid density (kg/m^3)
$\bar{\rho}_{ii}$	Intra-class correlation within a class *i*
ρ_{ij}	Statistical correlation between the individual loads
$\bar{\rho}_{ij}$	Inter-class correlation between class *i* and *j*
σ	Stefan-Boltzmann constant (W/m^2K^4)
σ_i	Standard deviation of single loads
σ^2	Composite covariance

1 Introduction

An increasing number of renewable energy resources are being installed in distribution systems. Larger units, usually above 10MW, are installed by commercial power producers and are connected to transmission facilities. Smaller units, which are no larger than 1 or 2 MW are, however, installed in distribution systems and are referred to as 'Distributed Generation' (DG) [1]. It is anticipated that with the proliferation of DG some distribution networks will face power flow congestion due to the thermally vulnerable components restricting the connection capacity and active energy yield of DG [2]. In conjunction with aging infrastructure and limited financial budgets for network reinforcement, the rapid growth of DGs is pressuring network operators to turn to real-time monitoring and operation solutions for distribution systems which potentially unleash the hidden capacities. Also, due to the increasing installation of DGs, switching operations reconfiguring feeders will be common in distribution systems, making the real-time thermal state monitoring of network components more expedient [3].

In general, to increase DG connectivity and to harness the generated renewable energy efficiently, there is a need for active dynamic distribution management systems (DMS). It is also in the interest of distribution network operators (DNO) to increase asset utilization in a safe manner, potentially allowing latent capacity to be used under strictly controlled conditions [2]. Traditionally, the main task of distribution system analysis tools has been to solve the power flow for one specific point in time, which is the predicted peak demand. Also, as a common practice, the thermal limits applied by DNOs tend to be based on fixed or assumed meteorological conditions that are not always accurate representations of the actual operating conditions [4], the result of which is potentially a conservative constraint on power flows. In place of the rigid capacity planning rules, the network operation planning process needs to incorporate more detailed and real-time simulations of capacity constraints. Hence, dynamic thermal models are expected to be a strong component in an active distribution network management system.

In this regard, the application of continuously changing (rather than seasonal) ratings, which can be updated in real-time, could enable generators to enhance their energy export, defer network reinforcement and also allow increased access to distribution networks for weather dependent forms of generation. Integrating real-time thermal rating in active power flow management schemes has been a research topic among the power systems

research community for a long time. EPRI's dynamic thermal circuit rating system released in early 1999, was among the first efforts which attempted to realize the higher equipment utilization offered by dynamic thermal rating [5]. Another methodology to forecast the real-time thermal rating of overhead lines, presented in [6], promises enhanced network operator decision making capabilities regarding network power flow management.

In [7], in addition to investment options such as substation or feeder expansions, installations of new DGs are presented as alternatives for utilities to solve network capacity limits. Nevertheless, it is also mentioned in [7] that on shorter feeders the ampacity limits could prohibit the utilization of economically beneficial DG installations. In [8], it is demonstrated that without careful engineering assessments, increased DG installations may have adverse system effects, such as exposing system and customer equipment to potential damage. The optimization of power output from DGs within a distribution network while maintaining thermal limits is proposed in [9]. In [10], a day-ahead scheduler which considers capacity limits, in the form of a specific upper bound to the current amplitude, is proposed. The scheduling procedure in [10] solves a non-linear multi-objective problem for the optimization of distributed resource production during the following day. A thermal state estimation based DG output control algorithm for a wide area network power flow control is proposed in [11]. The study in [11] verifies that the real-time rating system is able to estimate conductor temperature with an average error in the range of -2.2ºC to +1.4ºC.

Despite the numerous studies, the relationship between thermal states and stochastic DG generation has not been studied or quantified adequately in active distribution systems. Due to the variations in thermal time constants among overhead lines, underground cables and transformers, the thermal responses also differ accordingly. Hence, a look into the entire distribution network is necessary to identify potential bottlenecks with increased installations of DG. Up to day-ahead hour-by-hour thermal capacity limit forecasting and real-time thermal rating frameworks entirely based on thermal, DG and load models are presented in this thesis. The contribution extends also to the quantification of the benefits of real-time thermal rating (RTTR) for the efficient utilization and increased integration of DGs. The RTTR technique is simulated on two typical Finnish medium voltage (MV) test networks: NTK#1 in Section 3.3 and NTK#2 in Section 4.4.

The implementation of price and network based demand response programs, the pervasiveness of electric vehicles, the increasing installation of DGs, the rising customer load base of urban areas and other emerging factors are creating a distribution network loading curve which is stochastic in nature and previously unseen in shape. Hence, static distribution network rating is no longer a good enough network management tool. Rather, utilities need to adapt to the dynamism of load and generation behavior by applying programs such as RTTR for efficient and secure network operation.

The contribution of this thesis is in the improved analysis required for the development of RTTR systems for active distribution networks. The first research problem is the absence of non-conservative and accurate dynamic thermal models of distribution network components. In addition, with the improved measurement points in today's active distribution network, there has never been such a high degree of visibility and forecasting potential for distribution network component states and customer loads. The smart meter measurements are used in this dissertation to address the need for the understanding and forecasting of load profiles closer to customer connection points, which is also the second research contribution. As a third contribution, this dissertation untangles the complex interdependencies of weather and load variables in affecting the states of network components. Frameworks which enable the thermal state estimations and alleviate network capacity and voltage problems associated with high DG integration are proposed and simulated.

1.1 Background

Customarily, electricity distribution networks have so far been designed and operated as passive networks according to a design philosophy that requires them to handle all probable loading conditions. The network planning in a passive distribution network is based on worst case planning principles resulting in sub-optimal network efficiency. In active distribution networks, however, statistical network planning is envisioned with the consideration of the probabilistic nature of loadings and generation. Usually, in passive distribution network operation, congestions are managed by load curtailment and voltage problems associated with DGs are managed by curtailing DG output. These costly ways of operating network operations are destined to be past ways, with the development of ICT enabling monitoring and controlling technologies that create active distribution networks [2].

According to [12], the common global definition of active distribution network (ADN) is as follows:

'Active distribution networks (ADNs) are distribution networks that have systems in place to control a combination of distributed energy resources (generators, loads and storage). Distribution system operators (DSOs) have the possibility of managing the electricity flows using a flexible network topology. Distributed energy resources (DERs) take some degree of responsibility for system support, which will depend on a suitable regulatory, environment and connection agreement. '

Active networks not only connect DERs, but they also exploit them to optimize network asset investments and operational costs. This is the most fundamental difference between passive and active networks [13]. ADNs require active network management (ANM), aiming to add more flexibility to network management in order to utilize existing network

assets more efficiently [14]. In these regards, the real-time thermal rating (RTTR) system enables the utilization of the full capacity of the distribution network infrastructure. In this thesis, the fundamental components of the RTTR system, such as dynamic thermal models and load forecasting methods, are developed and discussed (see Fig. 1).

In active distribution networks, the RTTR system enables real-time monitoring and control activities by integrating with operational planning tools. Operational planning refers to short-term planning which organizes the network operation in the near future. The thesis comprehensively models and simulates the dependency of demand and network states on the common environmental variables such as wind speed, ambient temperature, solar irradiation and humidity in active distribution networks. Consequently, the potential of RTTR systems in increasing the integration potential of DGs and in enabling real-time coordinated voltage controls is demonstrated.

Distribution system analysis tools are expected to continue to play an important role in the real-time operation planning and analysis of the future smart grid [3]. The introduction of dynamic thermal rating to these tools is also becoming common practice, especially in transmission systems. The use of thermo-electric equivalent lumped parameter models for the dynamic estimation of the temperature in transmission cables is discussed in [15]. In [6], the application of dynamic thermal rating for forecasting the real-time rating of an active distribution network is discussed. However, the study in [6] presents only the overhead line ratings, also without the involvement of forecasted local generation. The study in [11] presents the integrated implementation of thermal state estimation and DG output control algorithms based on locally measured electrical and environmental parameters. Nevertheless, there has not been a comprehensive study looking into the possibilities of thermal state forecasting and real-time thermal rating of the main active distribution network components, such as distribution transformers, underground cables and overhead lines, in a one hour or longer period, such as 24 hours ahead. Since distribution system rating depends on the critically loaded component rating, there is a need for understanding the thermal response of the component types to their respective loading, especially in the presence of local generation such as wind turbines.

Distribution network components, such as underground cables, secondary substation transformers and overhead lines, have ratings set by manufactures under standard test conditions. However, it is customary for system operators to increase or decrease the ratings of the components based on the actual operating environmental conditions. The static rating is usually based on the standard loading guides provided by organizations such as IEC or IEEE. The wide applications of demand response programs and advent of distributed generation (DG) facilities are, however, imposing a more stochastic and increased loading scenario on distribution network components. Hence, a real-time thermal monitoring and rating capability is required, especially at the weak points of the network. Most static thermal models are suitable for practical approximations and hands

on computation, but the simplifications in such models inhibit their application for the dynamic thermal response of a stochastic loading scenario. The ambient temperature, wind speed and solar irradiation effect on local generation and component thermal rating at the time of loading has to be reflected in the hotspot temperature of transformers or conductor temperature of underground cables. The installation parts, such as the air-gap inside buried conduit carrying MV cables and vented prefabricated substation compartments, where natural convection is the dominant heat transfer component, are required to be modelled carefully in order to be suitable for real-time thermal state knowledge acquisition.

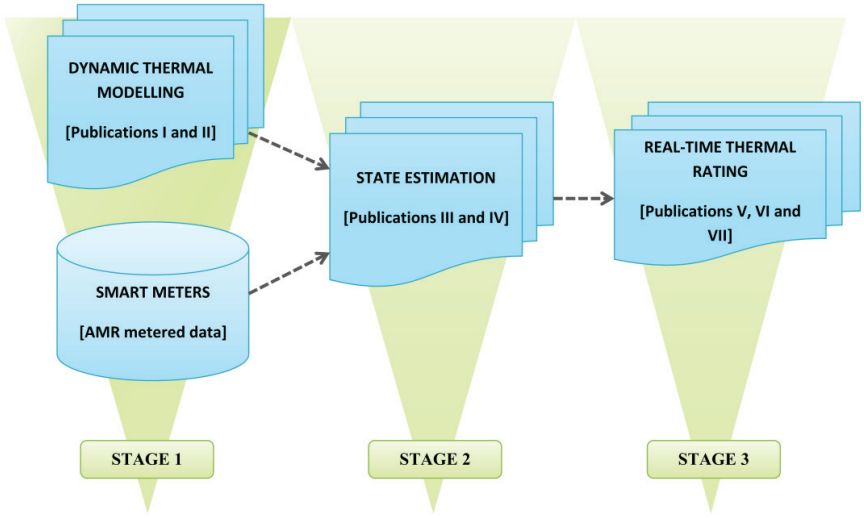

Fig. 1 *Requirements for real-time operation and management of an active distribution network*

1.2 Contributions of the thesis

In this work, relevant improvements and proposals have been presented in three stages on the path towards the development of a real-time operation and management system for active distribution networks. The principal topics that have been investigated are highlighted in Fig. 1. Besides the presentation of component level dynamic thermal models, this work has proved some of the advantages of real-time thermal rating, specifically in increasing the utilization and integration potential of DGs and in enabling a coordinated voltage control (CVC) with the involvement of DGs.

In this thesis, a real-time convection correlation has been developed for the air-gap heat transfer of underground cable installations inside unfilled conduit [Publication I]. The motivation for this contribution is the fact that, for dynamic thermal rating, the available simplified standard models are significantly conservative. For example, the IEC 60287 air-gap thermal resistance differs by 3-4 degrees on the safe side from the measured maximum conductor-insulation junction temperatures. Hence, the inclusion of realistic

installation set-ups in formulating real-time convection correlations is among the improvement measures. In this dissertation, it has also been shown that the use of the Raithby and Hollands Nusselt number correlation in the air-gap thermal resistance calculations of the inclined cylinders resulted in closer match with the measured conductor temperature than the IEC 60287 methods.

Another contribution of this work is the development of a working dynamic thermal model for prefabricated secondary substations [Publication II]. The most dominant but difficult to solve heat transfer mechanism, natural convection, is modeled through the introduction of the stack effect principle. In the work, a clear and expandable first principle approach is used to quantify heat transfer through ventilation openings. Besides measurements from a scaled model of a prefabricated substation, measurements from actual cabins and 3D Finite Element Method (FEM) simulations are used to validate the numerical model.

The thesis also investigates the potential for a bottom up load flow analysis based on customer level AMR measurements to compute the short time forecasts of demands and distribution network system states [Publications III and IV]. The main contribution in [Publication III] is the formulation and proposal of a distribution system load modeling framework based on AMR metered consumption data. In this dissertation it has been shown that AMR based load forecasts of individual customers can be used to forecast voltage profiles in distribution systems. A method to model and forecast secondary substation level loads based on classified customer group hourly consumption models is also presented [Publication IV]. It has been shown that the need to perform forecasting and monitoring of a distribution network in real-time can be met with the modeling of classified load type classes.

Tying up the preceding findings, the consequent work in this thesis has proposed and investigated a framework for day-ahead hour-by-hour thermal state forecasting of distribution network components [Publication V]. More importantly, the study has explored how well the thermal states of distribution network components can be forecasted based on smart meter measurements.

After the necessary components for the real-time thermal ratings are in place, the thesis moves further to showcase the benefits and practicalities of the method. In this regard, the proposal of an RTTR based active distribution network management framework with the inclusion of DG generation and load forecasts made the study in [Publication VI] among the first. In the study the potential for increased DG utilization and increased potential for new DG installations have been quantified. The study attempts to achieve better understanding of the real-time active distribution network management in its entirety with the inclusion of the emerging stochasticities and dynamics.

In this thesis, the deployment of the RTTR system for day-ahead operation planning of active distribution network with the objective of optimal voltage control is developed and simulated [Publication VII]. A framework comprising a synergy of the RTTR and CVC is proposed for solving the voltage variation and thermal limit problems that are associated with a high penetration level of DGs in an active distribution network. The benefit of incorporating RTTR with CVC has been proved to be two-pronged. On the one hand, the generated DG active power can be utilized better, due to an increased utilization of distribution network component load carrying capacity. On the other hand, the required reactive power for voltage regulation can be transferred without violating network component thermal limits if dynamic thermal rating (DTR) is applied in a real-time basis.

1.3 Structure of the thesis

This thesis is organized as follows:

Chapter 2 introduces the dynamic thermal modeling of three distribution network components: the overhead lines, the underground cables and the distribution transformers. The chapter mainly presents the two thermal models developed by the author. The first is for MV underground cables installed inside unfilled conduit and the second is the model developed for prefabricated secondary substations.

Chapter 3 presents the different ways the data from smart meters can be utilized in distribution systems for load modelling and load forecasting. In addition, the framework developed by the author for estimating and forecasting the thermal state of distribution network components is presented and explained in this chapter. The chapter further explores the impact of uncertainties in weather variable forecasts on distributed generation output and load forecasts.

Chapter 4 primarily presents the method to couple thermal and electrical models for the purpose of real-time thermal rating of the distribution system. Thermal and electrical state estimation utilizing smart meter measurements is also discussed. The chapter also presents the RTTR framework and algorithms for the investigation of the role of RTTR for both enhanced utilization of DGs and CVC involving DGs.

Chapter 5 The practical implication of the methods and frameworks developed in this dissertation is demonstrated, first, while trying to estimate more accurately the actual real-time capacity of distribution network components and, second, while attempting to involve DGs in the distribution system CVC. The benefits of RTTR are quantified and presented in this chapter.

Chapter 6 reiterates the main findings of this work and their implications. Furthermore this chapter points towards future research topics.

2 Dynamic thermal modelling

The absolute maximum loading capacities of underground cables, overhead lines and transformers are generally dependent on the thermal limits of their insulation. Hence, it is quite apparent that if one wants to know the true load carrying capacity of these power system components then the maximum loading without violating the hottest allowable temperature has to be known. The dynamic thermal models of the components are less conservative for tasks such as knowing the real-time carrying capacity and thermal states of the components.

Thermal modelling is the mathematical or numerical representation of every available heat transfer means, such as convection, conduction and radiation, from a material. With dynamic thermal modelling, the modelled heat transfer must be capable of representing a changing load and ambient weather conditions. In static thermal models only the thermal resistances of components and their immediate environment are considered; also, the calculated hotspot temperatures or ratings are steady state values. With dynamic thermal rating (DTR), however, the ratings of shorter time spans are computed taking into account the time constants of transient responses. Time constants are functions of the products of thermal resistances and thermal capacitances. As RTTR is the computation of the dynamic thermal rating of power system components in real-time; at each time step, the initial temperature, the ambient environmental variables and the loading of the component are variable.

Contrary to RTTR, a static line rating (SLR) matches the steady state maximum line current for which the line conductor temperature is less than the maximum allowable conductor temperature (MACT), under suitably conservative weather assumptions that are fixed or varying seasonally. The dynamic thermal ratings (DTR), however, match the line current for which the conductor temperature is less than the MACT for the existing weather situation. Nevertheless, due to the weather variability, DTRs are only valid for a limited time into the future, called the thermal rating period (e.g. the next hour) [16].

Regarding overload protection in a DTR regime, self-adaptive protection devices can be used. As the dynamic thermal models are capable of giving the next time step rating for the hottest conductor, the models can also give the ampere limit corresponding to the maximum allowable conductor temperature based on the standards. When a current limit is used for protection, as in static rating, the ampere level is fixed. However, when

temperature is used as a limit for protection the ampere value varies, following time-current curves which are dependent on historical loading and ambient weather conditions.

2.1 Thermal-electric analogy

The thermal-electric analogy network is a widely used and accepted way of modeling dynamic heat transfer from a heat source to the heat sink. Many heat transfer problems can be reduced to an equivalent RC circuit, where the distributed parameters can be lumped to a suitable combination of thermal capacitances and resistances. In some cases these elements must be nonlinear, such as the thermal resistance shown in Fig. 2. In general, most transformer top-oil or hot-spot, underground cables and overhead lines thermal models go through the following steps:

1. Identify all heat transfer components (i.e., convection, conduction and radiation)
2. Formulate the thermal resistances and capacitances of each medium between the heat source and the heat sink (Fig. 2).
3. Establish a simplified RC network, and from the respective first order linear differential equation, solve the temperature at the required node.

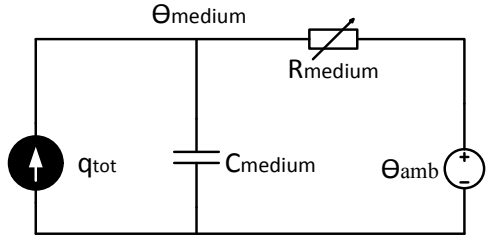

Fig. 2 *An RC thermal circuit*

$$q_{tot} = C_{medium}\frac{d\theta_{medium}}{dt} + \frac{(\theta_{medium} - \theta_{amb})}{R_{medium}} \quad \textbf{(2.1)}$$

The thermal resistance $R_{medium}(\frac{K}{W})$, analogous to electric resistance, obstructs the flow of heat $q_{tot}(W)$, which itself is the analogy of electric current in electrical circuits.

$$R_{medium} = \frac{1}{h_{medium} \times A_{medium}} \quad \textbf{(2.2)}$$

where h_{medium} is the heat transfer coefficient in $(\frac{W}{m^2K})$ and $A_{medium}$is the area in (m^2). $q_t(W) = I^2R_{ac}$, are the joule losses, where I is the current and R_{ac} is the ac resistance per length of conductor. In the case of transformers, $q_{tot}(W)$ are the total losses, including the load and no load losses.

The presence of thermal resistances and capacitances $(\mathrm{C}(\mathrm{J}/K)$in the network requires iterative numerical methods such as the Euler and Runge-Kutta methods to solve differential equations such as (2.1). This approach is used in almost all reviewed literature; for example, the IEEE guide for loading mineral-oil-immersed transformers [17].

The heat transfer coefficient in (2.2) depends on the physical parameters of the medium, which in turn might depend on temperature, hence giving nonlinearity to the thermal resistance. The coefficient may include both convection and radiation when the medium is air.

Natural, or free, convection results from the motion of fluid due to density changes arising from the heating process. Self-sustained natural convection might be initiated and continued either when there is an inclination from horizontal of the conduit, duct, tunnel, or other air-gapped cable container, or when deliberate height-differentiated vents are installed in horizontal installations [18]. The strength of natural convection is highly dependent on the installation setup. Hence, the respective convective heat transfer coefficients of different installation setups are detailed in Sections 2.3.1, 2.3.2 and 2.3.3. The heat transfer coefficient for natural convection is given in (2.3)-(2.6) [19].

$$h_{conv} = \frac{N_u \times k}{L} \tag{2.3}$$

$$N_u = C \times [G_r \times P_r]^n \tag{2.4}$$

$$P_r = \frac{c_{fluid} \times \mu}{k} \tag{2.5}$$

$$G_r = \frac{L^3 \times {\rho_{fluid}}^2 \times g \times \beta \times \Delta\theta_{fluid}}{\mu^2} \tag{2.6}$$

where N_u is the Nusselt number, P_r is the Prandtle number, G_r is the Grashof number, L is the characteristic dimension, length, width or diameter (m), g is the gravitational constant (m/s^2), k is the fluid thermal conductivity $(W/m.K)$, ρ_{fluid} is the fluid density (kg/m^3), C and n are empirical constants, β is the fluid thermal expansion coefficient $(1/K)$, c_{fluid} is the specific heat of the fluid $(J/kg.K)$, μ is the dynamic fluid viscosity $Pa\,s = (N\,s)/m^2$, $\Delta\theta_{fluid}$ is the fluid temperature gradient, (K) and h_{conv} is the convection heat transfer coefficient (W/m^2K)

Radiative heat transfer is the transfer of heat by electromagnetic waves, or photons, without interaction with the medium. The radiative heat transfer from a hot surface in air could be *surface_to_ambient* and/or *surface_to_surface* radiation, where the radiation heat transfer coefficient (h_r) is calculated as in (2.7) and (2.8), respectively.

a) *Surface_To_Ambient*: The ambient surrounding behaves as a blackbody. This means that the emissivity and absorptivity are equal to 1, and there is zero reflectivity.

$$h_r = \varepsilon\sigma\left(\theta_{surf} + \theta_{amb}\right)\left({\theta_{surf}}^2 + {\theta_{amb}}^2\right) \tag{2.7}$$

where ε is the surface emissivity and σ is the Stefan-Boltzmann constant (W/m^2K^4).

b) *Surface_To_Surface* (from both ambient and surrounding surfaces)

$$h_r = \frac{\varepsilon(\sigma{\theta_{surf}}^4 - G_m - F_{amb}\sigma{\theta_{amb}}^4)}{\theta_{surf} - \theta_{amb}} \tag{2.8}$$

where G_m is the mutual irradiation, going to other boundaries, $F_{amb}$is an ambient view factor whose value is equal to the fraction of the field of view that is not covered by other boundaries, and $\theta_{amb}$is the assumed far-away temperature in the directions included in F_{amb}.

The total heat transfer coefficient for a heat source body in a fluid medium (h_{medium}) is

given by:

$$h_{medium} = h_{conv} + h_r \quad \textbf{(2.9)}$$

Although various combinations of empirical correlations and modified solution mechanisms could be implemented, the general heat transfer theories explained above are the basis of the modeling in this thesis.

2.2 Overhead lines

Overhead bare lines have relatively low time constants, which makes them suitable for accommodating intermittent generation, such as wind generation, which is associated with high wind speed. Nevertheless, they also heat up rather quickly in the face of sudden increase in loading. The thermal characteristics of overhead lines are well understood compared to underground cables and transformer prefabricated substations. Hence, in this thesis the IEEE Std C57.91-2011 standard is used. The contribution of this thesis in regard to thermal modelling is limited to underground cables and prefabricated secondary substations, as discussed in the coming sections.

2.3 Underground cables

The underground cables commonly have a thick layer of insulation, grounded sheath, and a protective cover, and they are buried in the ground directly or within a duct or tube. The thermal modelling of underground cables has had a firm ground in the scientific community since the model presented by Neher-McGrath in the 1950s [20]. However, modelling the immediate environment has proved to be challenging inhibiting the utilization of the developed dynamic thermal models. In this section, the dynamic thermal model developed by the author for underground MV cables inside unfilled corrugated conduits and ducts or tunnels is presented.

The thermal states of cables placed in air-filled conduits, troughs and tunnels heavily depend on the heat transfer in the air-gap. Thermal radiation heat transfer from the cable surface to the surrounding duct or tunnel surfaces is significant, especially when the temperature difference increases and the cooling is natural ventilation. In [21], it has been reported that about 60% of the heat generated in cables (transmission network) is transferred to the retaining duct by radiation. Natural and forced convection is the other major heat transfer in the air-gap. As the air velocity increases the share of convective heat transfer grows, and in forced ventilated tunnels it may reach up to 90% of all heat transfer from cables [22].

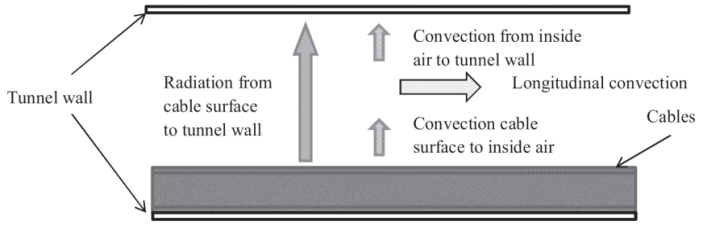

Fig. 3 *Heat transfer in the air-gap*

As shown in Fig. 3, the heat transfer in the air-gap has four components that can be represented by thermal resistances [23]:

- Convection from the cable surface to the air inside the tunnel (R_{ca}).
- Convection from the air inside the tunnel to the tunnel wall (R_{at}).
- Longitudinal convection due to either forced or natural flow of air along the tunnel (R_f).
- Surface-to-surface radiation from cable surface to inside conduit wall (R_r).

The installation in Fig. 3 can be represented by its analogous thermal-electric circuit using the principles explained in Section 2.1, as shown in Fig. 4. However the correct heat transfer coefficients have to be used for the respective installation setup. The horizontal circular concentric cylinders and the eccentric circle representations of tube installations, in this thesis, are defined by employing the Raithby and Hollands natural convection correlations. It has been shown that the simulation of the developed model and physical measurements are in agreement, as presented in [Publication I] and the later Section 2.3.4.

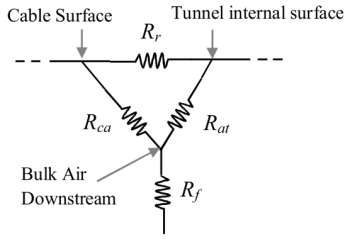

Fig. 4 *Air-gap equivalent thermal network.*

The strength of natural convection is exceedingly dependent on the installation set-up. In the next sections (Section 2.3.1 to Section 2.3.3) the installation setup dependent natural convection heat transfer coefficients are discussed. The Raithby and Hollands formulations of natural convection for the different installation setups are adopted from the studies in [24] and [25]. The Rayleigh and Nusselt number formulations in equations (2.10) to (2.21) embody the geometric factors and installation setup parameters dependencies.

2.3.1 Horizontal circular concentric cylinders

For horizontal concentric circular cylinders, the natural convection heat transfer from the inner to the outer cylinder is given in equations (2.10)-(2.14), [24].

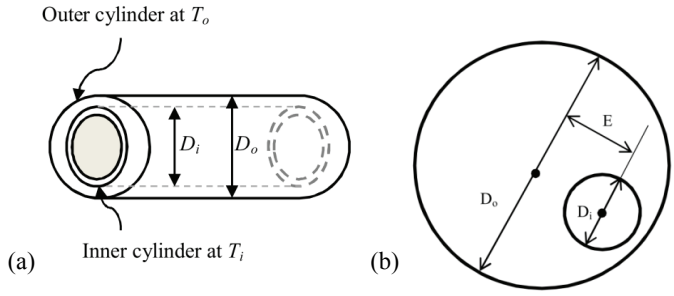

Fig. 5 *Geometry of the eccentric and concentric installations, (a) concentric horizontal annulus, (b) eccentric circular cylinders*

The characteristic length:

$$L_c = \frac{D_o - D_i}{2} \tag{2.10}$$

The effective thermal conductivity is:

$$k_{eff} = 0.386k\left(\frac{\Pr}{0.861+\Pr}\right)^{1/4}\left(F_{cyl}Ra_c\right)^{1/4} \tag{2.11}$$

where the Rayleigh number is given as

$$Ra_c = \frac{g\beta(T_i - T_o)L_c^{\,3}}{\nu\alpha} \tag{2.12}$$

and the geometric factor of concentric cylinders is

$$F_{cyl} = \frac{\left[\ln\left(D_o/D_i\right)\right]^4}{L_c^{\,3}\left(D_i^{-3/5} + D_o^{-3/5}\right)^5} \tag{2.13}$$

Natural convection heat transfer per unit length (Q_{conv}) is then obtained as:

$$Q_{conv} = \frac{2\pi k_{eff}}{\ln\left(D_o / D_i\right)}(T_i - T_o) \tag{2.14}$$

where D_o and D_i are the outer and inner cylinder diameters respectively, L_c is the characteristics length, k_{eff} is the effective thermal conductivity, k is the thermal conductivity, F_{cyl} is the geometric factor of concentric cylinders and Ra_c is the Rayleigh number of cylinders. In (2.12), g is acceleration due to gravity, ν is kinematic viscocity, α is thermal diffusivity and β is the thermal expansion coefficient. In case of multiple core cables, E is the distance between the center of the conduit and the center of the circle drawn around the cables. D_i represents the effective diameter of the three cables.

2.3.2 Horizontal circular eccentric cylinders

Raithby and Hollands were able to develop laminar and conduction layer heat transfer Nusselt number empirical correlations for non-overlapping eccentric cylinders [24]. The

overall Nusselt number will be then the maximum of the two Nusselt numbers as shown in (2.18).

$$Nu_l = 0.603\overline{C_l}\frac{\ln\left(\frac{D_o}{D_i}\right)Ra^{\frac{1}{4}}}{\left[\left(\frac{L_c}{D_i}\right)^{\frac{3}{5}}+\left(\frac{L_c}{D_o}\right)^{\frac{3}{5}}\right]^{\frac{5}{4}}} \tag{2.15}$$

$$Nu_{COND} = \frac{\ln\left(\frac{D_o}{D_i}\right)}{\cosh^{-1}\left[\left(D_o{}^2 + D_i{}^2 - 4E^2\right)\Big/ 2D_oD_i\right]} \tag{2.16}$$

$$\overline{C_l} = \frac{0.671}{\left[1+\left(\frac{0.492}{\Pr}\right)^{9/16}\right]^{4/9}} \tag{2.17}$$

For E≠0:

$$Nu = \left[Nu_l, Nu_{COND}\right]_{\max} \tag{2.18}$$

where Nu_l and Nu_{COND} are Nusselt numbers for conduction and laminar flow regimes respectively and they are formulated in (2.15) and (2.16). D_i and D_o are inner and outer cylinder diameters, as shown in Fig. 5b. $\overline{C_l}$ is an approximately universal function of Prandtl number (Pr).

2.3.3 Tilted cylinder (Raithby and Hollands)

For a long circular cylinder inclined θ degrees from the horizontal, the laminar flow Nusselt number correlation has been developed by Raithby and Hollands [25]. The flow, in this case, is considered to be directed along the length of the tube. For our concentric cylinder case, incorporating the longitudinal natural convection with the surface-to-surface radiation, we can use the formulation to calculate the air-gap heat transfer at a certain angle from horizontal.

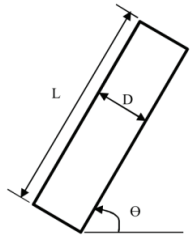

Fig. 6 *A tilted cylinder*

$$Nu_l = \frac{1.8}{\ln\left(1+\frac{1.8}{Nu^T}\right)} \tag{2.19}$$

$$Nu^T = \left\{0.772 + \frac{0.228}{1+0.676P^{1.23}}\right\}\left(\cos\theta + \frac{D}{L}\sin\theta\right)^{1/4}\overline{C_l}Ra^{1/4} \tag{2.20}$$

$$Ra = \frac{g\beta\Delta TD^3}{\nu\alpha}, P = 2\frac{L}{D}\cot\theta \quad \textbf{(2.21)}$$

where Nu^T is the average 'thin-layer-solution' Nusselt number for laminar flow, Nu_l is the average Nusselt number taken over the entire body, assuming laminar heat transfer prevails over the whole body, and $\overline{C_l}$ is expressed in (2.17). The parameters L, D and θ are shown in Fig. 6 and P is the perimeter. The Nusselt number for laminar flow computed in (2.19) is used in the air-gap thermal resistance formulated in (2.23).

2.3.4 Air-gap heat transfer: Natural convection

According to the classical Neher-McGrath method, the thermal resistance of the air-gap between the cables and the retaining duct is computed on the basis of empirical relationships [18]. The method not only reduces the three dimensional heat flow to one dimension, it also combines the radiation, convection and conduction heat fluxes together. The two main perspectives of the Neher-McGrath based models requiring review are the mathematical simplifications and temperature dependency avoidance of thermal resistance calculations. The simultaneous availability of unprecedented computational power and better convection correlations provides favorable ground for reviews and investigations. With the installation dependent correlations presented in Sections 2.3.1 to 2.3.3, it is possible to review the air-gap thermal resistance dependency on radial convection and the longitudinal convection dependency on installation set-ups.

We are thermally modelling a distribution system under various thermal challenges, such as riser-shafts, road crossings, inclinations and long horizontal alignment. It is evident that the ampacity of a cable passing through various thermal conditions is limited by the worst thermal scenario. Using the correlations in equations (2.10)-(2.21), cable surface to air-gap convective thermal resistances can be calculated as in (2.22) and (2.23).

$$T_{convec\_horizontal} = \frac{\ln(D_e/D_i)}{2\pi k_{eff}} \quad \textbf{(2.22)}$$

$$T_{convec\_inclined} = \frac{1}{\pi . k_{air} . Nu_l} \quad \textbf{(2.23)}$$

The cable surface to air convective thermal resistances in (2.22) and (2.23) are for horizontal and inclined installations, respectively. K_{eff} is given in (2.11) and Nu_l is given in (2.12). The radiation and conduction heat transfer formulations are adopted from [26].

In this thesis, the proposed Raithby and Hollands correlations based model of air-gap thermal resistance is compared with Electra 143 method (see [Publication I] and [23]) and the Dorison-Anders method [27].

2.3.5 Concentric vs eccentric approximation

Tube installations of underground cables are usually eccentric. In [28] it has been stated that a concentric approximation of an eccentric installation has minimal effect on the accuracy of the thermal model. However, finite element method (FEM) simulation results show otherwise. The finite element analysis software used in this dissertation was

COMSOL 4.2 [29]. Conjugate heat transfer and surface-to-surface radiation physics models were coupled to simulate the transient response. The physics model consists of a single phase flow interface, using a compressible formulation, in combination with a heat transfer interface. The default mode is solid with conduction heat transfer, and the fluid pre-defined domain uses the general (conduction and convection) heat balance equation. In addition, surface-to-ambient and surface-to-surface radiation boundary conditions are set with the hemicube method. The hemicube method calculates the view factors from one surface to all other surfaces and proceeds row-by-row through the view factor matrix. It is very accurate for geometries with a shadowing effect and small gaps.

The simulation results in Fig. 7 show that an assumption of concentric rather than eccentric alignment will be overly conservative. Without transposing, for a trefoil arrangement of cables inside unfilled conduit, the top cable will get significantly hotter than the bottom two, as the time dependent solution in Fig. 7a and Fig. 7b show. Hence, in this thesis the eccentric representation presented in Section 2.3.3 is used. The FEM simulation of the cradle formation is presented in Fig. 7c for comparison.

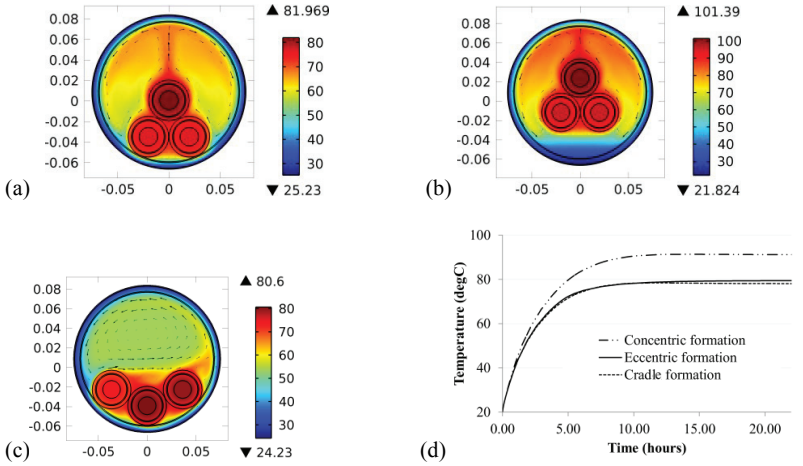

Fig. 7 *Time dependent solution of load 400A for eccentric (a) , concentric (b) and cradle (c) configuration. (temperature bar is in degree centigrade, while the x and y axis have dimensions in meters). Average of the three transposed cables' conductor-insulation junction temperature of the three cases (d).*

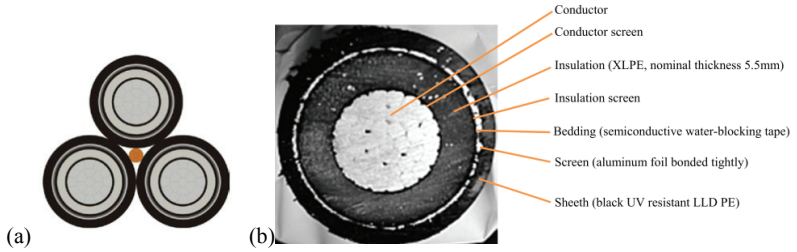

Fig. 8 *The* AHXAMK-W 3 x 240 Al + 70Cu 20kV cables used in the experiment (a) trefoil arrangement of three phase cables, (b) cross-section of single cable

2.3.6 Simulation and measurement results

Laboratory measurements were conducted in the high voltage laboratory of Aalto University in March, 2010. Two 6 m long corrugated conduits containing AHXAMK-W 3 x 240 Al + 70Cu 20kV cables were measured for different installation set-ups. The temperature measurements were taken using thermocouples (T- and K- type). The thermocouples were installed in the aluminum conductor (by drilling), on the surface of the aluminum conductor, on the cross-linked polyethylene (XLPE) insulation outer and inner edges, on the PE jacket outer surface, between the cables, in the middle of the air-gap middle air, on the inside, and outside surface of the conduit. The ambient temperature was also measured. The cable and tube specifications are provided in Tables 1 and 2. The specific cable tested in the experiment is pictured in Fig. 8.

Table 1 *Cable specification*

Name	Unit	Value
Number of cores x cross-section of conductor	mm^2	3x240Al+70Cu
Diameter over insulation	mm	31.3
Single cable diameter (aprox.)	mm	39
Complete cable diameter (approx.)	mm	88
Weight (approx.)	kg/100 m	530
Standard delivery length	m	500
Standard drum size	K	K28
Resistance of conductor	Ω/km	0,125
Resistance of earthing conductor	Ω/km	0,268
Inductance	mH/km	0,35
Reactance	Ω/km	0,11
Capacitance	µF/km	0,29
Charging current	A/km	1,1
Emissivity of cable surface	-	0.91
Insulation	XLPE	
Conductor	Stranded, round and compacted aluminum	
Screen	Aluminum foil bonded tightly to sheath	
Sheath	PE, black	
Highest permissible conductor temperature in continuous operation	ºC	90
Highest permissible conductor temperature in short circuit (duration up to 5 sec)	ºC	250

Table 2 *Tube specification*

Name	Unit	Value
Length of tube (each)	m	6
Inside diameter	mm	140
Outside diameter (max)	mm	150
Emissivity (HDPE and LDPE)	-	0.9
HDPE and LDPE wall thicknesses	mm	1

In the case of corrugated conduit installations, we studied four cases of each, with various inclinations and opening arrangements. For instance, Fig. 9a shows the measurement for a 10 degree inclined conduit. We also measured cables directly exposed to the ambient air for reference. There is a clear dependency of natural convection on the physical orientation of the installation, as is illustrated in Fig. 10. Natural convection increases as the degree of inclination from horizontal increases, where the best alignment would be vertical, for which there is a steady state temperature decrease of 12.5% compared with a 10 degree inclination from horizontal.

Another observation worth mentioning here from Fig. 10 is the absence of significant difference among the various degrees of inclination if either or both end openings are sealed. In a real life installation the scenario is comparable with a long tunnel or trough without forced convection. This in turn implies the importance of close enough openings to the outside air to provide a benefit from natural convection for thermally challenged short sections.

(a) 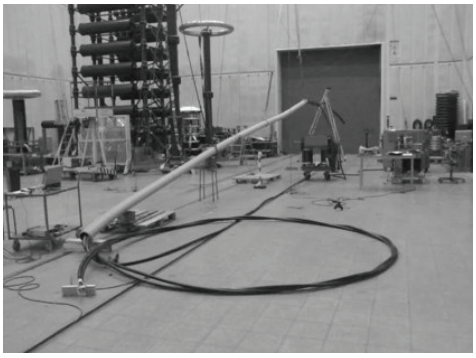 (b) 

Fig. 9 *Conduit measurements: 10 degree inclination (a) and concrete (trough) measurement with blocked openings (b).*

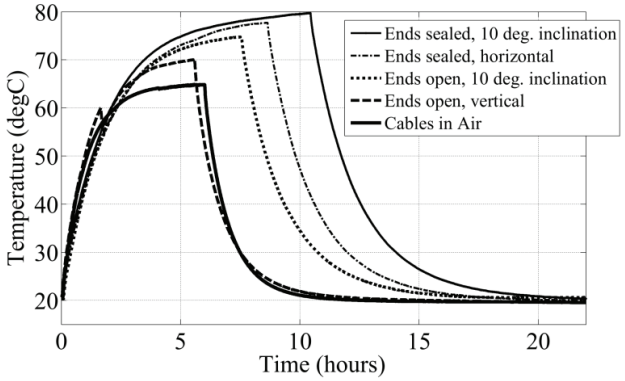

Fig. 10 *An equal 400A step load was supplied for different set-ups: 10 degree inclined conduit from horizontal where both ends are sealed as well as where both ends are open, horizontally positioned conduit with both ends sealed, and vertically positioned with both ends are open. Cables in air outside the conduit are also measured.*

For a horizontal setup with both ends of the conduit open, the trefoil MV cables were loaded with a step current of 250A, which was then increased to 450A, to compare the numerical solution with the measurement, as shown in Fig. 11. It should be noted that the correlations in equations (2.10)-(2.21) are used for the real time air-gap thermal resistance computation, which is part of the lumped 5-loop model shown in Fig. 12. The real time numerical algorithm is adopted from [30] and its formulation is presented in [Publication I]. For the horizontal installation, as can be seen in Figs. 11 and 13, with the presence of longitudinal natural convection, the equations in (2.10)-(2.21) are satisfactory.

In Fig. 12, R_{ins} is the insulation thermal resistance, R_j is thermal resistance of the cable jacket, R_{air_gap} is the thermal resistance of the air inside the conduit, R_{tube} is the corrugated tube wall thermal resistance and R_{ext} is the external thermal resistance representing the burial environment in real-life and the ambient environment in the laboratory measurements. In this thesis, the air-gap thermal resistance (R_{air_gap}) is formulated, to be installiation set-up dependent and less conservative (see (2.22) and (2.23)). For the detailed calculation procedures for the thermal capacitances in Fig. 12, please refer to [26] and [30].

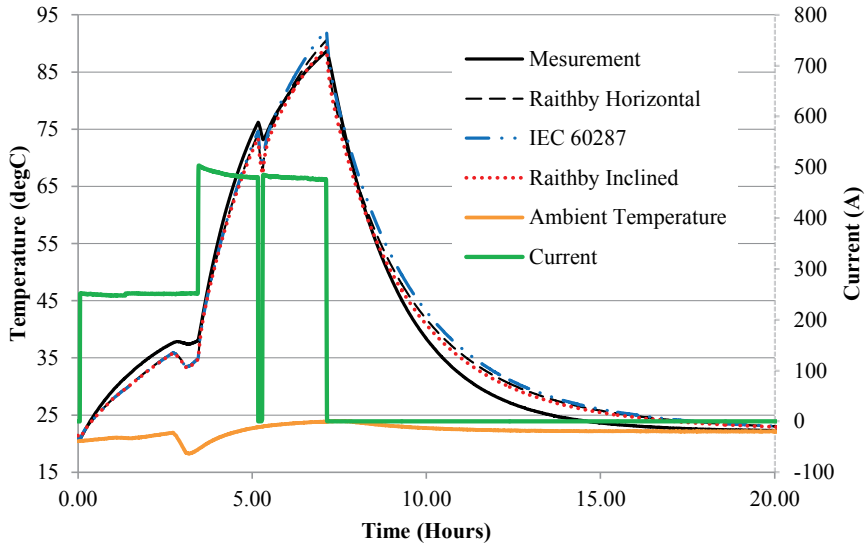

Fig. 11 *Conductor surface temperature measurement and numerical simulations for 12 m horizontal corrugated conduit with both ends opened*

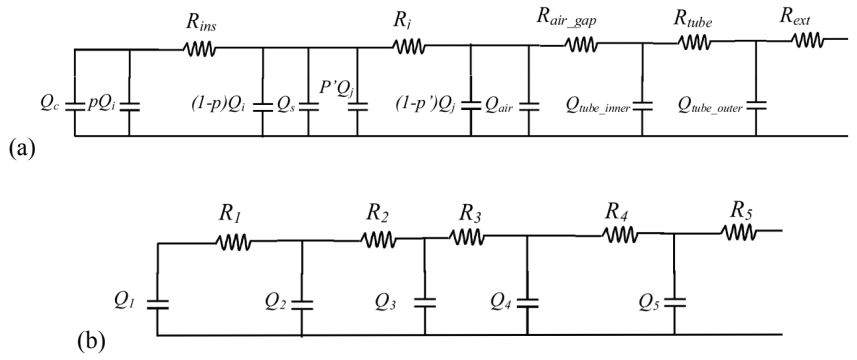

Fig. 12 *5-loop lumped thermal model of cables inside conduit (a) and the simplified circuit (b).*

The IEC 60287 air-gap thermal resistance is conservative, in that it differed by 3-4 degrees on the safe side from the measured maximum conductor-insulation junction temperatures. The Raithby and Hollands correlation for horizontal concentric cylinders is less conservative due to its inclusion of natural convection phenomena; but it didn't reflect angle inclination dependencies. The Raithby and Hollands Nusselt number correlation for inclined cylinders was very close to the measured values. Its reflection of inclination angle variations is visible in Fig. 13.

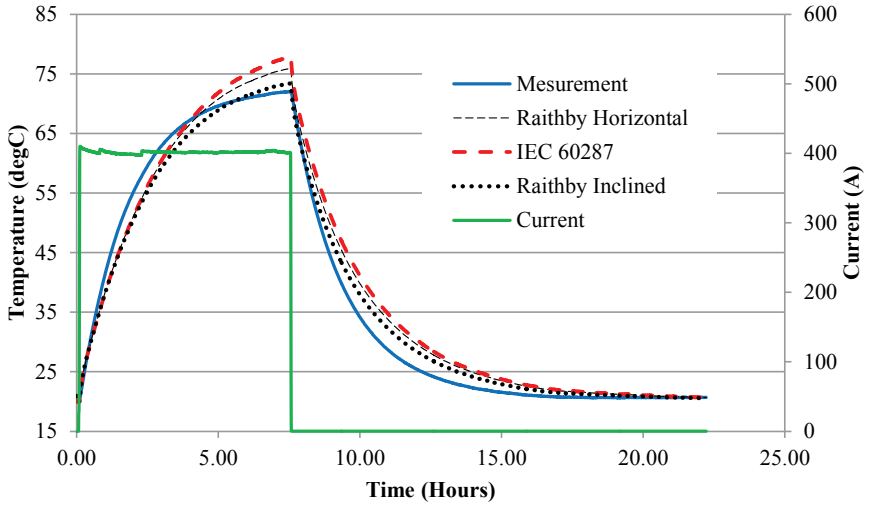

Fig. 13 *Conductor surface temperature measurement and numerical simulations for containing conduit inclined 10 degree, from horizontal with both ends opened.*

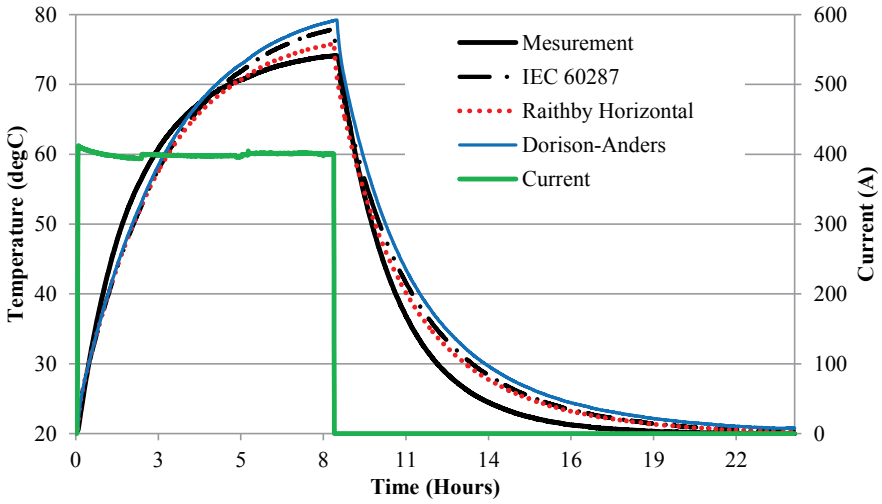

Fig. 14 *Conductor surface temperature measurement and numerical simulation for horizontal conduit both ends sealed.*

In Fig. 14, an additional method (Dorison-Anders) is evaluated based on the still air convective thermal resistance formulation presented in [27]. The study deals with the same important issue of separating convective and radiative heat transfer in order to properly model the effect of air movement inside the tunnel. A review of heat transfer in still air and a rating method for ventilated cables is presented in [27]. The dynamic behavior of all models are similar, as only the air gap modeling varies among the methods. The air-gap has an insignificant contribution to the overall thermal capacitance of the installation setup. Nevertheless, in Fig. 14 the methods show slight differences in their dynamic responses from the measurement values. This difference is likely due to the assumption of an infinite length installation while the conduit is actually only twelve meters long. The results in Fig. 14 show the need for deeper investigation into the air-gap thermal resistance problem.

For cables inside unfilled trough, in calculating external thermal resistance, the IEC 60287 standard uses the formulation for the cable in open air and adds an empirical temperature rise to account for the air-gap temperature [32]. By evaluating the effective (equivalent) diameter of the rectangular concrete, the Raithby and Hollands formulation for horizontal setup (Section 2.3.1) is applied and compared with measurements as shown in Fig. 9b. The results in Fig. 15 show a close correlation between the measurements and the numerical simulation when the Raithby and Hollands correlation for horizontal setup is used. In Fig. 15, the Raithby Horizontal models show a less conservative steady state conductor surface temperature than the IEC 60287 model. The applications of correlations for still air concrete ducts, however, needs further investigation.

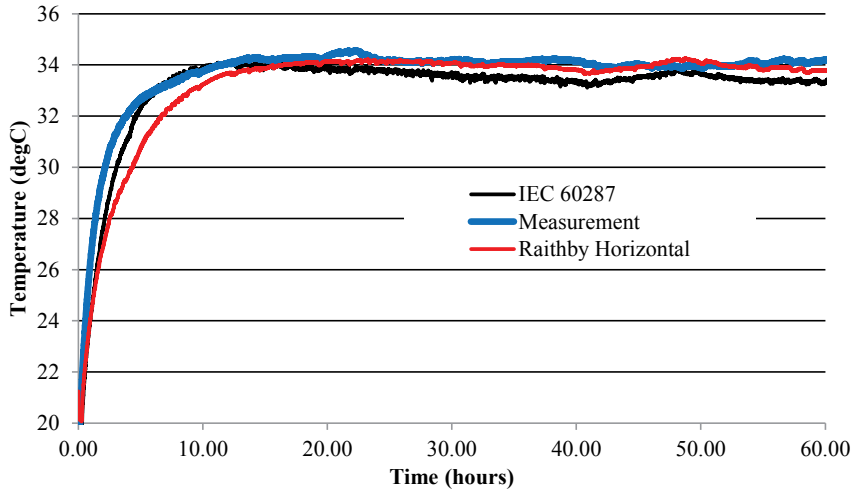

Fig. 15 *Conductor surface temperature measurement and numerical simulation for horizontal trough(rectangular concrete Fig. 9b) both ends sealed.*

Table 3 *Maximum temperatures (degC) at conductor-insulation junctions*

	Meas.	Raithby Horizontal	IEC 60287	Raithby Inclined	Electra 143
10 Degree , ends open	72.02	75.93	77.86	73.41	76.44
Horizontal, ends open	88.64	90.53	92.32	89.28	91.06
Horizontal, ends sealed	74.13	75.81	77.94	74.98	76.43

Table 3 presents the conductor temperature after being loaded with an equal load for an equal time span for a cable having similar dynamic properties (i.e. thermal capacitance) for all methods. Nusselt number correlations taking the actual installation situation into consideration showed a more accurate thermal state estimation. It is apparent that for optimum loading we need to switch to the actual real-time installation environment modeling, which used to be avoided due to computational burden. However, with today's computation power the overly conservative nature of the standards can be eased, as was also suggested in [31].

2.4 Transformers and prefabricated substations

Transformers are the most expensive components in power systems. The dynamic thermal modelling of transformers enables the exceeding of the steady-state ratings of power transformers, necessitated by economic reasons or the need to ensure continuous energy supply [33]. Short-time peak overloads, without significantly decreasing their life expectancy, are very often requested from distribution transformers installed in prefabricated substations [34]. The true capacity varies with the power system dynamics

as well as with varying environmental conditions. Dynamic thermal ratings utilize these factors to optimize and better manage the grid's power transfer capacity in real time. Hence, dynamic top-oil temperature models are required to be accurate enough for application in an online monitoring and real-time rating system of power transformers.

(a) 

(b) 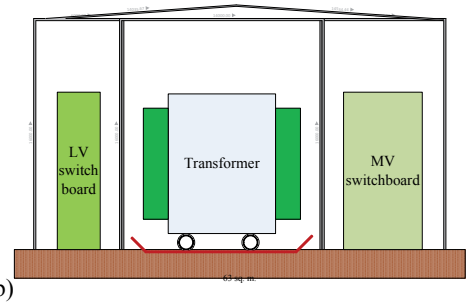

Fig. 16 *Prefabricated distribution transformer cabin layout (a) picture (source ABB) and (b) Schematic layout*

A prefabricated substation is defined as a type-tested assembly comprising an enclosure that includes a transformer, low voltage (LV) switchboard, MV switchboard, MV and LV interconnections and auxiliary equipment (see Fig. 16). The thermal-electric analogy model of a prefabricated MV/LV substation proposed in this thesis works in conjunction with the top-oil thermal model presented in [35]. In this transformer model Susa considered the changes in the oil viscosity and winding losses with temperature. Although some complex constant parameters are necessary in Susa's model, it has been shown that it yields good results [36]. In this thesis, the proposed model considers the thermal resistance and thermal capacitance of the immediate environment of the distribution transformer to be dynamically dependent on the transformer loading and ambient temperature. It also includes the effects of geometry and the orientation of components on the natural convection and thermal radiation heat transfers.

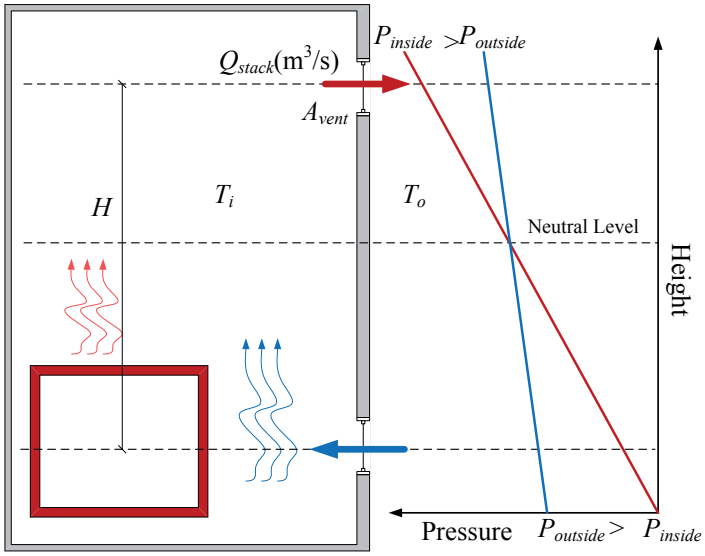

Fig. 17 *The potential for flow due to pressure variation with height*

2.4.1 Stack effect

Inside a cabin, after the air is heated at the surface of the transformer by natural convection, the hot air will rise to the roof. The accumulation of hot air at the top creates a positive pressure while the abandoned floor area of the cabin experiences a negative pressure (see Fig. 17). With the developed pressure difference and the presence of inlet and outlet openings at the bottom and top areas of the cabin respectively, a sustained circulation of air will occur. This phenomena is called the stack effect and it continues to act as long as the inside air is hotter than the ambient environment. This form of natural ventilation is so effective that, for instance, without the need to introduce forced ventilation, CFD (Computational Fluid Dynamics) techniques applied to partially ventilated cable troughs have shown an increase in the continuous rating of up to 31% [37].

The air streaming out of the outlet is quantified by the volumetric flow rate (Q_{stack}) and is given in (2.24) [36].

$$Q_{stack} = Cd * A_{vent} * \left(\frac{2gH * (T_i - T_o)}{T_i}\right)^{1/2} \quad \textbf{(2.24)}$$

where

Q_{stack} is the ventilation rate (m^3/s)

Cd = 0.65, a discharge coefficient

A_{vent} = free area of inlet opening (m^2), which equals the area of the outlet opening

g = 9.8 (m/s^2), acceleration due to gravity

H = vertical distance between inlet and outlet midpoints (m)

T_i is the temperature of indoor air (K)

T_o is the temperature of outdoor air (K)

The heat loss due to the ventilating moving air is given in (2.25) [38].

$$Q = Q_{stack} c_p \rho (T_i - T_o) \quad \textbf{(2.25)}$$

where Q is the heat loss (kW), c_p is the specific heat capacity air – 1.005(kJ/kg ^{o}C) and ρ is the density of air – 1.2 (kg/m^3)

Equation (2.24) consists of a discharge coefficient which directly incorporates the effect of the grill type and a covering panel just behind the vent openings. The discharge coefficient is a value describing the aerodynamic channeling of the airflow on discharge. It represents the ratio between the actual air flows compared with the theoretical airflow. The coefficient, ranging from 0 to 0.65, can easily be attained experimentally and is given in the manufacturer's specification of the specific grill or louver. The thermal resistance associated with ventilation openings will be as shown in (2.26), which is based on (2.24) and (2.25).

$$R_{vent} = \frac{(T_i - T_o)}{Q} = \frac{1}{Q_{stack} c_p \rho} \quad \textbf{(2.26)}$$

The temperature dependence of the air density and air viscosity could easily be incorporated in (2.24) to accurately account for the pressure driven ventilation and air humidity effects.

2.4.2 Simulation and measurement results

Before crafting the overall thermal circuit, we closely studied both a scaled down model of the cabins as well as a 3D FEM simulation. The model transformer has steel walls and wall attached cooling fins, and was filled with mineral oil. The heating load was supplied with 14 ceramic-walled hollow resistive rods with a connected resistance of about 31 ohms (see Fig. 18). Thermocouples were placed at different locations of the cabin, including on the surfaces of the resistive rods and inside the model transformer top-oil. The placement of the thermocouples was guided by results from a 3D FEM simulation shown in Fig. 19 and an analytical heat loss calculation of the parallel connected resistive loads.

The first measurement was conducted loading the resistors with 150 W and measuring the incoming and outgoing air temperature. The measurements, shown in Fig. 20, reveal that the hot air leaves the cabin at the very top of the upper windows, indicating that the rest of the openings are less relevant. The measurements also show that after a certain limit of opening area, further increasing the size of the ventilation opening does not have an

impact on the heat transfer. It is primarily the height and the placement of the outlet opening with respect to the inlet opening that will affect the top oil temperature of the distribution transformer. This observation supports the reasoning behind the stack effect.

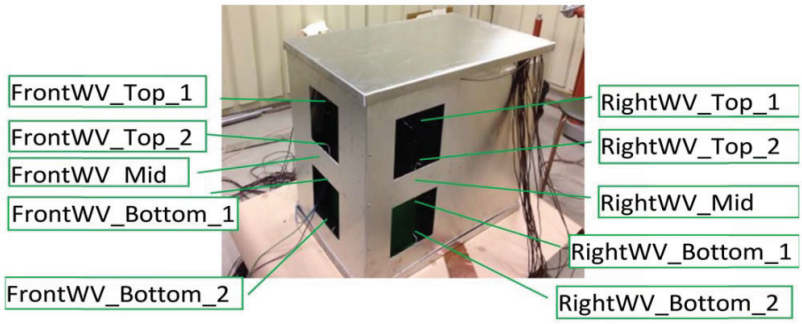

(a)

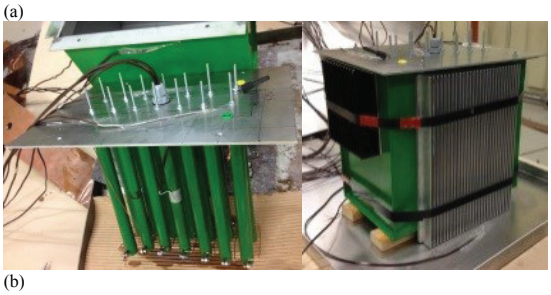

(b)

Fig. 18 *The transformer scale model, where dimensions are scaled by one third from a typical MV/LV transformer substation.(a) The aluminum cabin and (b) the model transformer filled with mineral oil*

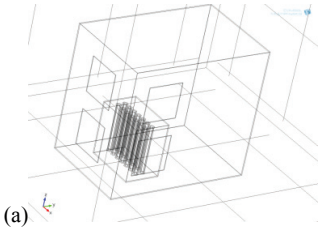

(a)

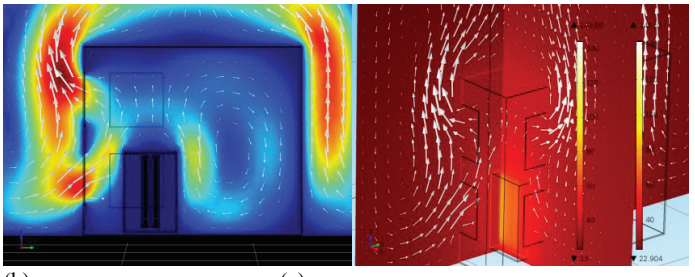

(b) (c)

Fig. 19 *FEM simulation for the transformer cabin scale model for a 150W heat supply from 14 ceramic resistors with a connected resistance of 31 ohms. (a) Geometry of scaled cabin model (see Fig. 18), (b) transformer cabin cross-section along its length showing airflow direction (arrows) and velocity (color gradient) and (c) transformer cabin ventilation air flow with temperature (℃) (slices) and air velocity (arrows) [29]*

The FEM simulation in Fig. 19 supports the fact that the hot air requires only a small area at the very top of the outlet opening to stream out, as explained above. Besides, the simulations show locally circulating air at the non-ventilated walls of the cabin. The heat transfer from the transformer surface to the non-ventilated cabin wall side, therefore, depends on surface-to-surface radiation and convection at the inside cabin wall surface.

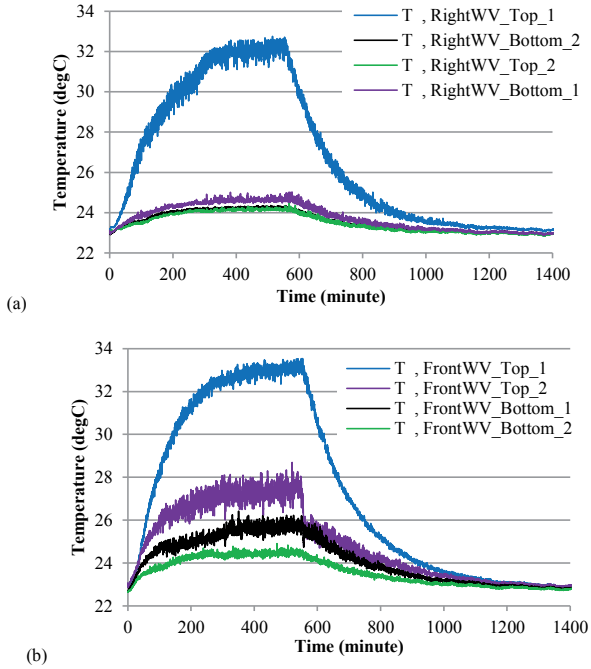

Fig. 20 *Air temperature measurements at different levels of the scaled down cabin model loaded with 150W heat supply. (a) Right side ventilation openings (b) Front side ventilation openings. See Fig. 18.*

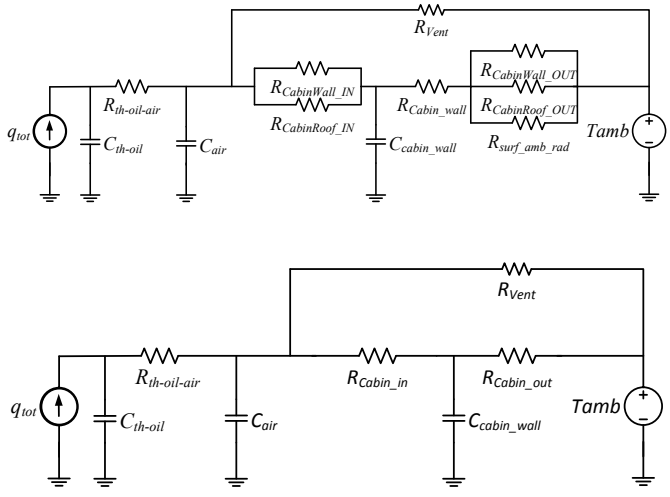

Fig. 21 *Overall thermal ladder network for the cabin installation (a) The detailed network consisting of the major thermal resistances and capacitances. (b) The simplified network.*

The thermal ladder network shown in Fig. 21 is proposed in this thesis. The network considers that the surface-to-surface radiation between the distribution transformer surface and the inner cabin wall surface is negligible. The thermal resistance for the heat transfer from oil to air ($R_{th-oil-air}$) is given in (2.27), which is elaborated in the top-oil thermal model of the ONAN transformer in [35].

$$\begin{aligned} C_1 &= C \times \left[{\rho_{oil}}^2 \times g \times \beta \times k^{\left(\frac{1-n}{n}\right)} \times L^{\left(\frac{3n-1}{n}\right)} \times c_{oil} \right]^n \\ \mu &= A_1 \times e^{\left[\frac{A_2}{\theta_{oil}+273}\right]} \\ h &= C_1 \times \left(\frac{\Delta\theta_{oil}}{\mu}\right)^n \\ R_{th-oil-air} &= \frac{1}{h \times A} \end{aligned} \tag{2.27}$$

where L is the characteristic dimension, length, width or diameter (m), g is the gravitational constant (m/s^2), k is the oil thermal conductivity(W/mK), ρ_{oil} is the oil density (kg/m^3), β is the oil thermal expansion coefficient $(1/K)$, c_{oil} is the specific heat of oil $(J/kg.K)$, μ is the oil viscosity $Pa\,s = (N\,s)/m^2$ and $\Delta\theta_{oil}$ is the oil temperature gradient

The empirical values for C and n are 0.59 and 0.25 respectively for laminar oil circulation, and 0.1 and 0.33 respectively for turbulent oil circulation. The thermal resistances R_{cabin_in} and R_{cabin_out} are computed based on the natural convection Nusselt numbers for vertical and horizontal planes facing either upwards or downwards, and either inside or outside, as shown in Appendix A of [Publication II] and also in [19]. The thermal resistance R_{vent} is given in (2.26). The thermal ladder network is implemented with an extended Matlab Simulink tool called Simscape, which is capable of authoring physical modeling components [39].

The output of the proposed thermal ladder network is compared with measurements from a 1000 kVA ONAN distribution transformer installed inside a prefabricated cabin of dimension (2.5×1.525×2) m. The technical specification of the 1000 kVA transformer is presented in Table 4. The measurement is conducted in an air-conditioned laboratory space with a room temperature of about 22°C. Heating power is supplied into the transformer MV (20 kV) side while the LV (410V) side is short circuited. During the transformer full load test (28.5A for our transformer), the transformer reached the critical temperature after 5 hours. This increment is due to the cabin environment, which causes the distribution transformer to perform below its rated current. During the test, we decreased the heating power associated with the total full load losses (11600W) to 9185W on the 5th hour and to 8500W after 1 hour and 45 minutes, and finally to 7500W after 2 hours, and the corresponding temperature can be seen in Fig. 22. For the 1000kVA distribution transformer inside the prefabricated cabin to stay under the upper thermal limit, it had to be loaded significantly less than when installed in free air.

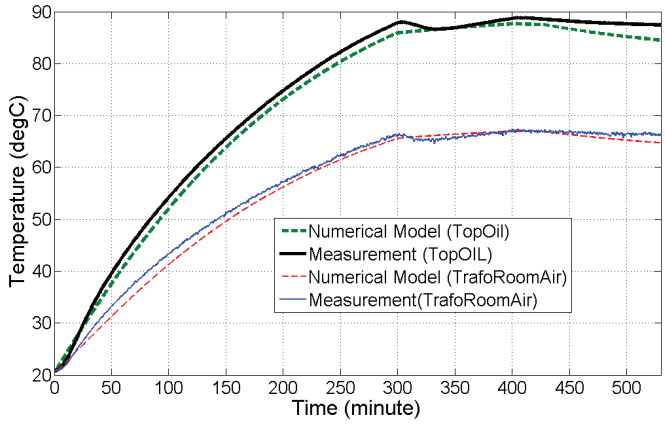

Fig. 22 *Top-oil and Transformer Room air temperature comparisons for a fully loaded 1000 kVA distribution transformer inside cabin.*

Table 4 *1000 kVA transformerspecification*

Name	Unit	Value
Rated power	kVA	1000
No-load voltage MV-side	V	20500
No-load voltage LV-side	V	410
MV-side tap steps	%	±2×2.5%
Frequency	Hz	50
Winding connection		Dyn11
Cooling		ONAN
No-load loss	kW	1100
Load loss	kW	10500
Short circuit impedance	%	6
Dimension L/W/H approx.	mm	1640/1000/1775
Gross weight approx.	kg	2645
Oil weight approx.	kg	495
Average winding temperature	K	65
Maximum oil temperature	K	65
Ambient temperature	°C	40

In another experiment, a temperature rise test on the prefabricated substation was done by heating the substation with external resistive heating elements. Heating power was adjusted according to the total losses of the substation. In the test, the LV switchgear side was heated all the time with a power of 240 W, which corresponds to the calculated losses of the low voltage side. The high voltage side was first heated with a power of 2960 W and finally at a power of 4540W, which corresponds to the total losses of the transformer. The outgoing air temperature measurement in comparison to the simulation results is presented in Fig. 23.

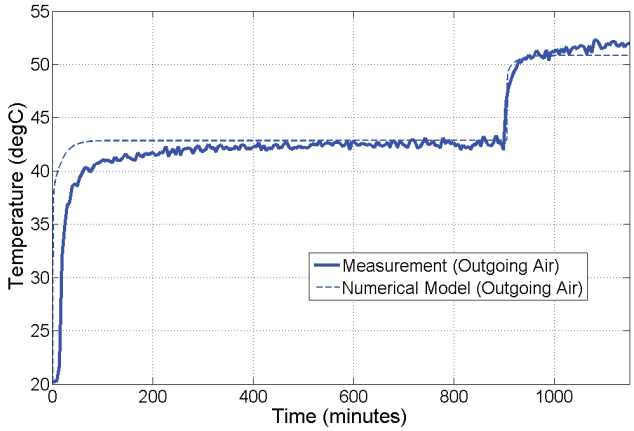

Fig. 23 *Step response of outgoing air temperature through the outlet ventilation of a prefabricated distribution transformer cabin supplied with 3200W followed by 4780W*

The Dormand-Prince based method solver ODE45 in Matlab was used to solve the step response for the ladder network shown in Fig. 24 [40]. The Simscape physical modeling enables the modeling of physical property components by the user, while allowing real time dynamism for viscosity, density, air pressure, etc.

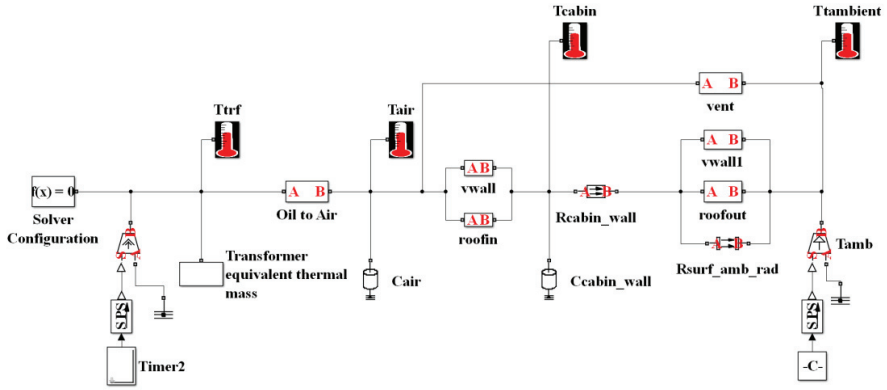

Fig. 24 *Simscape physical model*

The circuit parameters in Fig. 24 are represented in the thermal circuit layout in Fig. 21(a). Natural convection through the stack effect closely represents the ventilation scenario of prefabricated distribution transformer cabins. The proposed model estimated the top-oil temperature and temperature of hot-air streaming out of the top ventilation openings very closely, as shown in Figs. 22 and 23. The results in Fig. 23 show different dynamic responses in the two consecutive steps. Nevertheless, as one can imagine, convective wind temperature measurement is a very difficult task as the air movement can easily be altered relative to the thermocouple position. Although these kinds of discrepancies are unacceptable in more robust temperature measurements, such as the conductor surface,

the results presented in Fig. 23 are for a qualitative comparison of outgoing air temperatures.

Temperature differences and air pressure differences are the driving forces in natural ventilation. The requirement for safety and compactness forces the ventilation inlet and outlet openings to be single sided, meaning on the same wall. In addition, the safety requirements do not allow openings that grant direct view of the transformer from the outside, which makes temperature differences the dominant driving force for natural ventilation. In this thermal model we explained natural convection driven by temperature differences. However wind driven ventilation on prefabricated substations should be studied, especially for those cabins with a cross-ventilation set-up and significant openings in the direction of wind flow.

In an effort to introduce real-time thermal state monitoring and thermal rating system into active distribution networks, the first endeavor is to obtain credible dynamic thermal models of network components. In this thesis, a technique for the thermal modelling of underground cables installed inside unfilled conduit and prefabricated secondary substations was introduced and validated with measurements. In the consequent work in this thesis, the developed thermal models are combined with standard models of overhead lines and power transformers to establish a real-time thermal rating framework for active distribution networks.

3 Load and distributed generation forecasting

As a reminder, the main purpose of this thesis is to tie together the vital functions which enable the real-time operation and operational planning of active distribution networks. The basic work has been carried out in two parts. In part I, the dynamic thermal models of overhead lines, underground cables and secondary substation transformers have been developed to be usable in real-time. In part II, which is presented and discussed in this chapter, frameworks are developed to translate the load and weather data forecasting to the estimation of network component thermal states using smart meter measurements.

The load profiling practices and network calculation with load profiles have a long history in Finland, where load research projects started in 1983. Customer load profiles have been established and being utilized for purposes such as load flow calculation and state estimation as early as 1992. Although estimations of confidence intervals for several customers' cumulated load from the same customer class has been studied in previous works, the most general case of cumulated loads of several customers from different classes has not been dealt with sufficiently [41]. In active distribution networks, however, estimations of confidence intervals are crucial for load flow calculations as the number of customers is small. In [42], a pattern-recognition method for customer data classification based on AMR data is presented. Nevertheless, the consideration of within customer class and across customer classes' correlation and deviations to estimate confidence intervals has not been studied using AMR load data. In Sections 3.1 to 3.5, a statistical formulation based on clustered customer group's hourly consumption models is applied to calculate aggregated substation loads and day ahead load forecasts with the respective confidence intervals. The main contribution in these sections is the presentation of a method to forecast substation level loads with their respective confidence intervals using hourly AMR metered customer level consumptions.

Sections 3.6 to 3.8 present weather forecasting methods and existing DG models utilized in this thesis. Section 3.9 presents a method which enables the forecasting of distribution network thermal states based on load and weather variable forecasts. As estimating the future conductor and hot-spot temperatures is the foundation for the RTTR system, the framework presented in Section 3.9 is a strong contribution of this thesis.

3.1 Smart meter data for load modelling

There is a common understanding that a smart grid is one that incorporates information and communication technology into every aspect of electricity generation, delivery and consumption in order to: minimize environmental impact, enhance markets, improve service; reduce costs and improve efficiency. Distributed voltage control, enhanced demand response and load control are among the key applications enabled by the smart grid [3]. State estimation procedures and optimal on-line control tools are the most promising for electrical distribution networks to unleash smart grid applications curbed by the deterministic worst-case planning and operation limitations, which are based on steady state ratings.

State estimation can use load profiles to estimate the state of a distribution network. The process involves very short time load forecasts of individual classified load profiles and their aggregated loads. There are wide range of proposals presented in the literature on the methods of modeling load profiles and giving short and long term forecasts. The majority of them are time series methods such as: Fourier transforms, neural networks, Gaussian processes, Autoregressive, Fuzzy logic, wavelets and multiple regressions [43]. While short term load forecasting is the first step, the most difficult task is giving appropriate confidence intervals for the aggregation of the forecasted load. It requires a good understanding of the statistical distribution of customer loads within a classified class and across classes. The correlation between the loads of single customers has a central effect when defining the confidence limits of peak loads [44]. While research in this field is based on statistical methods, the conclusion has been that the distribution of electric load variation does not follow any commonly known probability distribution functions [45]. A study by Anssi Seppala proposes to use both normal distribution and log-normal distribution in the statistical model of customer load profiles [46], [47]. F. McLoughlin et al. on the other hand concludes that a Weibull probability distribution function is the best fit to the parameters of total electricity consumption and maximum demand, while a log-logistic probability distribution function gives the best fit to the load factor [43]. The classifying of customers into certain types enables better modeling of stochastic individual customers while still opening up customer level consumption behavior [48], [49]. However, changes in real-time as well as forecasted customer consumption have to be aggregated to understand feeder and substation level consequences.

The current DMS system is already shifting the static state estimations to dynamic and there is great interest in monitoring customer loads in higher spatial resolution [50]. We propose a practical method which uses AMR customer measurement database to model classified groups, and could then be aggregated to the substation level giving more spatial resolution to distribution system loads. The method is not affected by the existing limited access to real time customer load measurements. Besides, a formulation which takes into

account intra-class standard deviations and inter-class correlations is proposed for hourly measured consumption data. Statistically it is easier and more meaningful to model load classes rather than specific customers. In this dissertation we first investigate how well we can estimate primary and secondary substation load measurements from the aggregation of customer load classes. Subsequently we also compare the aggregation of day-ahead load forecasts of customer classes to substation level load forecasts.

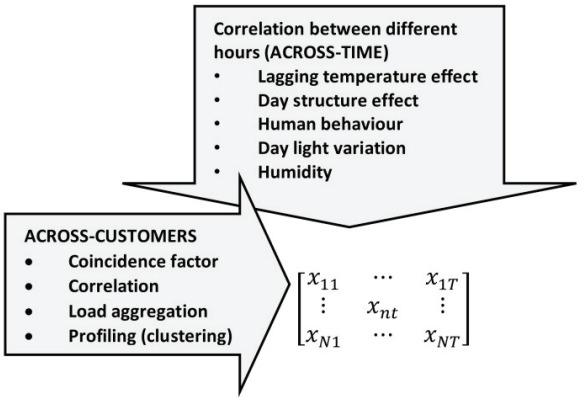

Fig. 25 *Two dimensional studies of load data. Where x_{NT} is hourly kWh consumption of households, N is number of households and T is the number of hours, which was 8760 in this* dissertation

A customer load measurement database can be investigated in two ways, from either the ACROSS-TIME perspective, which is from the time dimension for a specific customer, or the ACROSS-CUSTOMER perspective, which is from the customer dimension for a specific time. The ACROSS-TIME perspectives focus on variations with time and its relevance is for a short term load forecasts. The ACROSS-CUSTOMER perspective focuses on variations among customers at a specific hour, and is important for aggregating the forecasted or modelled load together and providing confidence intervals (see Fig. 25).

A distribution function describes how values are allocated across a population or sample space. The distribution function within a load class type is different from aggregated loads, due to the nature of the specific load class. Different techniques, such as fuzzy clustering can be applied to group similar load curves when background information of consumers is not available [51], [52]. However, a knowledge based clustering can also be applied when a database of background information is linked to a load cycle. In this thesis, a fully supervised classification of type loads is followed.

There are four predefined type load classes based on their primary heating systems. The information used for the classification is attained from a database containing statistical information of households gathered through questionnaires. The groups are: district heating (DIST), direct electric heating (DE), electric storage heating (STORE) and

ground source heat pumps (GSHP). The one year hourly load profile of typical households belonging to the four type load groups is presented in Fig. 26. It is worth mentioning here that only household loads are modeled in this thesis. No commercial, public or industrial loads are included.

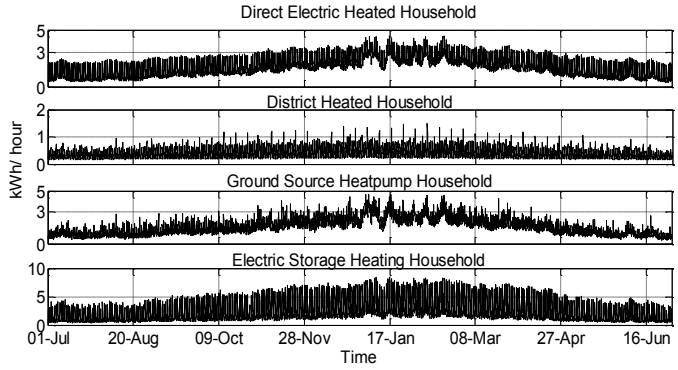

Fig. 26. The four household type load classes and their typical hourly load profiles for one year

According to the central limit theorem, the distribution of a sum of independent variables approaches the normal distribution when the number of variables increases. Nevertheless, in an LV distribution system the connected households are not in such a quantity to grant an automatic assumption of normal distribution. In this dissertation, probability distribution fits are compared using actual AMR measured data. A one year hourly measured data of 906 households is used. The fit is tried for each hour and the result shows the top three distributions to be Generalized Extreme Value, Generalized Pareto and Lognormal. Of all the four heating type households, those with electric storage heaters are very difficult to fit to known distribution functions (see Table 5).

Table 5 The best three fits out of 8760 fits for the four heating type groups

Rank	DE (N=550)	DIST (N=258)	STORE (N=81)	GSHP (N=17)
1	generalized extreme value 61.0%	generalized extreme value 32.8%	Birnbaum–Saunders distribution 17.7%	generalized pareto 33.4%
2	gamma 12.3%	loglogistic 22.6%	generalized pareto 15.7%	rayleigh 24.8%
3	Loglogistic 5.4%	lognormal 22.3%	gamma 15.4%	exponential 17.9%

3.2 Inter- and Intra-class correlations and standard deviations

There are four customer type load classes, as explained in the previous section. When these modeled classes are aggregated to give a composite load at a common connection

point, then correlations and standard deviations are required for the computation of confidence intervals. A fully represented load class will have hourly mean, standard deviation, inter-class and intra-class correlation values. According to T. Räsänen et al, there must be at least 100 monitored customers for each customer class with electricity records measured over the last 3 years in order to generate the relevant mean values and standard deviations of load curves for customers belonging to different classes [53]. Except for households in the ground source heating system class, there are close to 100 customers under each class in our database. For correlation terms, we used monthly values for each class due to the availability of only a single year of data. In Fig. 27 (a-d), the load models for direct electric heating load and district heating load types are presented. Households grouped under a similar heating type class behave in distinct ways within the class as well as across classes.

Although the primary heating type based grouping method is used in this study, one can cluster households considering the special conditions of the loads and also using robust clustering algorithms. In this chapter, however, households grouped by identical heating type can have significant variation in terms of heated area, number of residents and other appliance ownership. Hence, the grouping is admittedly not optimal. Nevertheless, the distinct temporal loading features of the household groups are demonstrated in Fig. 26.

There are two correlation computation methods used in this chapter. When the whole year scenario is considered, as in Fig. 27 c and d, the correlation of customers at individual hours is computed while it is varying in every day of the month. Hence similar hours of the month will have similar correlation values as shown in Fig. 27. On the other hand, when average day of the year is of interest the correlation values at individual hours is calculated from the time series matrix of rows equivalent to the number of columns and 365 rows. Hence, one can see better intra-class correlation values in Figs 32 and 33 compared to the intra-class correlation values presented in Fig. 27c. This is essential due to the heating type grouping method which manifests better correlation across the seasons in a year than, for instance, individual months.

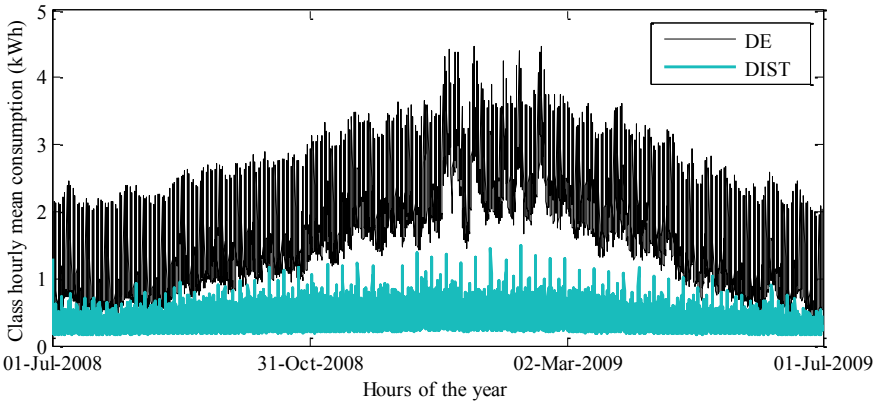

(a) *Class mean values of DE and DIST*

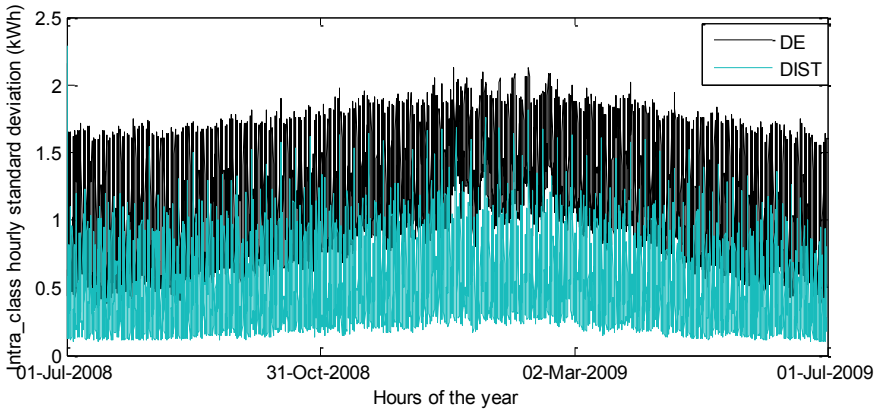

(b) Intra_class standard deviation values of DE and DIST

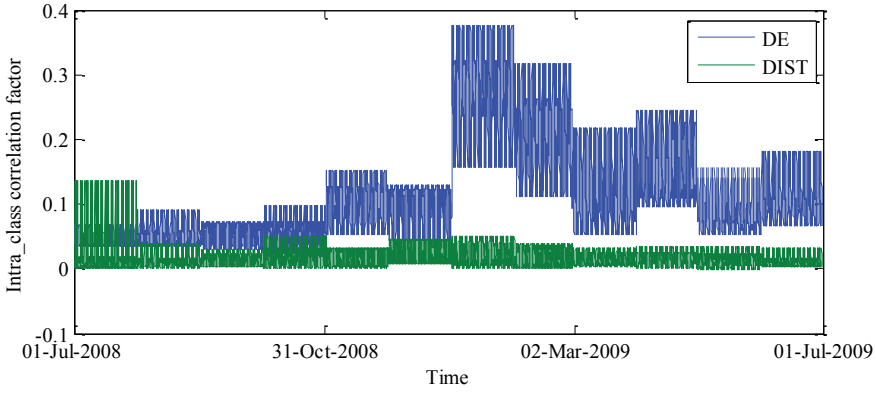

(c) Intra_class correlation values of DE and DIST

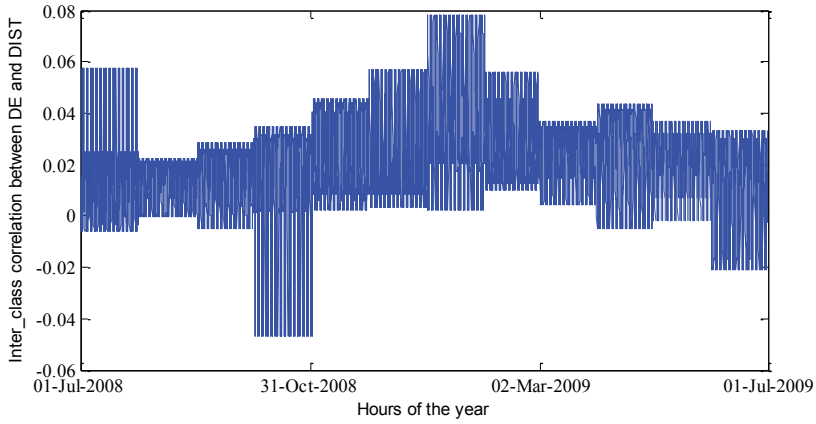

(d) Inter-class correlation values between DE and DIST

Fig. 27 *Class-mean, intra-class standard deviations and intra-class and inter-class correlation values of direct electric (DE) and district (DIST) heating load classes*

There is strong variance among households with electric storage heating systems, as shown in Fig. 28. Groups of other heating types experience similar variance trends in the 24 hour period, except for a significant difference in magnitude (see Fig. 28). Due to heating consumption, there is strong correlation among direct electric, electric storage or ground source heating equipped households (see Fig. 29). Also, all the three electric heating types correlate with district heated households in a very similar way (see Fig. 29 and Fig. 30). Correlation factors cannot be ignored in calculating composite load deviation. As shown in Fig. 31, there is an inverse relationship between correlation factor and standard deviation. Direct electric heated households are highly correlated within the group, as shown in Fig. 32. Besides, households with ground source heat pumps are more correlated to direct electric heated households than storage heaters (see Fig. 29 and Fig. 33). The lowest correlation among the four groups is experienced between the electric storage heated household class and district heated household class types (see Fig. 33).

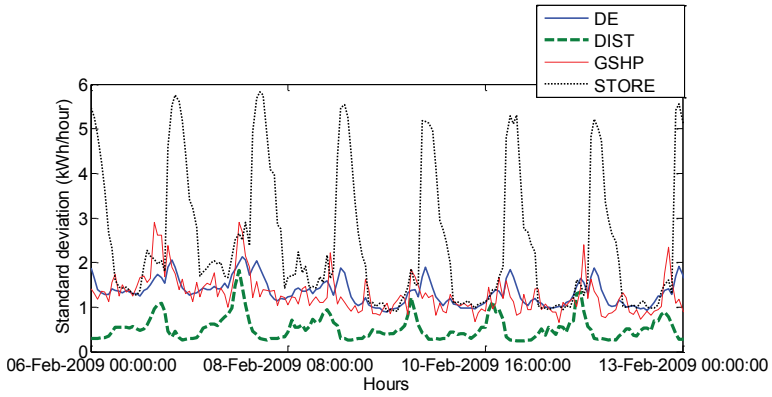

Fig. 28 *Hourly standard deviation for an average winter day of the four heating type groups*

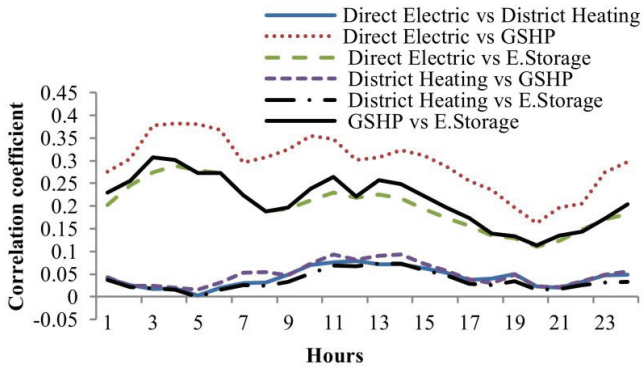

Fig. 29 *Hourly correlation between different heating type groups for an average winter day*

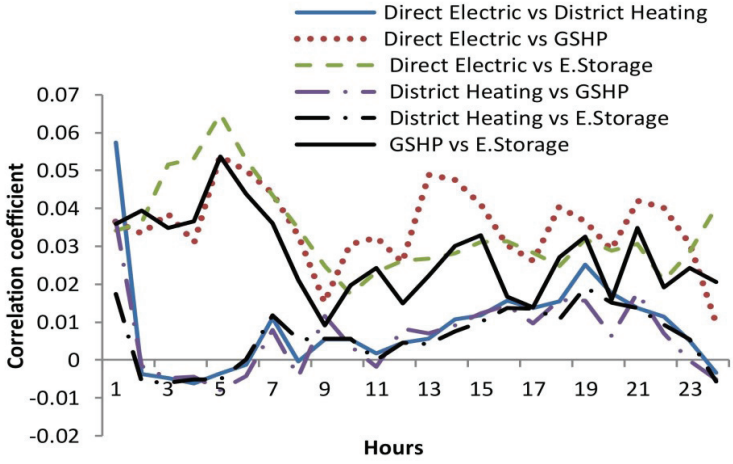

Fig. 30 *Hourly correlation between different heating type groups for an average Summer day*

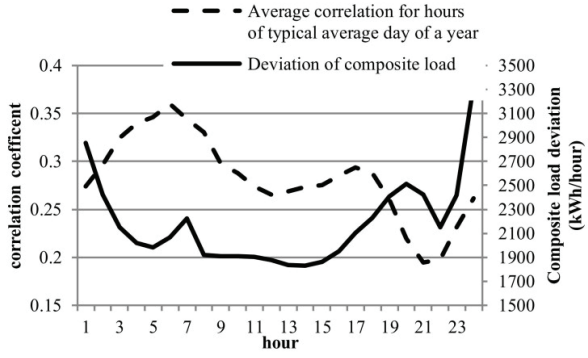

Fig. 31 *Relationship between correlation and standard deviation for a typical day of a year for 906 households.*

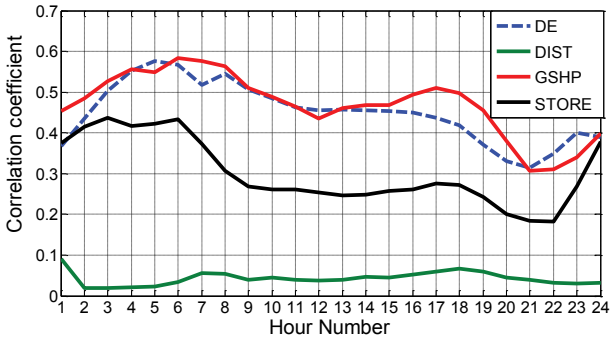

Fig. 32 *Intra-class correlations of the four heating type groups at each hour of the day.*

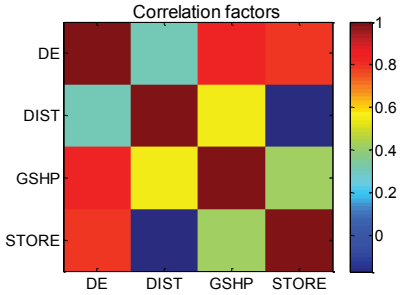

Fig. 33 *Correlations between different heating groups.*

3.3 The test distribution network (NTK#1)

In this thesis two test distribution networks were utilized for simulation purposes. The first test network (NTK#1) is used to compare local and aggregated level load modelling and forecasting capability, as shown in this section. NTK#1 is also used to simulate the benefits of a real-time thermal rating system in increasing the loading capacity of a distribution network as well as in increasing the utilization and integration potential of distributed generation (DG). The second test network (NTK#2) is used to simulate the role of RTTR in the coordinated voltage control (CVC) of an active distribution network, and is presented in Section 4.3.2.

Table 6 *Green-field radial distribution network data*

1 Primary Substation (40MVA, 110/20 kV)		
16 secondary substations (1.6MVA, 20/0.4 kV)		
1800 Households	Heating type	No.
	Direct Electric (DE)	673
	District heating (DIST)	960
	Ground Source HP (GSHP)	109
	Electric storage heating (STORE)	58

The test network is laid out by a network planning algorithm capable of producing close to optimal Greenfield networks or expansion and upgrade plans that utilize existing network. A fully radially operated network without distributed generation is used. The profile of household types connected to the test network is shown in Table 6, and Fig. 34a lays out the positions of the households with their heating system type in colors. Fig. 34b, on the other hand, shows the MV network in bold and the LV network in grey in the background.

As shown in Table 7, there are 1800 households belonging to one of the four primary heating type groups. These households are geographically distributed to build the simulated MV/LV network following geographical boundaries, street grids and the availability of, for example, district heating, as shown in Fig. 34 (a). On the other hand, we have actual hourly metered consumptions from one year, between 2008 and 2009, for the same number of households and heating type profiles. For both load forecasting and load flow analysis the actual one year hourly consumptions are randomly assigned to the individual households connected to the simulated network (see Fig. 34 (b)).

Table 7 *Distribution of LV customers of the four heating types under the sixteen secondary substations.*

No.	DE	DIST	GSHP	STORE
1	151	6	0	0
2	116	0	0	0
3	85	0	0	0
4	101	0	0	0
5	20	75	0	0
6	101	8	0	0
7	99	0	0	0
8	0	213	0	5
9	0	126	0	26
10	0	150	0	0
11	0	84	0	0
12	0	70	0	27
13	0	105	3	0
14	0	119	4	0
15	0	0	56	0
16	0	4	46	0

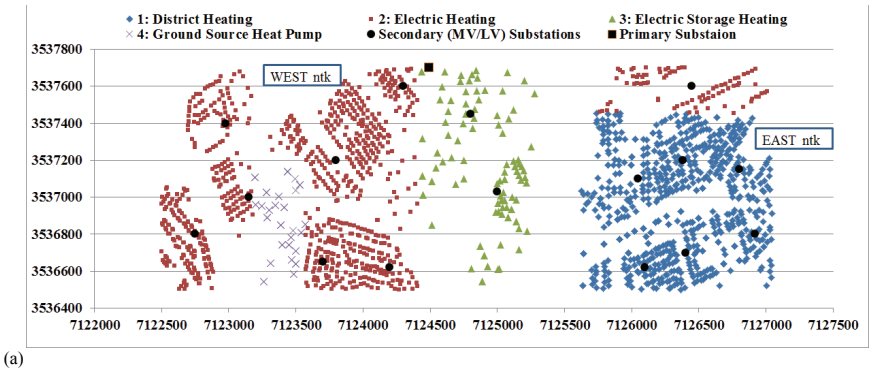

(a)

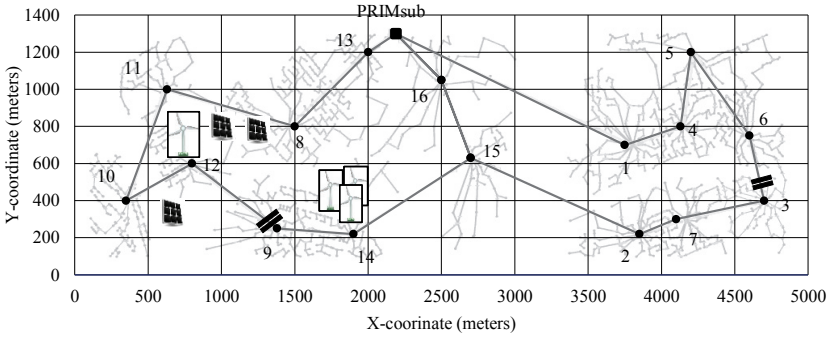

(b)

Fig. 34 *The Greenfield test network. (a) Showing the distribution of household types, MV/LV and HV/MV substations; (b) optimally planned distribution network to supply the households.*

The test network in Fig. 34 is a Greenfield network. That means, although it is routed using an actual geographical location scenario, it doesn't exist for real. When the network was planned, it assumed that the household types mentioned in Table 7 and also graphed in color in Fig. 34a are actually on the ground and planned an optimal network to supply the households from a single primary substation.

3.4 Composite load deviations for aggregated loads

Individual customers have intra-class (within a class) and inter-class (across classes) correlations, which vary with time in a given day. The standard deviation for a single load class containing *n* number of households can be calculated as in (3.1) [44].

$$\sigma^2 = \sum_{i=1}^{n}\sum_{i=1}^{n}\sigma_i\sigma_j\rho_{ij} \qquad \textbf{(3.1)}$$

where σ_i is the deviation of single loads, ρ_{ij} is the statistical correlation between the individual loads and σ^2 is composite covariance

For a network node in a distribution system supplying customers belonging to different load classes, however, a more robust standard deviation formula is needed. The

composite load deviation considering load types (multiple load type classes) and with the inclusion of both the intra-class and the inter-class correlations, can be calculated from the formula in equation (3.2) [44].

$$\sigma^2 = \sum_{i=1}^{k} n_i \bar{\sigma}_i^2 + \sum_{i=1}^{k} n_i (n_i - 1) \bar{\sigma}_i^2 \bar{\rho}_{ii} + \sum_{i=1}^{k} n_i \bar{\sigma}_i \sum_{\substack{j=1 \\ j \neq i}}^{k} n_i \bar{\sigma}_j \bar{\rho}_{ij} \quad \textbf{(3.2)}$$

where k is number of group types, n_i is the number of individual customers in each classified group, $\bar{\rho}_{ii}$ is the intra-class correlation within a class i, $\bar{\rho}_{ij}$ is the inter-class correlation between class *i* and *j*.

There is a similar formulation to (3.2), proposed by A.K. Ghosh et al to give the standard deviations of the aggregated load estimate of a node in a distribution network [54]. The formulation uses the standard deviations of individual load classes and the inter-class correlation terms. It doesn't, however, take the intra-class correlation term into account.

The calculation of the composite standard deviation in the above equations is vital for the calculation of both the prediction and confidence intervals. A prediction interval is similar in essence to a confidence interval, except the first is designed to cover a 'moving target', the random future value of *y*, while the second is designed to cover the 'fixed target', the average (expected) value of *y*, *E(y)*. The prediction interval must also take account of the tendency of *y* to fluctuate from its mean value, while the confidence interval (*l*) simply needs to account for the uncertainty in estimating the mean value. The formulations of the two intervals are slightly different to one another, and are given in equations (3.4) and (3.5). It is assumed that error term $e_n(l)$ has zero mean value (3).

$$e_n(l) = Y_{n+1} - \hat{Y}_n(l) \quad \textbf{(3.3)}$$

For an unbiased forecast, the expectation of the forecast error $E\big(e_n(l)\big) = 0$.

The prediction interval for Y_{n+1} is given by

$$\hat{Y}_n(l) \pm \alpha \sqrt{Var(e_n(l))} \quad \textbf{(3.4)}$$

And the confidence interval for mean value is given by

$$\hat{Y}_n(l) \pm \alpha \frac{s}{\sqrt{n}} \quad \textbf{(3.5)}$$

where $\hat{Y}_n(l)$ is the forecast value of Y_{n+1}, $Var\big(e_n(l)\big)$ is the variance of the forecast error and α is critical value for normal distribution, in the case of 95%, 99% or 99.5% non-exceeding probability the coefficient is taken to be 1.96, 2.326 or 2.576, respectively.

$$s = \sqrt{\frac{1}{n+1} \sum_{i=1}^{n} (Y_i - \mu)} \quad \textbf{(3.6)}$$

where s is standard deviation from the mean, μ is the mean of the sample Y and n is the sample number.

In this dissertation, both the prediction interval and confidence interval are of interest. The prediction interval is used when point measurements such as primary or secondary substations and class mean load are forecasted, whereas the confidence interval is used when models or forecasts of individual load classes are aggregated at the primary or secondary substation.

How well can we model substation level load profiles from an aggregation of customer load classes? In the previous sections we have shown that a customer class can be represented by its mean, intra-class standard deviation, intra-class correlation and inter-class correlation values. In equation (3.2) the computation of the composite standard deviation is provided. Hence, we can calculate the expected composite load and its confidence interval, as shown in equation (3.7).

$$P_{comp} = \sum_{i=1}^{k} n_i \cdot m_i + \alpha \cdot \sigma \qquad \textbf{(3.7)}$$

where P_{comp} is the substation composite load, i is the load class number, k is the total number of classes, n_i is the number of customers connected to the substation and belonging to class i, m_i is the mean value of class i, and σ is composite deviation as given in (3.2). In the case of 95%, 99% or 99.5% non-exceeding probability the coefficient α is taken to be 1.96, 2.326 or 2.576, respectively.

For the test distribution network NTK#1, explained in Section 3.3, the customer aggregated load is compared with the actual measured load at the secondary and primary substation. Hourly measured customer consumption is assigned randomly to each customer in the network from a database of actual customer AMR measurements. Primary and secondary substation measurements in this section refer to the direct sum of actual AMR measured household loads connected behind them, but not substation load measurements.

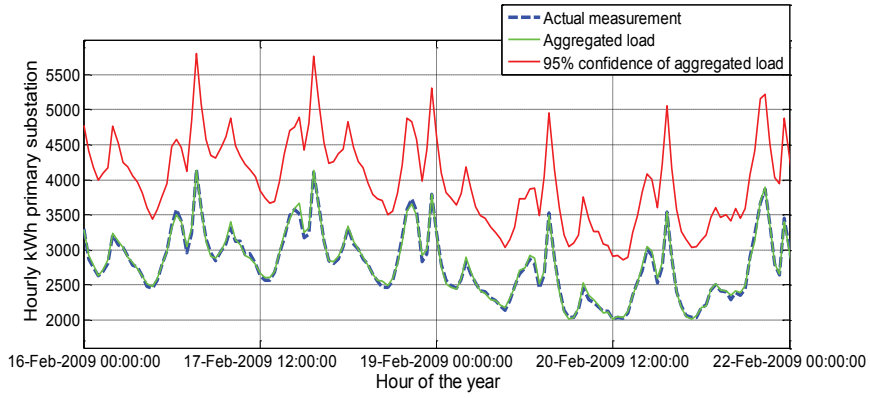

Fig. 35 *Aggregated customer loads and their 95% confidence limit at the primary substation*

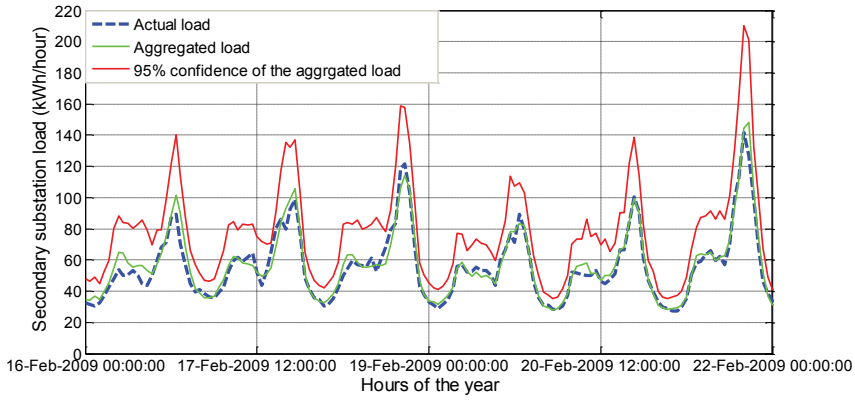

Fig. 36 *Aggregated customer loads and their 95% confidence limit at secondary substation (SUBs 13).*

Although the 95% confidence interval is violated at the secondary substation aggregated loads, as shown in [Publication IV], the aggregated load at the primary substation not only matched the actual consumption, but also its 95% confidence interval stayed way above the actual consumption all year (see Fig. 35). The one week load of secondary substation 13 shown in Fig. 36 illustrates significant error between the aggregated load and actual load compared to the primary substation in Fig. 35.

3.5 Day-ahead load forecasting

The time series model used for 24 hour ahead load forecasting belongs to the auto regressive with exogenous inputs (ARX) model group. It incorporates the lagging effects of temperature as well as consumptions from the previous week, as formulated in (3.8). The model has lagging hourly consumption information from the same hour in the previous week and the previous day same hour load. The effects of the previous two hours' temperatures together with real time temperature are included in the explanatory variable. The day structure effect is also included through weekday and weekend dummy variables.

$$y_t = C + \sum_{i=1}^{3} \alpha_i Y_{i,t} + \sum_{j=1}^{4} \beta_j x_{j,t} + \sum_{k=1}^{2} \gamma_k D_{k,t} + \varepsilon_t \qquad \varepsilon_t \sim N(0, \sigma^2) \tag{3.8}$$

where y_t is the output (target variable), C is constant or the intercept of the model. $Y_{i,t}$ are the lagging output values, which include: Previous Day Maximum Load, Previous Week Same Hour Load, $Y_{i,t-168}$, Previous Day Same Hour Load, $Y_{i,t-24}$,

$x_{j,t}$denotes external inputs (explanatory variables) which include: same hour temperature, amount of sun light (day length), Previous Hour Same Day Temperature, and previous 2 Hour Same Day Temperature.

$D_{k,t}$ denotes the dummy variables which include: the weekday dummy variable, and the weekend and holiday dummy variables. α_i, β_j and γ_k are coefficients estimated using ordinary least squares estimation. The lags are selected so that the error term ε_t is white noise.

Consumption lags are selected in the assumption that they reveal the repetitive activity patterns of residents. (i.e. the activity of residents at current hour is more likely to be similar to their activities same hour yesterday and same hour last week same day). Due to the thermal time constant of the building envelope, the impact of up to the previous two hours temperature variation in the ambient will only be reflected in the heating consumption lagging. Hence, ambient temperatures of up to two previous hours are selected as explanatory variable in the model.

The hourly AMR measured one year consumption data of thousands of households in Finland is used for the parameter estimation [55]. Only previous hours of the year are used to forecast every hour ahead, requiring at least a week length of consumption data for modelling. The validation of the model is conducted by the co-author of [Publication III] in [56].

Using the load forecasting technique presented in (3.8), comparisons of household level and substation level load forecasting are compared. Three cases are investigated. The results are plotted in Fig. 37 and the corresponding Root Mean Square Errors (RMSE) and Mean Absolute Percentage Errors (MAPE) are given for comparison in Table 8.

Case 1:

Forecasting individual customers: each and every household is modeled individually and a day-ahead forecast is carried out. The consumptions are then aggregated hierarchically at their feeding secondary substation and then the primary substation.

Case 2:

Forecasting at secondary substations: the consumption of individual households connected to a secondary substation is aggregated before application of the forecasting technique.

Case 3:

Forecasting at the primary substation: all consumption under the primary substation are aggregated and the aggregated load is modeled and forecast for the next day.

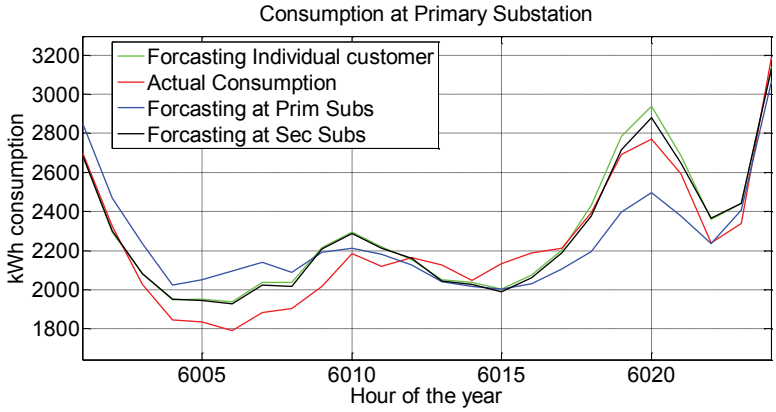

Fig. 37 *kWh at the primary substation connecting 1800 households in Fig. 34.*

The results presented in Figs 35 and 36 are based purely on statistical approaches. From the central limit theorem, as the sample size increases it will be more and more normally distributed strengthening the proposed method's assumption. This explains why the primary substation load prediction error is lower in Fig. 35 compared to Fig. 37. On the other hand, when temperature is used as an explanatory variable, the heating type of individual households would be better modeled using their specific load profiles than the aggregated load profile.

In Table 9, substations 8, 10, 11, 13 and 14 reveal better accuracy at the secondary substation level than for individual households. Those substations are supplying households with district heating. The load modelling formulation in (3.8) contains ambient temperature as an explanatory variable, which means that electric heated households can be modelled and predicted with better accuracy than households with a district heating system.

Table 8 *RMSE and MAPE comparisons*

	RMSE (kWh)	MAPE (%)
Case 1	196.61	9.27
Case 2	160.06	6.88
Case 3	173.46	7.36

Table 9 *RMSE (kWh) comparisons between individual customer forecasts and secondary substation forecasts for the 16 substations*

No.	Sub.	Customer.	No.	Sub.	Customer.
1	25.59	26.42	9	14.37	16.86
2	20.15	21.04	10	9.8	15.48
3	14.46	14.93	11	6.55	10
4	16.71	16.34	12	10.58	11.02
5	8.69	11.1	13	8.34	13.4
6	17.97	18.2	14	8.8	13.48
7	17.02	17.55	15	15.62	15.97
8	14.38	23.69	16	13.08	12.92

In the test network, the realistic geographical positioning of actual households is attempted to be represented. For instance, district heated apartments are likely to be in the same neighborhood and detached households with storage heaters in a separate neighborhood. This makes the household under secondary substations more homogeneous than primary substations. Hence the higher accuracy of the secondary substation forecast than the primary substation forecast in Table 8 is justifiable.

Nevertheless, the results in Tables 8 and 9 shows that there is little difference in the errors committed when load forecasting is performed at customer points and at secondary substations. Nevertheless, those secondary substations supplying mainly households with district heating are better modelled at the secondary substation than at the customer level, revealing the failure of the temperature explanatory variable in (3.8) in explaining the consumption of district heated households. The RMSE of voltage forecast using customer forecasted loads was about 0.004 pu and the MAPE is less than 1%. Hence, customer level load forecasting can be used to conduct load flow analysis giving forecasted customer level voltages. Voltages are not measured in the test network. All voltage computations based on actual household AMR consumption measurements are referred to as 'measured voltages' in the text. When the voltage values are computed from the load flow analysis using forecasted customer level loads, they are referred to as 'forecasted voltages'.

The error is expected to be greater with the attempt to model individual customer level electric loads as these loads do not follow any known distribution function [46]. There is, therefore, a trade-off between the interest in a customer level detailed load flow analysis and obtaining a model with an acceptable error margin. Nevertheless, the results in our study suggest that individual customer level modeling can be attained with a comparable error level to the secondary substation or primary substation level load modeling (see Table 9 and Fig. 37). However, the modeling technique needs to be robust and capable of providing error margins. In addition, it has to take into consideration the coincidence and correlation factors among individual customers. In that sense, the secondary substation aggregated load based modelling is a preferred choice.

3.6 Weather variable forecasting

The four weather variables affecting the load forecasting, the distributed generation forecasting and the thermal rating of network components are ambient temperature, soil temperature and moisture content, wind speed and solar irradiation. There is a strong correlation among the variables, though, for instance between customer loads and ambient temperature. There are four distribution network components this dissertation aims to monitor. They are the underground cables, the overhead lines, the indoor secondary substation transformer and the prefabricated secondary substation transformer. Concerning the distributed generation, the outputs from the solar panels and the wind turbines are forecasted.

The four distribution network components and their respective relevant environmental variables are listed in Table 10. Weather forecasting is an extensive research area in its

own right. The usual practice among system operators is that they either buy the next day forecasted data series from meteorological institutes or use in-house modeling based on their own measurements. However, besides the introduction of dynamic thermal rating to an active distribution system, the scope of this thesis is limited to show the dynamics and dependencies among the various distribution network variables affecting the accuracies of thermal state forecasts. Hence, we chose to use a simple Autoregressive Integrated Moving Average (ARIMA) model to forecast the weather variables.

Table 10 *Components and Relevant Environmental Variables*

Component	**Environmental variable**
Underground cable	Soil temperature
Overhead line	Wind speed, solar irradiation and ambient temperature
Indoor substation	Room temperature (ventilation type)
Prefabricated substation	Wind speed, solar irradiation and ambient temperature

The ARIMA method is widely applied to climate variables such as solar irradiation, wind speed and ambient temperature [57-59]. With its simplicity and clarity, the ARIMA method outperforms other methods such as neural networks, especially in lower time resolutions [57]. In this dissertation, the four environmental variables are forecast for the next day 24 hours based on measurements up to the previous day last hour.

The ARIMA models for wind speed and solar irradiation were fitted on transformed data as in [58]. The transformation

$$Y_t = [F_N^{-1}(\hat{F}_{t_t}(Z_t)], \tag{3.9}$$

where $\hat{F}_t$ is the estimated cumulative distribution function (CDF) and F_N^{-1} is the inverse CDF of the standard normal distribution, transforms the measured data at time t, Z_t, to normally distributed Y_t for all t. The transformed data is easier to treat in an ARIMA model. Also, the residuals (estimated error terms) of the ARIMA models, as built on transformed data, were approximately normally distributed, which allows the calculation of confidence intervals in forecasting. For wind speed data, the estimated CDF in (3.9) was a Kernel smoothing estimate with the same $\hat{F}_t$ for all t. For solar irradiation data, with significantly different expected values for different hours of the day, a different empirical CDF was estimated for each hour of the day giving 24 different $\hat{F}_t$, where the correct CDF is defined by the hour of the day and month specified by t.

After closely examining the Autocorrelation Function (ACF) and the Partial Autocorrelation Function (PACF) of the four univariate time series variables (see Figs. 38 and 39), the parameters of *ARIMA(p,d,q)* were selected as presented in Table 11. p is the number of autoregressive terms, d is the number of non-seasonal differences needed for stationarity and q is the number of lagged forecast errors in the prediction equation. In forecasting, the data were transformed from normally distributed forecasted Y_t to the final

estimated Z_t for the transformed wind and solar data. The 24-hour-ahead forecasted ambient temperature and its 95% prediction intervals are presented in Fig. 40.

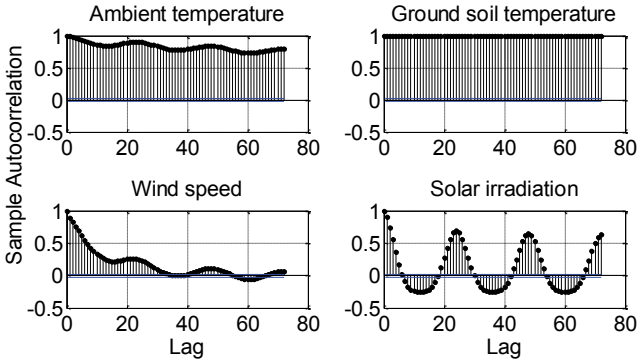

Fig. 38*Autocorrelation (ACF) of hourly measurements for ambient temperature, soil temperature, wind speed and solar irradiation (up to 72 hours lag)*

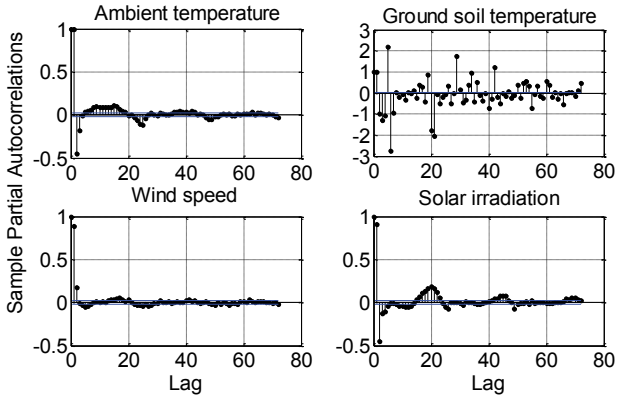

Fig. 39 *Partial autocorrelation (PACF) of hourly measurements for ambient temperature, soil temperature, wind speed and solar irradiation (up to 72 hour lag)*

Table 11 *The ARIMA p, d, q Parameters for The Environmental Varibales*

	p	*d*	*q*
Solar Irradiation	[1,2,3,4,24,48]	0	0
Ambient Temperature	[1:24]	0	0
Wind Speed	[1,2,3,24]	0	0
Soil Temperature	[1,2]	5	0

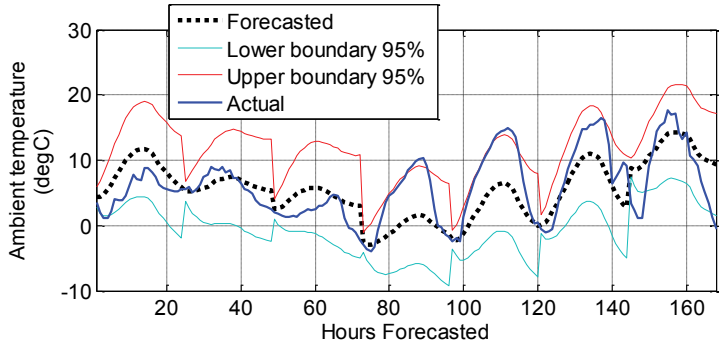

Fig. 40 *An example of ambient temperature 24-hour-ahead moving window forecasts for a week (168 hours) based on ARIMA (see Table 11)*

3.7 Wind turbine model

In this thesis, a simple wind turbine model, which uses its nominal power, cut-in speed, speed of rated output and wind speed, is used to calculate the corresponding generated power. The model approximates the power characteristics curve of the wind turbine with two straight lines, and is given in equation (3.10). One year hourly weather data for wind speed was attained from the Finnish Meteorological Institute (FMI) [60]. For a 50 kW wind turbine the hour by hour generation profile for one year is plotted in Fig. 41.

$$P_{wind} = \begin{cases} S \cdot w_{meas} + K, & w_{cut\_in} < w_{meas} \text{ and } w_{nomin} > w_{meas} \\ P_{nomin}, & w_{meas} \geq w_{nomin} \end{cases}$$

$$S = \frac{P_{nomin}}{w_{nomin} - w_{cut\_in}} \qquad \textbf{(3.10)}$$

$$K = -S \cdot w_{cut_{in}}$$

where P_{nomin} is rated power, w_{nomin} is wind speed at rated power, w_{cut_in} is cut-in wind speed (m/s), w_{meas} is wind speed (m/s), S is slope and K is constant.

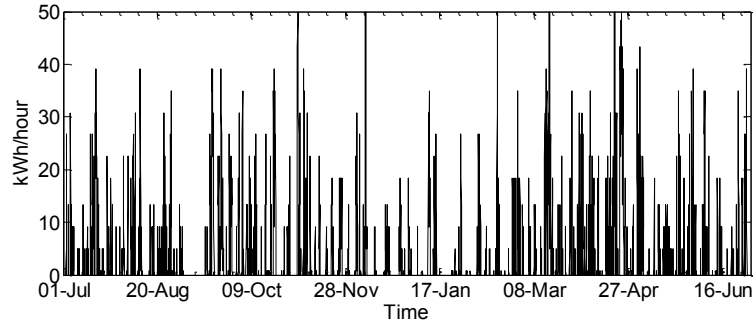

Fig. 41 *One year hourly generated energy from a 50 kW wind turbine (kWh/hour) (July, 2008 to June, 2009)*

3.8 Solar panel model

A practical model developed by Jones and Underwood for the production of optimal output power from a photovoltaic module is used in this dissertation [61]. The approach uses the simple relationships from the diode model of irradiance and temperature, with short circuit current and open circuit voltage to calculate the maximum power output. In equation (3.11), except for the ambient temperature and solar irradiance values, all other values can easily be taken from the manufacturers' datasheet of the considered module. The one year hourly weather data for ambient temperature is from the Finnish Meteorological Institute (FMI), and the solar irradiation data is from the Solar Energy Services for Professionals (SoDa) website [60], [62]. The hourly generation profile for a 215Wp (peak) solar panel installed at 64.2º N, 27.7º E is plotted in Fig. 42.

$$
\begin{aligned}
P_{pv\_max} &= FF \cdot \left(I_{sc} \cdot \frac{G}{G_{ref}} \right) \cdot \left(V_{oc} \cdot \frac{ln(P_1 \cdot G)}{ln(P_1 \cdot G_{ref})} \cdot \frac{T_{jref}}{T_j} \right) \\
FF &= \frac{PV_{max}}{V_{oc} I_{sc}} \\
P_1 &= \frac{I_{sc}}{G} \\
T_j &= T_{air} + \frac{NOCT-20}{80} \cdot S
\end{aligned}
\qquad \textbf{(3.11)}
$$

where T_j is photovoltaic (PV) cell temperature (K), T_{jref} is the reference cell temperature (K), FF is the filling factor, S is the insolation (mW/cm2), I_{sc} is the short circuit current (A), V_{oc} is the open circuit voltage (V) and PV_{max} is the maximum power under Standard Test Conditions (STC) (for our PV: irradiance of 1000W/m^2 and NOCT is 25 ^{o}C). The Nominal Operating Cell Temperature (NOCT) is defined as the temperature reached by open circuited cells in a module under standard conditions. With the assumption that the panels are equipped with solar tracking system, the incident solar irradiation is considered to be perpendicular to the module surface.

T_{air} is air temperature (degC), G is irradiance (W/m^2), G_{ref} is standard irradiance (W/m^2), PV_{max} is the maximum power under STC conditions (W) and P_{pv_max} is the maximum power output (W).

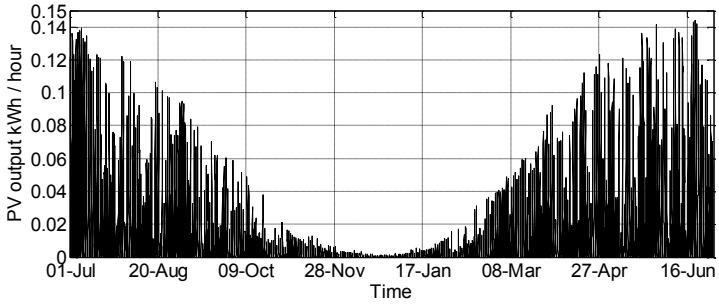

Fig. 42 *One year hourly generated energy from a single 215Wp solar panel (kWh/hour) (July, 2008 to June, 2009)*

3.9 Network component thermal state estimation and forecasting

In this thesis we investigate how well we can forecast the thermal state of distribution system components 24 hours ahead. The distribution system under consideration is one with a high penetration of distributed generation, such as solar panels and wind turbines (see NTK#1, Fig. 34). The day-ahead distribution network operational planning fundamentally depends on the thermal loading risks of the components. Hence, the uncertainties in loading, weather conditions and DG generation forecasts have to be translated to the thermal state forecast risk factors. In this dissertation, the required variables for the thermal state forecasting of distribution network components are gathered together with the presence of local generation to show the entire dynamics of an active distribution network.

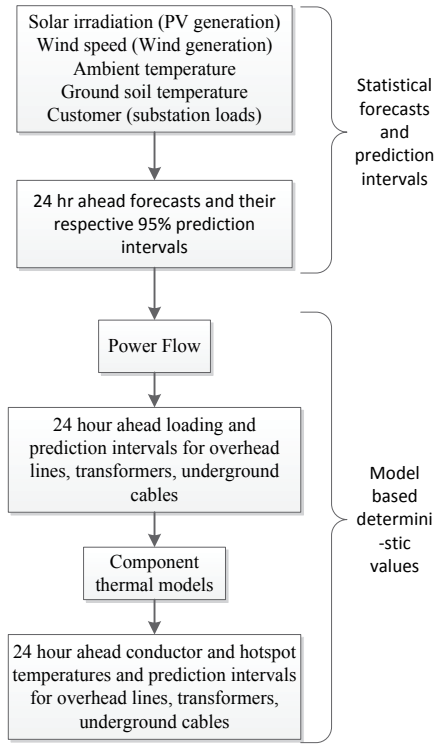

Fig. 43 *Workflow for distribution network thermal state forecasting*

With the advent of distributed generation, which is intermittent in nature, how well can we monitor and manage an active distribution network with the full utilization of network capacity by allowing temporary overloading? The combined effect of uncertainty in weather and local generation forecasting together with customer load forecasts needs to be translated to thermal state forecasts. Due to the inherent dependency of customer loads and local generation on the weather variables, it is logical to start with the relevant weather variable forecasts. The subsequent procedures up to the thermal state forecasts are presented in Fig. 43.

After the 24 hour ahead loadings of network components are evaluated from the deterministic power flow, the loadings will be input to the thermal model. Once the 24 hour loading of a network component, say an underground cable branch, is known, the dynamic thermal model starts calculating the conductor temperature at every hour for the next 24 hours. Hence, at every hour the model uses the previous hour's conductor temperature as the initial temperature and calculates the next hour temperature using the predicted next hour's loading from the power flow and the forecasted weather variables for the next hour.

The modeled and forecasted variables are the secondary substation loads, the ambient temperature, the wind speed, the solar irradiation and the ground soil temperature. The time series data for all the stated variables span from June 1, 2008 to May 31, 2009. The first 300 days are used to model the time series data and the last 65 days are used for validation. There is the assumption that the four variables are uncorrelated for the sake of simplicity. Nevertheless, for substation load forecasting, the dependencies of the loads on the previous day data series of ambient temperature and sunlight are included as exogenous variables, as shown in (3.8). To compute thermal state forecasts using the respective dynamic thermal models, the relevant forecasted variables are used. For the upper and lower prediction interval a knowledge based approach is used, where, except for the environmental variable wind speed, all the other variables affect the thermal state positively. Hence, the upper boundaries of environmental variables such as ambient temperature, solar irradiation and soil temperature are associated with the upper boundary of the thermal state forecast. Given 95% prediction intervals for the variables, the logic stated above gives a conservative boundary leading to a greater than 95% prediction interval for the thermal state forecasts. The actual values are values calculated from actual weather variable measurements and the component thermal models.

Table 12 *The Values of RMSE and Percentage of Time the Actual Thermal State Violated the Upper Boundary*

		RMSE	**% time upper boundary violation**
Overhead Line	Near DG (Line 14)	7.3645	2.05%
	Away from DG (Line 2)	3.6743	7.5%
Underground cable	Near DG (Line 12)	0.5472	0.78%
	Away from DG (Line 1)	0.0249	0.025%
Indoor transformer (at node 12)		3.69	2.72%
Prefabricated substation transformer (at node 1)		5.4176	0

As shown in Table 12, the thermal state of underground cables can be forecasted with better accuracy due to the predictable soil temperature and higher time constant of cables. For overhead lines, however, the error gets bigger due to its dependency on the wind speed, ambient temperature and solar irradiation, which themselves are stochastic and relatively difficult to forecast. The case for prefabricated substations is similar, where the error term gets higher than for indoor substation transformers due to direct exposure to the variation in ambient temperature. The actual and forecast temperatures of the four

components of the distribution network shown in Fig. 34 are plotted in Figs. 44-47. For the conductor and hotspot temperatures in Figs. 44-47, 'actual temperature' refers to temperature calculation based on actual consumption and weather data while 'forecasted temperature' refers to calculations based on forecasted load and weather data.

The underground cable supplying node 12 connects the wind turbine to the rest of the network, while the LV-connected PVs supply the local loads. Hence the thermal states for underground cable 12, in Fig. 45, show very light loading, except for the times when the wind turbines are generating.

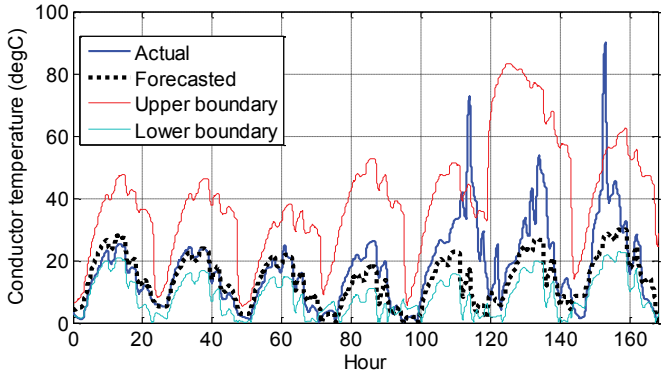

Fig. 44 *Overhead line 24-hour-ahead conductor temperature forecasts for one week (line connecting node 14, NTK#1)*

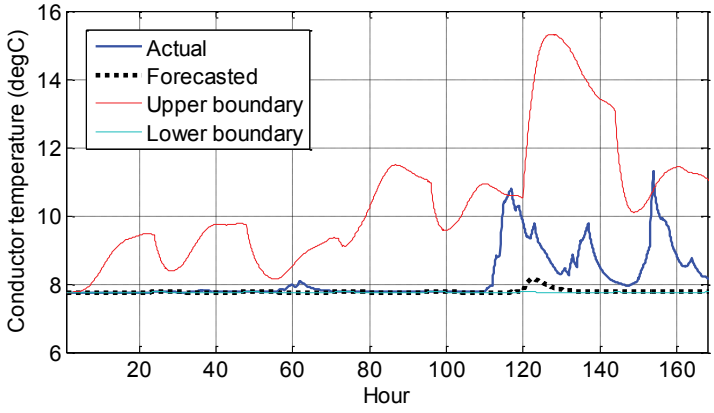

Fig. 45 *Underground cable 24-hour-ahead conductor temperature forecasts for one week (line connecting node 12, NTK#1)*

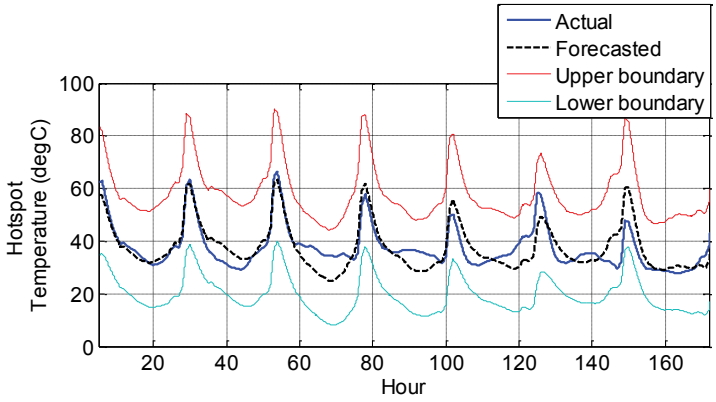

Fig. 46 *Prefabricated substation transformer 24-hour-ahead hotspot temperature forecasts for one week (substation at node 1, NTK#1)*

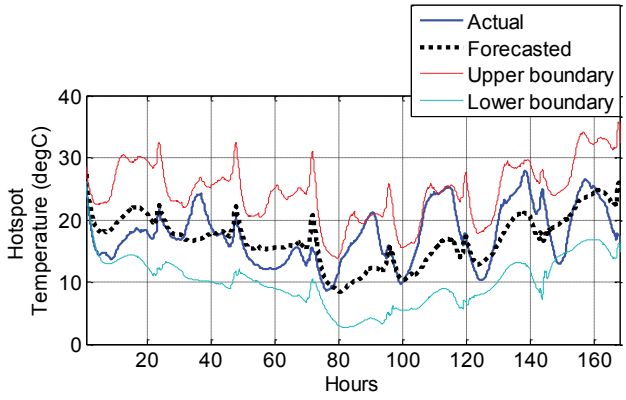

Fig. 47 *Indoor substation transformer 24-hour-ahead hotspot temperature forecasts for one week (substation at node 12, NTK#1)*

The 24-hour-ahead forecasting of network component's thermal state is highly inaccurate especially as the forecasting hours are longer as it can be seen in the violations of the confidence intervals in Figs 44 and 45. This volatility is essentially due to the errors associated with weather variable forecasts. Especially, as can be seen in conductor temperature of the overhead line connecting node 14 in Fig. 44, inaccuracies associated with wind speed forecasting are the main sources of errors. Nevertheless, at no times do conductor and hotspot temperatures violate the 95% confidence interval for three hour ahead forecasts in the analysis. The main sources of errors, environmental variables and distributed generation forecasts, are known to be forecasted with an acceptable predication interval for three hours ahead. In the presented analysis, by using the dynamic thermal models of components, it has been demonstrated that conductor and hot spot temperatures can be forecasted while reliably staying within the 95% confidence intervals for up to three hours ahead.

In this chapter load, weather variables and distributed generation forecasting methods were presented and discussed. More importantly, a method to use smart meter measurements of household level loads for substation load modelling and forecasting was evaluated. Utilizing the dynamic thermal models proposed in Chapter 2 and the forecasting techniques presented in this chapter, a framework for distribution network component thermal state estimation and forecast was proposed and evaluated in this chapter. The next chapter, tying up the methods developed in Chapters 2 and 3, will present a real-time thermal rating method for active distribution network. The benefit of the developed RTTR system is also weighed for its impact on the integration potential of DGs and their utilization for voltage control.

4 Formulating the RTTR algorithms

This chapter presents the RTTR frameworks and algorithms developed for an increased utilization and integration potential of DGs and for distribution system coordinated voltage control involving DGs. In addition, the test distribution network (NTK#2) utilized for CVC simulations is presented in the last section of this chapter. The framework in Section 4.2 targets to investigate the role of RTTR in alleviating network capacity problems and the framework in Section 4.3 mainly aims to relieve voltage problems in active distribution network. In the simulation of the framework presented in Section 4.2 the smaller test network (NTK#1) is utilized and the results are presented in Section 5.1. On the other hand, for the framework presented in 4.3, the relatively larger test network (NTK#2) is employed and the results are discussed in Section 5.2.

4.1 Real-time thermal rating

Static distribution system ratings are usually calculated assuming conservative weather conditions, for instance, for overhead lines, low wind speed conditions and high ambient temperature. The ratings are usually provided for the different seasons in a year. Besides ratings supplied by the over-head line manufacturer, distribution system operators use their own experience in either increasing or decreasing ratings depending on the operating environmental conditions. The loading guides of international standard organizations, such as IEC and IEEE, are the main guides for system operators. IEEE Std C57.91-2011, for instance, is one such loading guideline for oil-immersed transformers [17]. According to [17], a continuous hottest-spot temperature of 110 ºC can be handled with normal life expectancy. Emergency loadings of up to 200 ºC hottest-spot temperature can be applied; however this would incur a 1% loss of life per emergency if the emergency loading is maintained for 1 hour. Hence, in this dissertation dynamic thermal rating utilization is considered in real-time normal network operation where the compromise of loss of life is avoided.

Component thermal models, such as those explained in Chapter 2, are prerequisite for power system real-time thermal rating. The dynamic thermal models of the three major distribution network components are used to compute the system rating. These components are overhead lines, electric cables and power transformers. Except for cables buried inside unfilled conduit and secondary transformers installed in cabins, IEEE

standards are used to develop the thermal models. For cables inside unfilled conduit a suitable air-gap thermal model has been proposed by the authors in [Publication I]. A dynamic thermal model for prefabricated MV/LV substations, presented in [Publication II], is used for secondary substation transformer thermal ratings.

The component models can either be dynamic or static. The dynamic model involves time constants, which are functions of thermal resistances and capacitances emulating the transient responses. The time constant for overhead bare lines is very small, as the maximum possible hotspot steady state temperature for a given loading scenario shows up in the order of minutes. IEEE standard [63] is used for the thermal modeling of overhead lines and [17] is used for oil-immersed distribution transformers indoor installations. However, for underground cables installed inside buried air filled conduit, a seven loop dynamic thermal model is used, which has been developed by the authors in Aalto University, [Publication I] and [64]. The thermal-electric analogy circuits of the components are presented in Fig. 48.

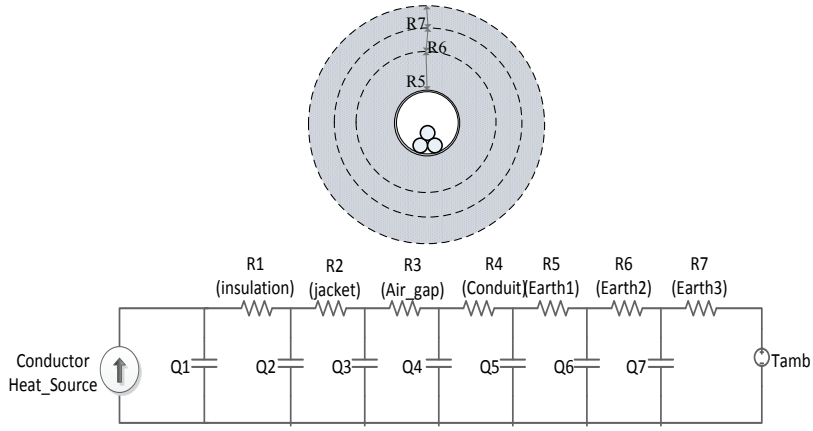

Fig. 48 *A seven loop thermal model for an underground cable inside an unfilled conduit*

By definition, a thermal time constant is the amount of time necessary for a particular body or system to change to 63.2% of the total difference between its initial and final body temperatures when it is subjected to a step change in load. The three components in a distribution system network have very different time constants, which can be translated as how fast the component responds to favorable or unfavorable environmental conditions. Components with high time constants reach the hotspot temperature increment corresponding to temporary overloading in the very far future. Besides, the future response of such components is strongly influenced by their past thermal-loading history. The advantage of a high time constant is the ability to handle high over loading followed by an extended period of normal loading. Contrary to that, low time constants have the advantage of fast response to favorable (cooling) environmental conditions, such as high wind speed for overhead bare lines. For transformers, the hotspot temperature time constant, which is the combination of winding and top oil time constant, is usually tens of

minutes, whereas for top oil temperature the time constant is in hours. The time constants for underground cables are the highest, giving the potential for temporary overloading, whereas for overhead lines the time constant is the lowest, giving the most opportunity when overloading and favorable environmental conditions are coinciding (see Fig. 49). All the thermal models are based on real-time ambient temperature and therefore measurements for the ambient temperature are assumed to be readily available.

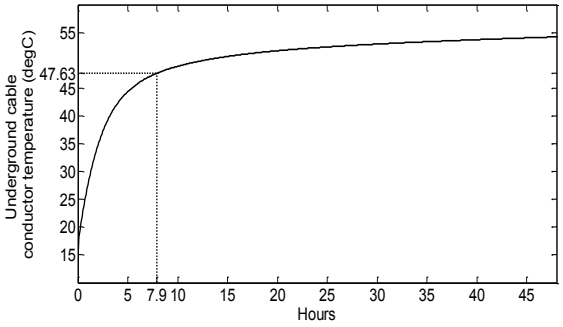

(a) Underground cable conductor temperature time constant 8 hours

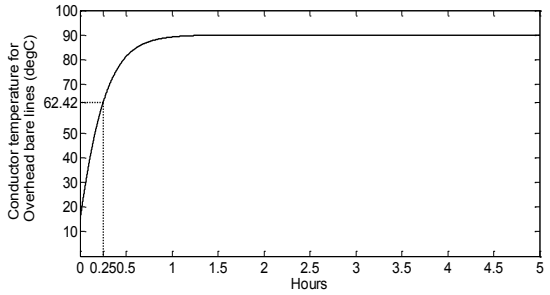

(b) Overhead bare line conductor temperature time constant 0.25 hours

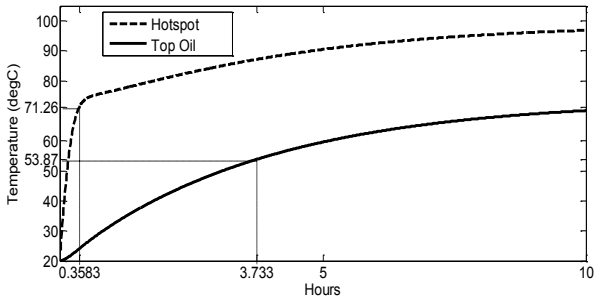

(c) Secondary substation transformer hot spot temperature time constant 0.358 and top oil temperature time constant 3.733 hours

Fig. 49 *Time constants of the typical distribution network components for rated step loading from cold start*

As requirements, the RTTR system needs measurements of ambient temperature, wind speed and solar irradiation at least at a single location at each primary substation. Nevertheless, weather measurements at the location of each component would significantly increase the accuracy of the system. Moreover, more intrusive measurements such as top oil temperatures of secondary substation transformers, cable and overhead line surface temperatures will increase the accuracy of the rating further. In this chapter, however, weather variable measurements at a single location at each primary substation are considered. The study of the impact of increased measurement points in the RTTR system accuracy is left for future works, and is mentioned in the 'Future Prospects' section.

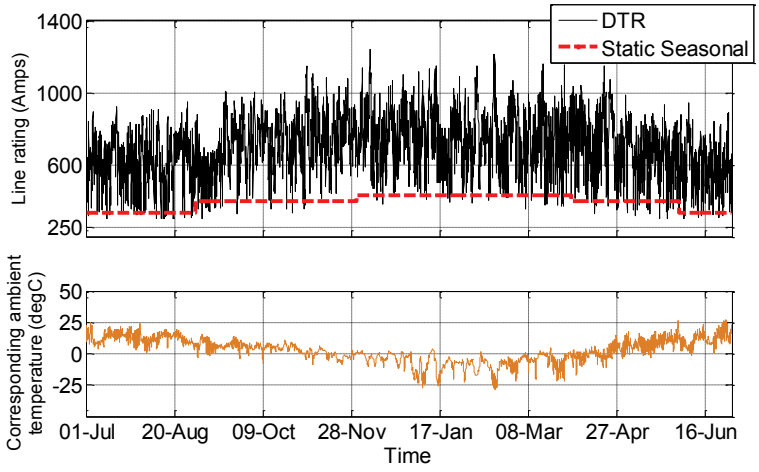

Fig. 50 *RTTR vs Static rating for overhead bare line (July, 2008 to June, 2009)*

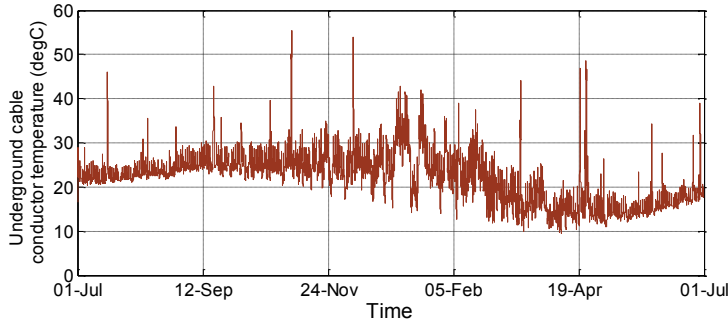

(a)

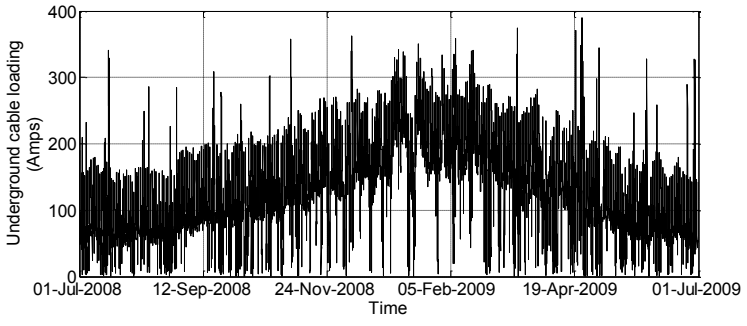

(b)

Fig. 51 *One year conductor temperature (a) and the corresponding hourly load profile (b) of an underground cable*

Based on hourly Finnish weather data, Fig. 50 shows the hourly rating of an overhead line with the parameters shown in Table 13. It is compared with seasonal static ratings. Fig. 51 shows the conductor temperature of an underground cable installed inside unfilled conduit and loaded with current moderately influenced by the stochasticity of distributed generation. For underground cables, the model takes measured ground temperature as a reference. The ground temperature where the distribution system is operating varies slowly from +5.5 ºC to +20.5 ºC annually, following a sinusoidal shape. This variation is also reflected on the conductor temperature of the underground cable. It is assumed that ground conditions are otherwise thermally stable, but where this is not acceptable, moisture migration can also be included, using methodology given in [65] and [66].

Table 13 *Line and Cable Parameters*

	Res (Ohms/m)	React (Ohms/m)	Rated Current (A)
Underground cable (240Wiski)	0.000138	0.00011	330
Overhead Line (Al132)	0.000279	0.000344	430

4.2 The RTTR framework for increased utilization of DGs

The optimal power flow (OPF) is a technique deployed in power systems to address problems ranging from economic dispatch to loss minimization [Publication III]. In this dissertation the OPF function utilizes the static rating or real-time thermal rating of the system to decide the permissible loads of network components. Whenever static rating or thermal violation is experienced, only curtailment of DGs or loads is considered as correction measures, as shown in the flow chart in Fig. 52. The objective for the OPF is to minimize the total cost of load and DG curtailment whenever ratings are exceeded. Within the scope of this work, only the potential that a dynamic thermal rating function brings to a distribution network has been shown, especially with regard to the increasing connection of distributed generation. Real-time network reconfiguration can also be an alternative remedy for network capacity violations, but is not considered in the presented framework.

Table 14 *Static loading thermal limits for decision making*

One Hour Maximum	OH (conductor)	UG (conductor)	TRAFO (hotspot)
Static Rating	430A	330A	1600kVA
Temperature	110ºC	90ºC	110ºC/120ºC

As shown in Fig. 52 there is a decision making step depending either on whether a thermal violation or static rating violation is detected. The logic behind the limit violation decision is given in Table 14. Since the loading scenario in this dissertation is hourly, the emergency limits of components with less than an hour loading limit are not an option. For oil immersed transformers, normal life expectancy occurs when a transformer is operating at 110 ºC continuously. The normal life expectancy IEEE loading guide also allows up to 120 ºC hotspot temperature and a corresponding 1.17pu loading for a short period during the day. Besides, according to the IEEE guide, a planned loading beyond the nameplate rating is allowed up to 130ºC hotspot temperature or 1.27pu loading [17]. In this analysis, however, the RTTR is chosen to operate within the normal life expectancy loading limit. Hence, a 110ºC limit is used during the comparison of 8 scenarios of DG penetrations (Table 14) and a 120ºC limit is used for the identification of substation loading and DG penetration limits.

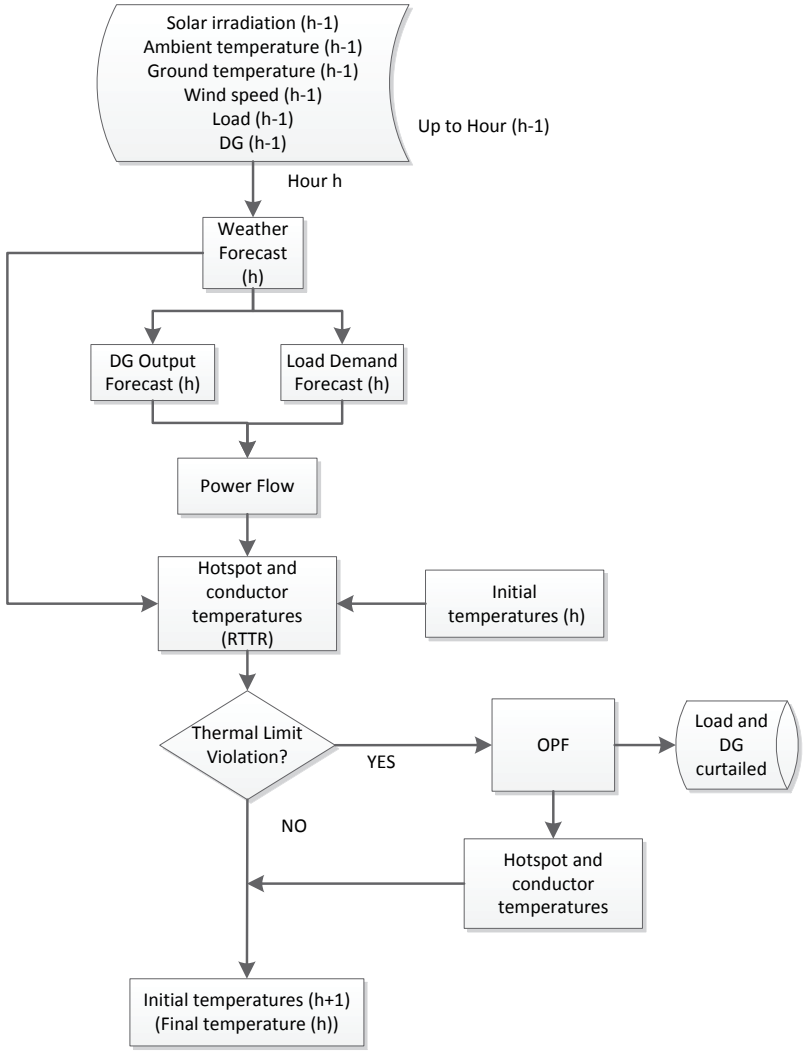

Fig. 52 *Real-time thermal rating framework for hour ahead dispatching*

The algorithm shown in Fig. 52 is applied for 8 scenarios over a period of one year for different levels of DG (see Table 15). As shown in Fig. 52, RTTR and a power flow are applied at every hour. Nevertheless, the OPF is called only when there is a thermal limit violation requiring corrective actions. As the primary substation transformer rating is 40MVA, it is used as the system capacity to decide the DG level. The solar panels are connected behind secondary substations whereas the wind turbines are connected to the MV network. The stressed network components (in test NTK#1) are: secondary substation transformer at node 1, overhead line Section 14 and underground cable section 12. The loadings and the respective thermal responses are analyzed for these components in the next section.

In the Finnish environment the solar panel yearly generation trend goes in the opposite direction to the actual consumption due to higher heating consumption in winter, which is also the darkest season. This trend is depicted in Fig. 53, showing the loading on transformer substation 12, where solar panels are connected to the LV side. The negative power implies solar panel generated power flowing to the MV network after fully supplying the local loads. Since our load measurements are AMR based with one hour resolution, the corresponding current loads on the line sections are also hourly, as shown in Fig. 54. Also shown in Fig. 54, the thermal violations in this dissertation were assessed by the real-time state of hotspot temperatures, not from steady state temperature.

Table 15 *DG prevalence scenarios for MV distribution network operating radially (NTK#1)*

	DG level (out of 40MVA)	DG Cumulative Maximum (MVA)	WIND			SOLAR		
			Node12 (Number of 50kW turbines)	Node14 (Number of 50kW turbines)	Total (kVA)	Node10 (Number of 215Wp solar panels)	Node12 (Number of 215Wp solar panels)	Total (kVA)
Scenario#1	0	0	0	0	0	0	0	0
Scenario#2	50%	20	107	285	19600	1017	1763	598
Scenario#3	100%	40	214	570	39200	2034	3525	1195
Scenario#4	110%	44	235	627	43120	2237	3878	1315
Scenario#5	120%	48	257	684	47040	2441	4231	1434
Scenario#6	150%	61	321	855	58800	3051	5288	1793
Scenario#7	200%	81	428	1140	78400	4068	7051	2391
Scenario#8	315%	127	675	1799	123676	6418	11125	3772

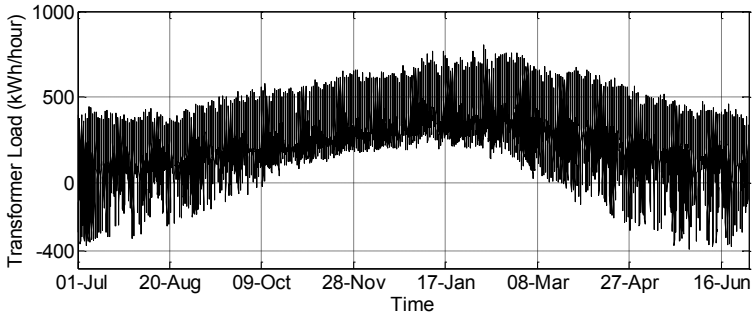

Fig. 53 *Secondary substation 12 transformer load for scenario#6 (July,2008 to June,2009) (negative power is associated with LV connected solar panels supplying power to MV network)*

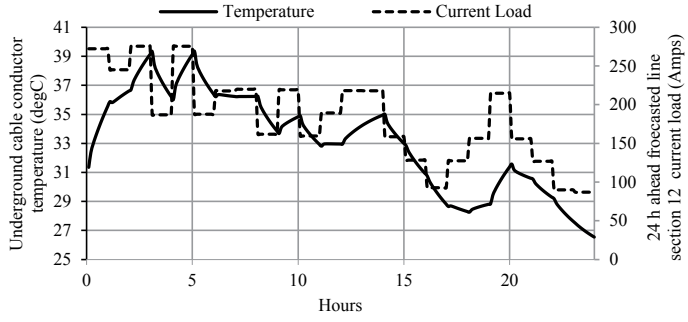

Fig. 54 *Line section 12 underground cable forecasted load and the corresponding conductor temperature for scenario#3*

4.2.1 OPF plus RTTR formulation

The optimization routine is called whenever violation in static or real-time thermal rating limits is detected. The choices considered to counter rating violations here are load curtailment and DG curtailment. An hourly NordPool market price is used as the cost of DG curtailment and an average cost is used for load curtailment, as presented in [67]. Hence the OPF tries to minimize the total cost of load and generation curtailments while keeping loadings under the limits of the specific hour. Real-time network reconfiguration is not realized in this work; however, it will be an interesting research topic combined with stochastic loading and real-time thermal ratings. On the other hand, network investment could also be considered as an alternative solution; nevertheless, provided that DG and load curtailment costs are quantified it will be a straightforward comparison to make. The formulation of the OPF is presented in (4.1).

$$\text{Minimize} \sum_{i} \left(\rho_{lc}^{i,t} P_{lc}^{i,t} + \rho_{gc}^{i,t} P_{lvgc}^{i,t} + \rho_{gc}^{i,t} P_{mvgc}^{i,t} \right) \tag{4.1}$$

where, t and i are indices for the time span and buses. ${\rho_{lc}}^{i,t}$ is the compensation cost for the curtailed load ${P_{lc}}^{i,t}$ and ${\rho_{gc}}^{i,t}$ is the compensation cost for the curtailed low voltage side generation (${P_{lvgc}}^{i,t}$) and medium voltage side generation (${P_{mvgc}}^{i,t}$) at time span t and bus i. The objective function (4.1) is subject to the following constraints:

$$P_f^{ij,t} = -Y_f^{ij} V_i^t V_j^t \cos(\delta_i^t - \delta_j^t + \theta_f^{ij}) + Y_f^{ij} {V_i^t}^2 \cos(\theta_f^{ij}) \tag{4.2}$$

$$Q_f^{ij,t} = -Y_f^{ij} V_i^t V_j^t \sin(\delta_i^t - \delta_j^t + \theta_f^{ij}) + Y_f^{ij} {V_i^t}^2 \sin(\theta_f^{ij}) \tag{4.3}$$

$$S_f^{ij,t} = \sqrt{{P_f^{ij,t}}^2 + {Q_f^{ij,t}}^2} \tag{4.4}$$

$$P_s^{i,t} = P_l^{i,t} - P_{lc}^{i,t} - P_{lvg}^{i,t} + P_{lvgc}^{i,t} \tag{4.5}$$

$$Q_s^{i,t} = Q_l^{i,t} - Q_{lc}^{i,t} - Q_{lvg}^{i,t} + Q_{lvgc}^{i,t} \tag{4.6}$$

$$S_s^{i,t} = \sqrt{{P_s^{i,t}}^2 + {Q_s^{i,t}}^2} \tag{4.7}$$

$$P_{mvg}^{i,t} - P_{mvgc}^{i,t} - P_s^{i,t} - \sum_j P_f^{ij,t} = 0 \tag{4.8}$$

$$Q_{mvg}^{i,t} - Q_{mvgc}^{i,t} - Q_s^{i,t} - \sum_j Q_f^{ij,t} = 0 \tag{4.9}$$

$$\underline{V_i} \le V_i^t \le \overline{V_i} \tag{4.10}$$

$$0 \le P_{lc}^{i,t} \le P_l^{i,t} \tag{4.11}$$

$$0 \le P_{lvgc}^{i,t} \le P_{lvg}^{i,t} \tag{4.12}$$

$$0 \le P_{mvgc}^{i,t} \le P_{mvg}^{i,t} \tag{4.13}$$

$$P_{lc}^{i,t} Q_l^{i,t} - Q_{lc}^{i,t} P_l^{i,t} = 0 \tag{4.14}$$

$$P_{lvgc}^{i,t} Q_{lvg}^{i,t} - Q_{lvgc}^{i,t} P_{lvg}^{i,t} = 0 \tag{4.15}$$

$$P_{mvgc}^{i,t} Q_{mvg}^{i,t} - Q_{mvgc}^{i,t} P_{mvg}^{i,t} = 0 \tag{4.16}$$

$$-S^{ij,t}_{f,Static} / S^{ij,t}_{f,RTTR} \leq S^{ij,t}_{f} \leq S^{ij,t}_{f,Static} / S^{ij,t}_{f,RTTR} \quad \textbf{(4.17)}$$

where f and j are indices for the feeders and buses. $P_l^{i,t}$ $\left(Q_l^{i,t}\right)$, $P_g^{i,t}$ $\left(Q_g^{i,t}\right)$, and $P_s^{i,t}$ $\left(Q_s^{i,t}\right)$ are the load, generation, and injected active (reactive) powers at time t and bus i. $P_{lvg}^{i,t}$ $\left(Q_{lvg}^{i,t}\right)$ and $P_{lvgc}^{i,t}$ $\left(Q_{lvgc}^{i,t}\right)$ are the LV side generation and curtailment of active (reactive) power. $P_{mvg}^{i,t}$ $\left(Q_{mvg}^{i,t}\right)$ and $P_{mvgc}^{i,t}$ $\left(Q_{mvgc}^{i,t}\right)$ are the MV side generation and curtailment of active(reactive) power. δ_t^i is the voltage angle and θ_f^{ij} is the power flow angle. V_i^t is the voltage magnitude at bus i and time t, respectively, whose limits are specified in (4.10), and $S_f^{ij,t}$ in (4.4) is the apparent power of feeder f between buses i and j at time t. $S^{ij,t}_{f,Static} / S^{ij,t}_{f,RTTR}$ stands for static rating and RTTR limits at time t. $P_s^{i,t}$, $Q_s^{i,t}$ and $S_s^{i,t}$ are the active, reactive and apparent powers injected at the bus. Finally, $P_f^{ij,t}$ $\left(Q_f^{ij,t}\right)$ is the active (reactive) power flowing at time t through feeder f connecting bus i to bus j. (4.2) and (4.3) calculate the active and reactive power flowing through the feeders. (4.4) calculates the apparent power flowing through the feeders. (4.5) and (4.6) calculates the active and reactive power absorbed from the buses. (4.7) calculates the apparent power absorbed from buses. (4.8) and (4.9) are the active and reactive power balance at the buses. (4.10) forces the voltage magnitudes at the buses to be within an acceptable range. (4.11) ensures that load curtailment at each bus is less than the total load at that bus. (4.12) and (4.13) ensure that the generation curtailment at each bus (low voltage and medium voltage) is less than the available generation at that bus (low voltage and medium voltage). (4.14)-(4.16) guarantee that the power factor remains the same after and before either load or generation curtailment. (4.17) guarantees that static rating and RTTR limits are not violated for feeder f at time t.

Although the formulation presented in (4.1) is general, a DC power flow is used in both pre-optimization load flow and the optimal power flow of the test case scenarios (see Fig. 52). A DC power flow is used for its computational simplicity. It should be noted that the accuracy of the DC power flow model is not of concern, since the focus in this section is on capacity limit violations (not under voltage). Besides, for the suburban test network utilized in this case, the difference between an AC and DC power flow has been checked to be trivial. In fact, the worst voltage drop in a year experienced by the test network one (NTK#1), which is laid out on area of 7 square km, is 5.5% of nominal value.

The real-time thermal rating is solved in MATLAB whereas the optimal power flow is solved by the General Algebraic Modeling System (GAMS).

The results attained using the framework formulated in this section is presented in Section 5.1. The next section discusses the RTTR framework for CVC in distribution systems.

4.3 The RTTR framework for CVC involving DGs

Among the various limiting factors inhibiting the further installations of DGs are feeder thermal capacity limits and the steady state voltage rise problem [68]. With regard to dealing with the voltage rise problem, reactive power contribution by distributed generation (DG) units is one of the most commonly proposed approaches [69]. Wind turbines, for instance, by virtue of the power electronic converters that come with them are able to control active and reactive power independently [70]. The voltage source inverter in PVs is also an interface enabling the control of reactive power. These non-dispatchable DGs, such as PV and wind, operate a significant fraction of their time much below their rated power, during which they can provide reactive power service. Nevertheless, the present grid codes does not allow distributed generation to participate in distribution network voltage control in any way [71]. Moreover, the currently used distribution network planning tools and procedures are not capable of taking active voltage control into account as discussed in [72]. Nevertheless, nowadays, reactive power control capability is required in many countries and it is also recommended by Finnish Energy Industries

There have been numerous studies solving optimization problems for coordinated voltage control in distribution systems. Some studies considered the coordination of only two voltage control methods, while others investigated all the available methods, including the reactive power control of DG units. For example the study in [73] presents a coordination of OLTC and Static-var-Compensators (SVC) in an unbalanced distribution system. The proposed approach is a two-stage decision making procedure, where in stage one, an optimization problem of loss minimization is solved and in stage two, the minimization of switching due to economic and technical considerations is solved. Nevertheless, in [73] the DG units have been assumed to operate with unity power factor; no reactive power supply is considered from the DG units. In the studies in [72] and [74], the authors presented a method to enable distribution system operators to integrate the voltage level management potential of DG units in their network operation and planning principles. The coordination between substation voltage and DG reactive power is claimed to be the least cost method in [72], which used statistical distribution planning to select voltage control strategy. In the statistical planning, one year load and production curves were used to conduct load flows, which can then be used to evaluate the costs of different control strategies [72]. Nevertheless, the rule-based procedures in [72] and [74] do not investigate the costs of the optimal coordination of different voltage control strategies.

Only a few studies (such as [75] and [76]) tackle the real-time management of voltage and thermal constraints local to DG connections. The decentralized approach in [75] aims to avoid extensive sensing and communications, where the thermal constraint is managed by setting a constant line capacity threshold that triggers the trimming of wind

generation if violated. A centralized management of thermal constraints, while inhibiting violation of voltage limits, is presented in [76] by employing remotely controlled switches to reduce the DG curtailment. The study claims that the additional degree of freedom provided by remotely controlled network switches leads to less DG curtailment. However, as in [75], in [76] the thermal limits of all lines are set to a constant value.

In practice, both the capacity threshold and DG generation fluctuates a lot, following weather variations in real-time. Hence, dynamic thermal rating is proposed in this thesis to manage the voltage level and network losses while the real-time line thermal limit is being respected in the constraint. In addition, in this thesis OLTCs, DG units and SVCs are coordinated in addressing the voltage and thermal constraints in an active distribution network.

The purpose of this manuscript is to provide a CVC strategy for the day-ahead operation of an active distribution network with updated network capacity using real-time thermal rating (RTTR). The CVC involves tap changing transformers, switchable static VAR compensators and DG units. The day-ahead control strategies use day-ahead forecasts of load, weather variables and DG generation. A voltage penalty function and network loss minimization objectives are compared in solving the CVC problem involving DG units.

This section presents the voltage control strategies utilized in this thesis and also assesses their effectiveness in today's active distribution network.

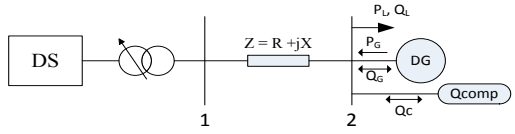

Fig. 55 *A simple illustration of Voltage dependency in a distribution network [68]*

There are two typical voltage level problems in distribution systems. The short-term problem, which lasts for not more than a minute; and the long-term problem, where the voltage level remains outside the $\pm 10\%$ limit for more than one minute. Over voltage and under voltage events require proper management that utilizes the dependencies of voltage and other variables, such as active and reactive load and generation as shown in Fig. 55 and (4.18). The voltage at busbar 2 in Fig. 55 can be approximated as:

$$V_2 \approx V_1 + \frac{R(P_G - P_L) + (\pm Q_G - Q_L \pm Q_C)X}{V_2} \quad \textbf{(4.18)}$$

where P_G and Q_G are local generations connected with local load P_L and Q_L . Q_C is supplied from a reactive compensator.

4.3.1 Distribution system voltage regulation devices

4.3.1.1 On-load Tap-changers (OLTCs)

An OLTC is a transformer component controlled automatically by a relay to increase or decrease voltage by altering the tap position of the transformer [77]. Usually, OLTCs operate following the connection point voltage level with a feedback control loop. In a CVC scheme, however, the operation of OLTCs might be needed for correcting voltage level problems elsewhere in the distribution network. The CVC scheme, therefore, needs to communicate the optimized set-points for the OLTCs. Nevertheless, the OLTCs might also need to take corrective actions for local contingencies without waiting for the centrally running optimization. Hence, an intelligent OLTC operating with two layers of control regimes, central and local, is the solution. This control scheme is presented briefly in Section 5.2.2. Nevertheless, in the test case, OLTCs receiving only centrally optimized set-points are considered.

The OLTCs are mainly installed in the HV/MV primary substation transformer. In this dissertation, the optimal placement or optimal OLTC installation problems are not discussed. However, with a given OLTC installation level and without further device investment, we attempt to improve the voltage variation through CVC involving DGs and an RTTR system.

4.3.1.2 Switchable static VAR compensation devices (SVC)

An SVC is a shunt-connected static var generator or sink whose output is adjusted to exchange capacitive or inductive current. Hence, SVCs are capable of either supplying or absorbing reactive power. The response time of SVCs is also fast enough to respond to transitional voltage fluctuations. In this dissertation, the SVCs comprise either thyristor-switched capacitors or reactors.

4.3.1.3 DG Reactive power control methods

The reactive power capability of DGs (wind turbines and solar PVs in this dissertation) originates from their inverter circuits connecting to the grid. Except for limiting the maximum reactive power intake or supply, the active power generated does not have an impact on the reactive power capacity of DGs, as formulated in (4.19). This fact enables solar PVs to be utilized in reactive power balance even during the night time where no generation is possible. The inverter apparent power rating, however, sets the absolute possible reactive power capacity, as shown in (4.19) and Fig. 56.

$$Q_{\max}(t) = \sqrt{S_{\max}{}^2 - P_{act}(t)^2} \quad \textbf{(4.19)}$$

where S_{max} (red line in Fig. 56) is the inverter apparent power rating, $P_{act}(t)$ is the actual active power generated by DG at time *t* (green line in Fig. 56) and $Q_{max}(t)$ is the corresponding maximum reactive power supply or intake capability.

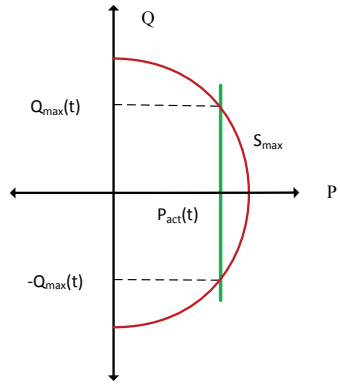

Fig. 56 *Inverter loading capability chart*

Standards such as IEEE 1547 do not currently allow active voltage regulation by DG inverters at the point of common coupling (PCC) to access the maximum amount of real power and to avoid unnecessary interaction among voltage controllers. Otherwise, there is no other technical limitation inhibiting the usage of the reactive power of DG units. Many inverters have the capability of providing reactive power to the grid. Inverters can also be oversized just to increase the capacity of their reactive power balance. In a highly resistive network, such as a low voltage distribution network, the voltage is more dependent on active power rather than reactive power. Conversely, when the reactance of a power system network is more significant than the resistance the voltage will be more sensitive to changes in reactive power. Hence, in the former scenario a P/V droop controller is recommended and in the latter case a Q/V droop controller would be more effective. DG control for voltage regulation involves either soft or hard curtailment. With hard curtailment, we disconnect the DG altogether. However, with soft curtailment either of the P/V or Q/V droop control methods can be utilized.

4.3.1.3.1 Q/V droop controller

This type of control is also called voltage dependent reactive power control. The DGs considered in this dissertation are PVs and wind turbines. The Q/V droop method does not need a source of real power for generating the necessary reactive power for compensation. Since the main objective of PV generators is to produce active power, their reactive power is limited to the maximum apparent capacity of the inverter.

$$Q = \begin{cases} \frac{V}{|V|} \cdot Q_{max},\ V < 0.9 \text{ or } V > 1.1 \\ 0,\ 1-D \le V \le 1+D \\ \frac{Q_{max}}{0.1-D}(-V+1+D),\ 1+D < V \le 1.1 \\ Q_{max}\left(\frac{-V+1-D}{0.1-D}\right),\ 0.9 \le V < 1-D \end{cases} \quad \textbf{(4.20)}$$

$$Q_{max} = \sqrt{S_{\max}{}^2 - P_{act}{}^2} \quad \textbf{(4.21)}$$

where S_{max} is the inverter apparent power rating, P_{act} is the actual active power generated by DG at time t and the deadband range setting value is D. The graphical presentation of (4.20) and (4.21) is presented in Fig. 57.

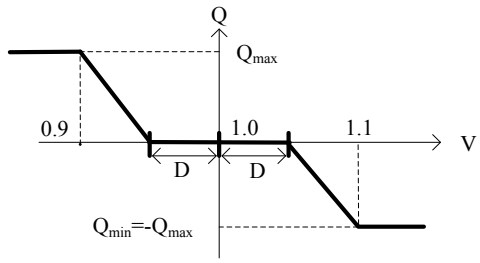

***Fig. 57** Q/V control with dead-band*

4.3.1.3.2 DG P/V droop controller

The P/V droop can be implemented with either soft curtailment in the case of dispachable DGs or disconnection of the DG altogether in the case of non-dipatchable DGs. The P/V droop controllers are effective in resistive networks. Both the P/V and Q/V-control could be a constant droop or with a dead-band. In this way, the DG units would only react to voltages that exceed a certain threshold voltage. In the P/V droop control, the DG units contribute to the load sharing depending on both their ratings (droops) and the line impedances. The P/V droop control strategy is based on the formulation shown in (4.22).

$$P_i = \begin{cases} P_{\max,i} - k_i\left(V_i - V_{crit,i}\right) \forall V_i \geq V_{crit,i} \\ P_{\max,i} \qquad\qquad\qquad\qquad \forall V_i < V_{crit,i} \end{cases} \tag{4.22}$$

where $V_{crit,i}$ is the voltage above which the power injected by the DG is decreased with the droop coefficient k_i and $P_{max,i}$ is the nominal power or the maximum power available by the DG. V_i and P_i are voltage level and DG output, respectively, at node i. The P/V droop equation in (4.22), hence, executes the active power curtailment required for keeping the bus voltage within an acceptable range. In this dissertation, the Q/V droop controller method with dead-band is used to control the reactive power supply or intake of DGs.

4.3.2 Optimal Day-Ahead CVC Formulation

The main goal of CVC in distribution networks is to compensate for the load and DG generation variations so that the customer supply voltages are kept within certain bounds. The utilization of DGs coordinating with static VAR compensators (SVCs) and OLTCs for voltage control can impose higher loading on the network. In other words, to tap the supply and absorption capacity of reactive power in a distribution system the lines and cables are required to cope with increased loading. The network loading capacity in a static rating regime, however, is heavily limited compared to real-time thermal rating.

The day-ahead CVC framework presented in Fig. 58 comprises weather variable and load forecasts. The DG output forecast is based on the weather variables while the component ratings depend on both the weather variables and forecasted loading. The errors in the forecasting will, in fact, be carried through to the CVC settings. Hence, evaluating the uncertainties in the control settings is also equally crucial. Besides, except for being the general day-ahead guideline for the voltage regulating devices, the optimal control settings from the proposed framework require updates within each day. In this dissertation, we mainly focus on providing optimal CVC set-points for day-ahead distribution network operation. The practical issues, such as communication, uncertainties and contingencies, are briefly discussed in Section 5.2.2 from the multi-agent system perspective.

In the optimal decision of set-points for CVC, the ratings of components such as lines and cables must be considered. However, these capacity limits could either be set based on static rating principles or real-time thermal rating methods. The incorporation of an RTTR system with CVC brings two main benefits: the first is the lower cost of operation of a facility involved in CVC and the second is a higher utilization and integration potential of DGs. The loss minimization objective is formulated from (4.23) to (4.31).

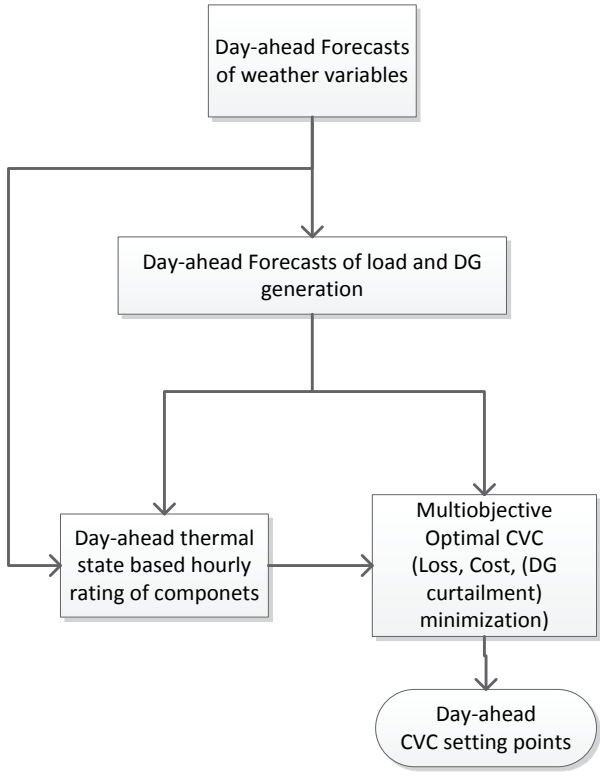

Fig. 58 *Three level CVC strategy procedure*

4.3.3 Objective functions

Defining an objective function to conduct voltage regulation and reduce losses is a challenge. For loss minimization, the reactive power flow along the branch is preferred to be zero (i.e. $Q_{ij} = 0$). Nevertheless, to maintain the voltage variation between buses i and j at a minimum, the reactive power flow is preferred to be equal to $-(r_{ij}/x_{ij}) \cdot P_{ij}$. In [78], it is suggested that a control scheme should be adaptable to easily allow for smooth transitions between emphases on voltage regulation and distribution losses. The minimizations of loss and penalty objective functions formulated in (4.23) and (4.24), respectively are compared in Section 5.

Loss minimization demonstrates the economic aspect while voltage deviation in the objective represents the technical limitations. The utilization of DG reactive power and impact of real-time thermal rating for CVC is the focal point of this study. Ultimately, however, advanced centralized optimal coordinated voltage controls are expected to be multi-objective, encompassing the following:

- Maintain voltage within permitted range and flatten voltage profile along feeders
- Minimize the sum of:
    - Energy losses
    - Curtailed DG energy
    - Operation (wear) of network components (OLTC, VR, SC etc.)
    - Reactive power flow through HV/MV transformer
    - Reactive power injection/absorption by DG

4.3.3.1 Loss minimization

The loss minimization objective is formulated in (4.23)

$$Min\, P_L = \frac{1}{2}\sum_{i=1}^{N}\sum_{\substack{j=1 \\ j\neq i}}^{N} g_{i,j}\left[V_i^2 + V_j^2 - 2V_iV_j\cos\left(\delta_i - \delta_j\right)\right] \quad \textbf{(4.23)}$$

where N is the total number of buses and g_k $(g_{i,j})$ is the conductance of branch k or the line connecting node i to j. V_i and V_j are the voltage magnitudes and δ_i and δ_j are the voltage angles for nodes i and j, respectively.

4.3.3.2 Voltage penalty function objective

In addition to the loss minimization objective defined in (4.23), a penalty function for the voltage exceeding a certain threshold can be defined as in (4.24).

$$W_i = \begin{cases} k\left(V_{imin} - V_i\right)^2; & V_i < V_{imin} \\ 0; & V_{imin} \le V_i \le V_{imax} \\ k\left(V_i - V_{imax}\right)^2; & V_i > V_{imax} \end{cases} \quad \textbf{(4.24)}$$

where k is the penalty factor.

The objective function in (4.24), also drawn in Fig. 59, can be used when voltage variation is more of an issue than overall distribution network losses. In Section 5.2, the minimizations of loss and penalty objective functions are compared.

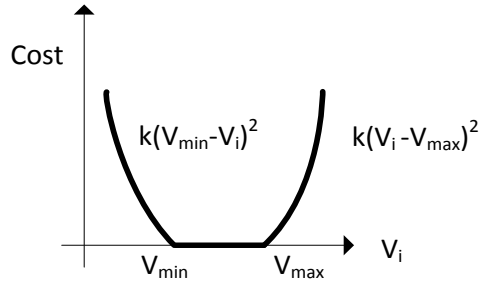

Fig. 59 *Voltage penalty function*

4.3.3.3 The equality constraints:

$$-P_{DGi} + P_{Di} + |V_i| \sum_{j=1}^{N} |V_j| \left(G_{ij} \cos\left(\theta_{ij}\right) + B_{ij} \sin\left(\theta_{ij}\right) \right) = 0 \quad i = 1, \ldots, N \quad \textbf{(4.25)}$$

$$-Q_{Ci} - Q_{DGi} + Q_{Di} + |V_i| \sum_{j=1}^{N} |V_j| \left(G_{ij} \sin\left(\theta_{ij}\right) - B_{ij} \cos\left(\theta_{ij}\right) \right) = 0 \quad i = 1, \ldots, N \quad \textbf{(4.26)}$$

$$Q_{DGi} = \begin{cases} \dfrac{V_i}{|V_i|} P_{DGi} \cdot \tan\left(a\cos\left(PF_{\lim}\right)\right), & V_i < 0.9 \; or \; V_i > 1.1 \\ 0, & 1 - D \le V_i \le 1 + D \\ \dfrac{P_{DGi} \cdot \tan\left(a\cos\left(PF_{\lim}\right)\right)}{0.1 - D} \left(-V_i + 1 + D\right), & 1 + D < V_i \le 1.1 \\ P_{DGi} \cdot \tan\left(a\cos\left(PF_{\lim}\right)\right) \left(\dfrac{-V_i + 1 - D}{0.1 - D} \right), & 0.9 \le V_i < 1 - D \end{cases} \quad \textbf{(4.27)}$$

where $\theta_{ij} = \delta_i - \delta_j$ is the voltage angle difference between connected buses i and j. Q_{DGi} is the reactive power supplied or absorbed by the DG connected to bus i.

4.3.3.4 Inequality constraints:

$$V_{imin} \le V_i \le V_{imax}, \; i = 1, \ldots, N, \quad \textbf{(4.28)}$$

$$Q_{DG_i min} \le Q_{DG_i} \le Q_{DG_i max}, \quad \forall i \in N_{DG_q} \quad \textbf{(4.29)}$$

$$Q_{C_i min} \le Q_{C_i} \le Q_{C_i max}, \quad \forall i \in N_{C_q} \quad \textbf{(4.30)}$$

$$a_{kmin_i} \le a_{k_i} \le a_{k\max_i} \quad \forall i \in N_{OLTC} \quad \textbf{(4.31)}$$

$$\left|S_{ij}\right| \le S_{ij,max} \quad \textbf{(4.32)}$$

where (4.25) and (4.26) calculate the active and reactive power injections at bus i respectively. The network admittance matrix is given by $Y_{ij} = G_{ij} + i \cdot B_{ij}$. (4.25) sets the DG reactive power supply following the Q/V droop characteristics, (4.28) limits the

upper and lower voltage magnitude at bus *i*, (4.29) sets the limits for the DG reactive power at bus *i*, (4.30) limits the reactive power supply from the SVCs, (4.31) gives the range of OLTC set-points and (4.32) gives the real-time dynamic thermal rating or static rating of branch *ij*. N_{DG_q}, N_{C_q} and N_{OLTC} are the sets of all DGs, SVCs and OLTCs connected at bus i, respectively.

$S_{ij,max}$ is the capacity of the line or cable, which is calculated using the dynamic thermal models of the overhead lines and underground cables. The previous hour optimal loading of the branch is used to attain the initial conductor temperature for calculating the coming hour's line or cable rating. Hence, the iteration between the OPF with CVC and the RTTR is established. Due to the nonlinearity of power systems, linear programming loses accuracy due to linear assumptions [79]. Hence, the OPF is solved using the nonlinear IPOPT solver of the General Algebraic Modeling System (GAMS) while the RTTR has been implemented in MATLAB [80]. For numerical efficiency within the power flow or the OPF solution, all discrete variables (transformer taps and shunt steps) are treated as continuous until the optimal solution is found. Then they are rounded off to their nearest discrete values.

The day-ahead dynamic thermal rating of the distribution network components in Fig. 58 is attained from the load and weather variable forecasts input into the dynamic thermal models of the components. The day-ahead dynamic thermal rating procedure is presented in [Publication V]. The iterative implementation of the RTTR framework is illustrated in Fig. 60. In the optimization problem defined in (4.23)-(4.32), the control variables are the reactive power of DGs (Q_{DGi}), the reactive power of SVCs (Q_{Ci}) and the tap set-point (a_k). The state variables, on the other hand, are the bus voltage magnitude and angle, while the line load flows are output variables.

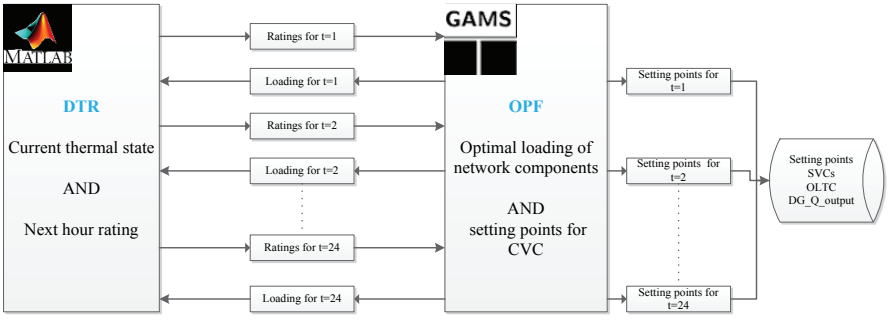

Fig. 60 *The implementation of the RTTR framework*

The results obtained by using the framework developed in this section for distribution systems CVC is presented in Section 5.2.

4.4 The test distribution network (NTK#2)

For the test case, a Greenfield distribution network plan based on actual loading data and geographical location is used, as shown in Fig. 61. In the single line network diagram the green lines represent MV underground cables while the red lines are overhead. The test distribution network has 146 secondary 20/0.4 kV substations and a 110/20 kV primary substation.

The distribution network has voltage regulating devices, OLTCs and SVCs, installed at different locations. Besides, wind turbines are installed at 4 locations and solar panels are installed at 3 locations. The network also has a mix of underground cables and overhead lines. The research investigated various formulations of the CVC problem for day-ahead distribution network operation. The alternative solutions studied are the involvement of DGs in supplying or absorbing reactive power through the CVC scheme and the implementation of a real-time thermal rating system.

In the test network, the secondary substation one day loading is selected randomly from a pool of hourly AMR meter measurements from actual households. The random selection considers the data pool to be uniformly distributed. The respective reactive power loads are calculated to correspond to the residential loading power factor range of 0.955 to 0.98.

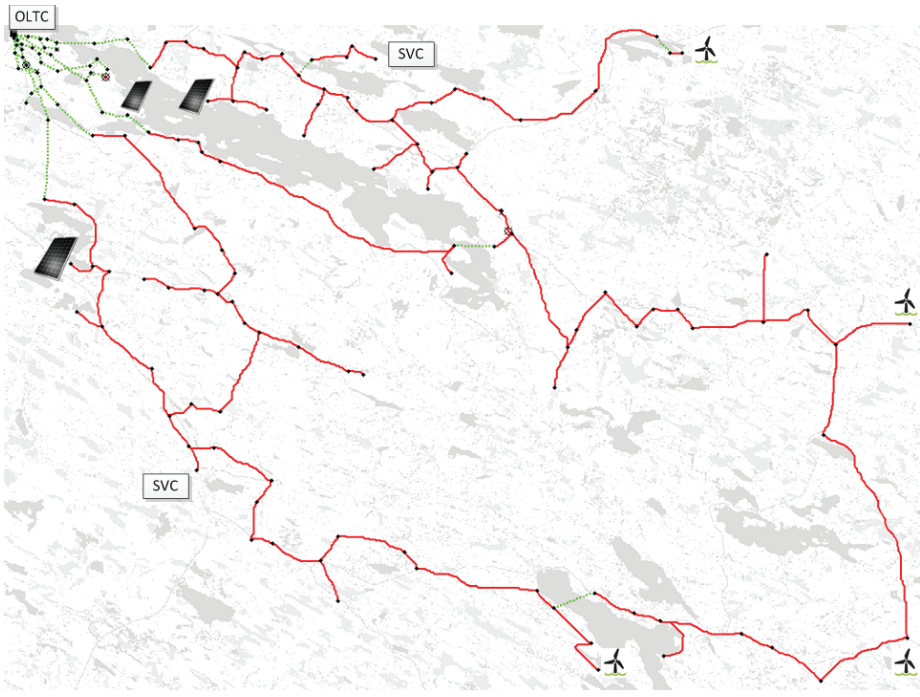

Fig. 61 *Greenfield network plan based on actual loading data and geographical location [66]*

The full parameters of test network two (NTK#2), including the location and ratings of DGs, are presented in the appendix (Table A1 and Table A2).

5 Results and discussions

The two main results of this dissertation are summarized in this chapter. The first is the development of real-time thermal rating program for increased utilization and integration potential of distributed generation in distribution systems. The second is the utilization of DGs in a coordinated voltage control framework for distribution systems involving RTTR based distribution network operation planning. The results presented in Section 5.1 are obtained by using the method developed in Section 4.2 and the test network presented in Section 3.3 (NTK#1). Conversely, the results presented in Section 5.2 are attained by using the framework formulated in Section 4.2 and the test network presented in Section 4.4 (NTK#2).

5.1 Role of RTTR in increasing the utilization of DGs

For the static rating a constant current limit is set, where the steady state temperature of the conductor, in the case of overhead lines and cables, and the hotspot temperature in the case of transformers are set to their maximum according to manufacturers' datasheets. However, in RTTR, the conductor and hotspot temperature are monitored based on thermal models to decide loading limits. Therefore, in static rating constant loading limits (at least seasonal limits) are used whereas in RTTR time varying loading limits are set. Hence, the overall loading capacity increment, for example, of overhead lines is tightly linked to the ambient temperature, wind speed and solar irradiation. In Finnish weather conditions for a 20kV bare overhead line, about 58% more delivered energy in one year would be possible in the case of real-time thermal rating rather than static rating (see Fig. 50). For underground cables, however, the time constant is too long to react to instantaneous loading and DG output profile. Hence temporary overloading, especially in the case of contingencies, is viable as long as it is followed by an extended period of low loading. Transformers lie somewhere in between, where whether it is installed inside a room or in the outside environment influences the real-time thermal rating. In this dissertation, an indoor installation is considered since our test network is for a sub-urban area. Hence, the real-time thermal rating for transformers focuses more on overseeing upcoming thermal violations than setting the maximum hourly load limit for the next 24 hours.

A 110°C limit for each secondary substation transformer is used during the comparison of the eight scenarios of DG penetrations (Table 16, Figs 59 and 60) and a 120°C limit is used for the identification of substation loading and DG penetration limits (Table 17, Table 18).

Usually, it is not probable that the best DG installation area will be near highly populated loads, especially in the case of wind turbines. In the test network the most congested line section is the overhead line section 14. It supplies the wind turbine generations connected to the MV side. In the case of RTTR implementation, there is no major overloading up to a 120% penetration level of DGs in the network. However, for static rating the expected energy not served is remarkably high at only a 100% penetration level. Underground cable line section 16 shows 2.5 times more unserved energy in the case of static rating rather than RTTR. Although for most line sections in the distribution network loading has decreased with the increasing penetration level of DGs, those components near to DG installations experience highly volatile loading and even increased temporary overloading. Assuming more DGs are to be installed in the already selected favorable area, RTTR can defer network investment by allowing 10-20% more DG penetration than the static rating can handle. This can be realized by installing RTTR capability, which increases DG installation potential before the need for additional network investment. Also, for the installed DG, the efficient utilization of the generated renewable energy increases by the same percent. This can be achieved with negligible loss of life (see Table 16 and Fig. 62). Nevertheless, there is also mechanical stress imposed by highly stochastic loading on network components. This issue needs to be investigated, especially for termination points and joints in high and medium voltage underground line sections connecting wind turbines [81]. In Table 16, the cumulative DG unserved energy in the distribution network is presented. The unserved energy is calculated by solving the OPF model, which was described and formulated earlier.

The differences between the secondary substations in Tables 17 and 18 are due to the types of households connected, which affect the load factor and shape very distinctly based on their proportions in Table 7 (NTK#1). Without installation of DGs, the loads are increased starting from the existing annual peak load up to the static rating and RTTR limits. According to the results in Table 17, on average RTTR has a 48% greater loading possibility of the existing load compared to the static rating limits. In an additional analysis, keeping the existing load constant, the penetration of DGs (solar panels) under each secondary substation was increased up to the secondary substation transformer static rating and RTTR limit as shown in Table 18. In general there is higher potential for connecting more DGs than the potential of load increment, as can be seen in Tables 17 and 18. When we look into hourly annual peak distributed generation and load demand, even if they have the same per-unit values, the historical and future generation or load have very distinct profiles. The stochasticity in distributed generation helps the RTTR

since the occasional spikes in generation usually occur for only a very short period compared to the time constants of the components, as shown in Table 18. RTTR allows a margin of approximately 40% more capacity compared to static ratings, for both additional loading and DG integrations, as the results in Tables 17 and 18 show.

Table 16 *Comparison of real-time thermal rating and static rating for different penetration levels of DGs*

DG scenario	Number of hours in year		Undelivered energy STATIC rating (MWh)		Undelivered energy RTTR (MWh)	
	Violations of Static Rating	Violations of RTTR	Load Curtailed	DG Curtailed	Load Curtailed	DG Curtailed
Scenario#1	0	0	0	0	0	0
Scenario#2	54	0	0	77.65	0	0
Scenario#3	430	191	0	2243.73	0	969.97
Scenario#4	433	258	0	2993.36	0	1434.80
Scenario#5	603	294	0	3858.65	0	1972.13
Scenario#6	618	440	0	6881.58	0	4046.98
Scenario#7	893	624	0	13111.73	0	8822.90
Scenario#8	1295	1087	0	31224.89	0	23594.88

* The scenarios are explained in Table 14

Table 17 *Percentage of load increment up to the static and RTTR rating limits for the 16 secondary substations*

Substation Number	Annual peak demand (pu)	% of Additional Load Increment Limits		
		Static Rating (1.17pu)	RTTR (120 ºC)	Difference
SUB#1	1.2	Overloaded	10.00%	10.00%
SUB#2	0.970	20.64%	40.00%	19.36%
SUB#3	0.635	84.33%	100.00%	15.67%
SUB#4	0.839	39.50%	60.00%	20.50%
SUB#5	0.317	269.46%	310.00%	40.54%
SUB#6	0.760	53.89%	70.00%	16.11%
SUB#7	0.810	44.42%	60.00%	15.58%
SUB#8	0.578	102.41%	170.00%	67.59%
SUB#9	0.533	119.69%	150.00%	30.31%
SUB#10	0.415	181.84%	230.00%	48.16%
SUB#11	0.322	262.86%	530.00%	267.14%
SUB#12	0.503	132.75%	170.00%	37.25%
SUB#13	0.283	312.70%	400.00%	87.30%
SUB#14	0.382	206.57%	260.00%	53.43%
SUB#15	0.480	143.93%	170.00%	26.07%
SUB#16	0.371	215.53%	240.00%	24.47%

From the presented values in Tables 16 and 17, it is apparent that wind turbines connected to overhead lines will benefit the utmost from the loading capacity unleashed by the RTTR framework. On the other hand, solar panels connected to underground cables will be less restricted by capacity limits than when they are connected to overhead lines. This is due to the positive correlation of overhead lines' capacity with wind speed and due to the negative correlation with solar irradiation. Hence, the impact of the RTTR system would surely be affected by the location of DG in the network. While our simulation

showcases the scenario for a determined test network, one can further study the optimal locating of DG considering the incorporation of the RTTR system.

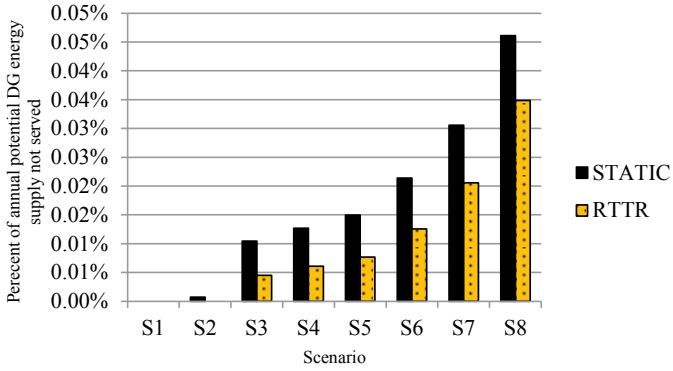

Fig. 62 *Unserved DG generation due to capacity limit with RTTR and Static rating*

Table 18 *Percentage of DG increment up to the static and RTTR rating limits for the 16 secondary substations*

Substation number	Percentage of Solar panel installment compared to the peak load connected to each secondary substation			
	Annual peak demand (pu)	Static Rating (1.17pu)	RTTR (120 ºC)	Difference
SUB#1	1.2	90.00%	170.00%	80.00%
SUB#2	0.970	130.00%	150.00%	20.00%
SUB#3	0.635	200.00%	230.00%	30.00%
SUB#4	0.839	150.00%	170.00%	20.00%
SUB#5	0.317	390.00%	440.00%	50.00%
SUB#6	0.760	170.00%	240.00%	70.00%
SUB#7	0.810	160.00%	180.00%	20.00%
SUB#8	0.578	220.00%	300.00%	80.00%
SUB#9	0.533	240.00%	270.00%	30.00%
SUB#10	0.415	300.00%	340.00%	40.00%
SUB#11	0.322	370.00%	420.00%	50.00%
SUB#12	0.503	250.00%	280.00%	30.00%
SUB#13	0.283	430.00%	490.00%	60.00%
SUB#14	0.382	320.00%	370.00%	50.00%
SUB#15	0.480	260.00%	340.00%	80.00%
SUB#16	0.371	330.00%	380.00%	50.00%

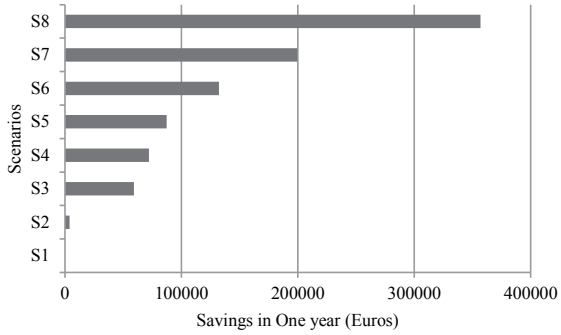

Fig. 63 *One year cumulative cost savings of curtailed load and DG generation for RTTR system compared to static rating system*

The objective function in (4.1) calculates the total cost of load curtailment using average cost and the cost of DG curtailment based on the Nordpool hourly spot price. Comparing the total yearly costs for the RTTR and static rating systems, the saved cost is plotted in Fig. 63. The monetary benefit of RTTR increases exponentially with the penetration level of DGs, as shown in Fig. 63. The extra network capacity released by the RTTR system has also some indirect impacts on aspects of distribution network operation, such as the dispatch of resources and network reconfiguration, as well as planning aspects such as postponing investments. Hence, an overall economic analysis would be a valuable future research topic in its own right.

With regard to the practical deployment of the RTTR system, measurement sensor installation and existing distribution management system (DMS) system compatibility are needed. In [5], it is mentioned that EPRI's dynamic thermal circuit rating program will run on a PC that is networked to the SCADA/DMS system where the required measurements are accessed. A field trial thermal controller installed on a Scottish distribution network deployed relays to collect weather data such as wind speed and direction, ambient temperature, soil temperature, soil moisture and solar irradiation [11]. For the RTTR system to be used for real-time network reconfiguration or DG control, a high resolution of such weather data has to be communicated with the RTTR system hosting computer. Also, to implement and harness the benefits of the above control strategies based on real-time thermal rating for smart distribution networks, reliable communication infrastructures are needed, as is pointed out in [82]. Conditional to the quality of the available measurements, there is a need for thermal state estimation programs to be integrated with active distribution network state estimation algorithms. According to the practical experiences of companies attempting to develop the RTTR systems, certain criteria have to be fulfilled before RTTR solution will be considered by utilities. RTTR solutions are considered when demand is not exceeding the firm capacity of the asset, the demand is correlated with seasonal temperature and there is some uncertainty of the evolution of the demand over time.

5.2 Role of RTTR for CVC

The forecasts of the day-ahead load and weather variables are used to compute the optimal CVC set-points for day-ahead network operation. The forecasting methods are presented in Chapter 3. The day-ahead dynamic thermal ratings and weather and load forecasting procedures utilized in this dissertation are also presented in [Publication V]. The coordinated voltage control framework involving RTTR method and utilizing reactive power potential of DGs is formulated and presented in Section 4.3.

By definition, the DG penetration level in a system is the ratio of gross annual energy generated by the DG to the total annual energy demand in the system. In this dissertation DG penetration levels of 1.13%, 11.3%, 22.6% and 65% are investigated. The installed DGs, however, are not evenly distributed throughout the network; rather, only the installed capacities are varied at their respective fixed geographical locations, as shown in Fig. 61.

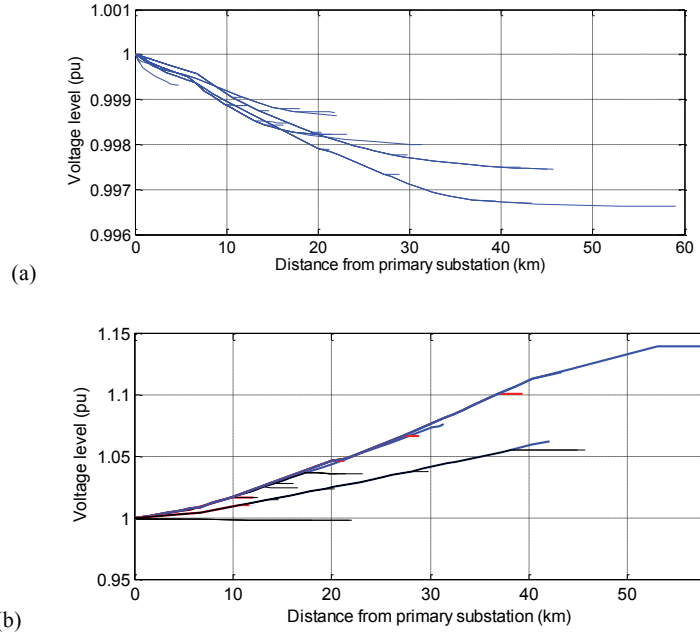

Fig. 64 *Daily average voltage levels of buses on the 30 feeders radiating from the primary substation for the test distribution network without DG (a) and with 65% DG penetration (b) (in (b) the blue feeders are connected with wind turbines and the red feeders are connected with solar panels). In both (a) and (b), there is no CVC applied*

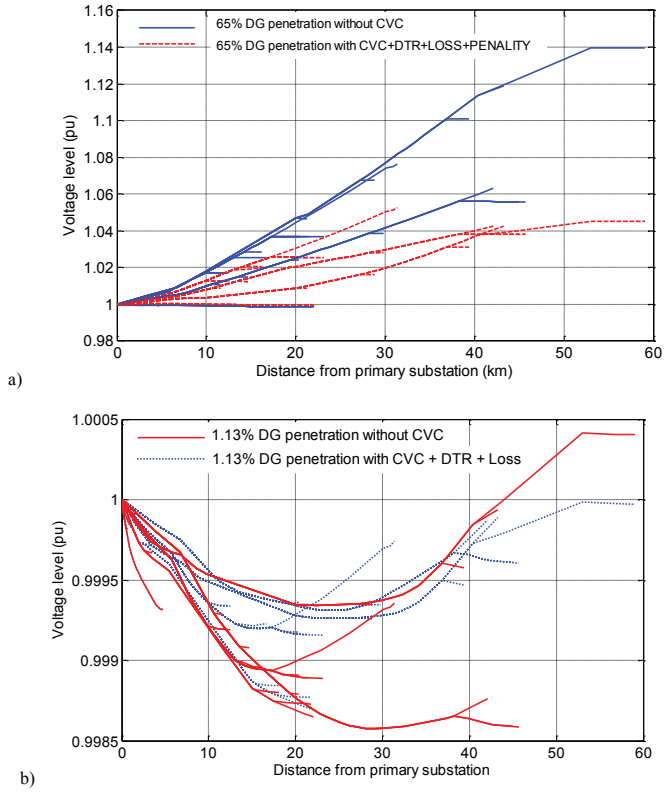

Fig. 65 *An average day-ahead voltage level profile of the secondary substations on the 30 feeders with and without the implementation of CVC. (a) shows the profile with 65% of DG penetration and (b) shows the result with 1.13% DG penetration level.*

There are around 30 radial feeders connected to the primary substation, of which the longest line is 60 km. Details of the test distribution network are provided in Tables A1 and A2 in the Appendix. In Fig. 64, the bus voltages of the feeder starting from the primary substation are plotted for a network without DGs and a network with 65% penetration of DGs. There is no CVC applied in the case shown in Fig. 64 and the voltage levels are the average of the 24 hour voltage levels. The test distribution network without DG integration (see Fig. 64a) has 2.4% higher losses on the selected day than the DG integrated test network (see Fig. 64b) with a 65% DG penetration level. In Fig. 65, the substation voltage level on the 30 feeders of the test network is plotted before and after the CVC is applied. Fig. 65a shows the case for a 65% DG penetration level while Fig. 65b shows the case for 1.11% DG penetration. The CVC corrects both the overvoltages caused by DG connected at the end of radial feeder and undervoltages due to long distances from the primary substation. From Fig. 65 it is also apparent that the two-third rule [83] for SVC placement on a radial feeder does not apply in the test network, where the DGs are scattered at the ends of the feeders.

5.2.1 Simulation results

In this dissertation, the day-ahead model predictive CVC strategy is applied on the test distribution network (NTK#2) by varying the CVC objective functions and the network rating types. The results in Table 19 compare the six types of CVC formulation, involving DGs at 1.13% penetration level with DG curtailment, and at 11.3% and 22.6% penetration level, with and without DG curtailment. Table 19 presents the overall network losses after applying the control set-points for a period of 24 hours. Besides, the number of OLTC and SVC operations per day, and the cumulative reactive power supplied by DGs and SVCs are presented. The lowest network losses are attained, as expected, for a CVC formulation where loss minimization is the objective. Apparently there is no difference between static and dynamic rating when loss minimization is the only objective as RTTR does not directly reduce losses. Nevertheless, the DG soft curtailment is too high when voltage loss minimization is the objective. RTTR shows a clear advantage over static rating in terms of maximizing the utilization of the DGs, while SVCs are effective for voltage control and reducing the stress on OLTCs. However, the greater utilization of active power generation from the DGs came with a slight increment in losses. A voltage penalty function can minimize the voltage burden on the customer. As shown in Fig. 66, the static and RTTR ratings coupled with both the voltage penalty function and loss minimization gave the voltage level closest to the nominal. RTTR, therefore, enables the proper utilization of resources for CVC, where a superior benefit can be attained by using RTTR coupled with the penalty function and loss minimization objectives.

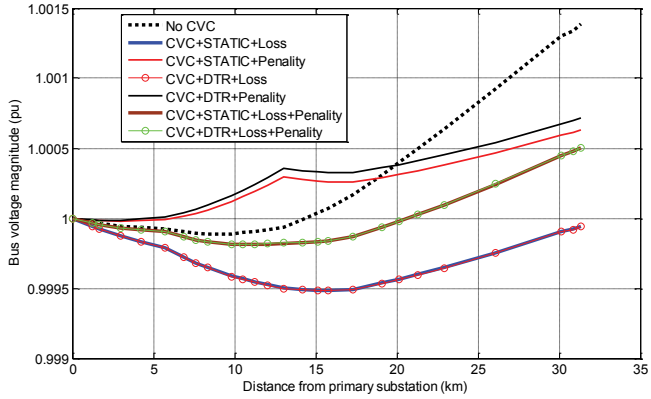

Fig. 66 *Voltage level at hour 4:00 on feeder 10 where a wind turbine is connected at the furthest node. The DG penetration level is 1.13% and the CVC involves DG curtailment*

Table 19 *Evaluation of the CVC formulation techniques for the period of 24 hour ahead implementation*

No.	Specification (Objective and Rating)	DG Penetration	DG Curtailment	Loss (kWh)	Max. V_{dev}* (%)	No. of OLTC opera'n	No. of SVC oper'n	DG Qgen. (MVARh)	DG Pgen Curtailed (%)	SVC Qgen. (MVARh)
1	Obj: Loss & Rating: Static	1.13%	YES	25.6	0.14%	0	0	2.439	31.63%	0.856
		1.13%	NO	34.5	0.14%	0	0	1.016	0%	0.994
		11.3%	YES	23.0	0.14%	0	0	1.459	90.39%	0.946
		11.3%	NO	2610.7	0.91%	0	12	-36.455	0%	7.521
		22.6%	YES	22.8	0.14%	0	0	1.457	94.97%	0.946
		22.6%	NO	10352.5	1.83%	0	27	-73.620	0%	15.146
2	Obj: Loss & Rating: RTTR	1.13%	YES	25.6	0.14%	0	0	2.438	31.64%	0.858
		1.13%	NO	34.5	0.14%	0	0	1.017	0%	0.991
		11.3%	YES	23.0	0.14%	0	0	1.459	90.39%	0.947
		11.3%	NO	2609.6	0.89%	0	10	-36.161	0%	6.584
		22.6%	YES	22.831	0.14%	0	0	1.454	94.97%	0.954
		22.6%	NO	10352.5	1.83%	0	25	-73.620	0.00%	15.147
3	Obj: Penalty & Rating: Static	1.13%	YES	47.9	0.24%	11	1	-1.506	2.27%	9.866
		1.13%	NO	55.8	0.28%	9	2	-2.185	0%	11.915
		11.3%	YES	2981.9	3.56%	10	20	-48.952	0.69%	50.989
		11.3%	NO	3261.6	3.56%	16	31	-50.713	0%	56.733
		22.6%	YES	10798.6	1.86%	16	31	-87.857	0.12%	63.214
		22.6%	NO	11502.7	3.88%	17	32	-92.136	0%	78.740
4	Obj: Penalty & Rating: RTTR	1.13%	YES	49.8	0.21%	5	0	-1.647	2.10%	10.292
		1.13%	NO	57.0	0.29%	13	0	-2.296	0%	12.351
		11.3%	YES	2926.5	1.94%	13	19	-49.411	1.39%	53.125
		11.3%	NO	3041.3	2.54%	12	27	-48.449	0%	48.768
		22.6%	YES	10867	1.92%	7	22	-89.359	0.14%	68.587
		22.6%	NO	11546.9	3.99%	16	36	-94.552	0%	87.551
5	Obj: Loss + Penalty & Rating: Static	1.13%	YES	36.0	0.16%	6	2	0.929	4.23%	1.867
		1.13%	NO	34.5	0.14%	0	0	1.021	0%	0.979
		11.3%	YES	2544.5	0.89%	5	0	-36.076	0.97%	6.775
		11.3%	NO	2613.9	0.91%	2	3	-36.641	0%	8.051
		22.6%	YES	10302.7	1.83%	4	4	-73.316	0.31%	14.752
		22.6%	NO	10352.5	1.83%	0	3	-73.619	0%	15.143
6	Obj: Loss + Penalty & Rating: RTTR	1.13%	YES	34.6	0.14%	8	0	1.026	3.77%	1.454
		1.13%	NO	34.5	0.14%	0	0	1.018	0%	0.990
		11.3%	YES	2542.9	0.89%	4	0	-36.113	0.82%	6.752
		11.3%	NO	2610.1	0.90%	2	1	-36.352	0%	7.213
		22.6%	YES	10338.9	1.83%	4	3	-73.553	0.14%	15.142
		22.6%	NO	10352.5	1.83%	0	3	-73.619	0%	15.144

*$V_{dev} = max(|1 - V_{ij}|), i = 1{:}24, j = 1{:}147$

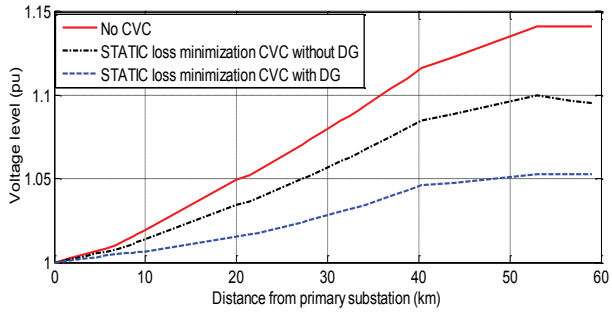

Fig. 67 *Voltage level on the longest feeder of the network after implementation of CVC with and without involvement of DG reactive power supply. (In all the three scenarios, 65% DG penetration).*

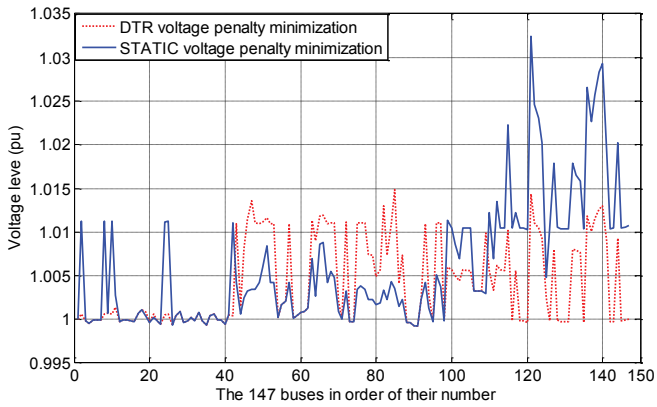

Fig. 68 *The voltage level at hour 16:00 after the static and RTTR based CVC control settings are applied with voltage penalty minimization objective and 20% DG penetration*

The results in Table 19 compare the six types of CVC formulation involving DGs. The table presents the overall network losses after applying the control set-points for the period of 24 hours. Besides, the number of OLTC and SVC operations per day, and the cumulative reactive power supplied by DGs and SVCs are presented. The lowest network losses are attained for a CVC formulation where both the penalty function and loss minimization involving RTTR are included in the objective. As presented in Table 19, the loss minimization objective produces set-points with a higher number of switching of SVCs. If only the loss minimization objective is used for CVC, the set-points would give a customer voltage near to the upper limit (+10% in this dissertation). A voltage penalty function can minimize the voltage burden on the customer. As shown in Fig. 68, the static rating coupled with the penalty function gave the voltage level closest to the nominal. However, this is achieved at the significant expense of overall network losses, as shown in Table 19. RTTR, on the other hand, inherently minimizes losses, which entails the superior benefit of using RTTR coupled with the penalty function and loss minimization objectives. In practice, only CVC formulations 5 and 6 in Table 19 are implementable, as both voltage level and losses are considered in existing distribution management systems.

The following characteristics of the CVC objective function formulation methods are observed:

Observation#1: The CVC formulation experienced a higher voltage level from the nominal without the involvement of DG reactive power capacity than with (see Fig. 67). In addition, the optimal set-point is achieved at significantly higher network loss values for CVC without DG reactive power involvement.

Observation#2: With the voltage deviation penalty function objective; there is a higher requirement for the operation of the SVCs and OLTCs, as shown in Table 19. In both Static and RTTR rating methods, the voltage penalty function objective utilizes a higher reactive power supply from the SVCs and OLTCs while injecting reactive power into the DGs. This is because the objective gives less emphasis for losses, leading to a greater tendency to use reactive power absorption and supply to keep the voltage level in the entire network close to unity. With the voltage penalty function objective, the voltage level stays closer to the flat one per unit compared to the loss minimization objective function. However, the network losses increased tremendously with the voltage penalty function objective, as shown in Table 19. With the penalty function objective, RTTR can use the reactive power resources and also lower the DG active power generation curtailment better than static ratings, as shown in Table 19.

Observation#3: RTTR shows no significant difference from static rating when loss minimization is an objective. In principle, the RTTR utilizes the opportunities provided by the weather for the cooling of distribution network components. It is evident that with RTTR network losses could even increase as long as they remain within the economically acceptable level. As shown in Fig. 68 and Table 19, the voltage penalty minimization objective provides better voltage levels with RTTR than with static rating, even though the total losses are the same.

Observation#4: The combined loss minimization and voltage penalty objective function with both static and RTTR rating reduced significantly the operations of OLTCs and SVCs, while utilizing both the active and reactive power resources of the installed DGs to the utmost. This has been observed in all the four cases presented in Table 19.

5.2.2 Discussions on Practical Implementations

Planning CVC for day-ahead distribution network operation requires reliable load and environmental variable forecasting. Nevertheless, the control setting planned a-day-before faces two fundamental challenges. The first is the question of where to conduct the central optimization for CVC and how to communicate the optimal set-points to the respective equipment such as OLTCs, SVCs and DGs. The second challenge is how to react to contingencies during the same day and the requirements for updating.

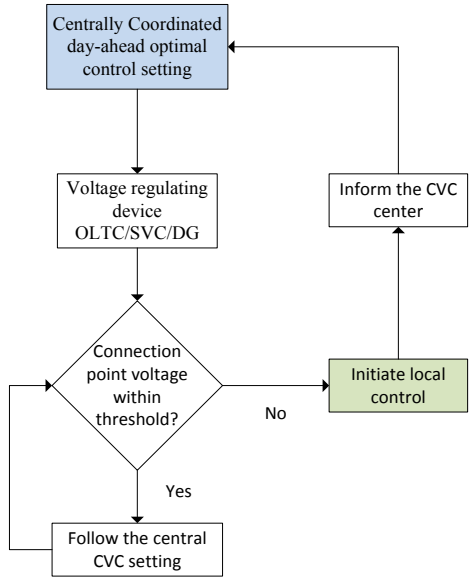

Fig. 69 *Integrated local and central voltage control strategy*

Usually voltage regulators operate by following the voltage level at their connection point. In CVC strategy, however, the optimal set-points are computed and communicated from elsewhere. We propose a connection point voltage dependent on central and local control strategies for the specific voltage regulators as shown in Fig. 69. The day-ahead optimal setting point will be sent to the specific voltage regulating device that it follows unless the connection point voltage level does not violate a certain threshold. When the connection point voltage level violates a given preset level, however, the local closed loop control system will be initiated (see Fig. 69). This strategy can be implemented naturally with the Multi-Agent System (MAS) control architecture of active distribution networks. With the specified MAS approach, the voltage regulating devices need to be agents with decision making and communication capability. Another challenge in executing the optimal control settings is the proper queuing of the control actions. Hence, not only do we need to communicate the day-ahead control settings but the associated time lags are also needed.

The proposed method is mainly for active distribution network operations planning, which might range from minutes ahead to up to a day-ahead. For real-time application, as is discussed briefly in this section, we propose a cooperative central and distributed control strategy. In the proposed scheme, the day-ahead centralized operation planning (which can be referred to as coordinated control agents) will be used as a guideline for local controls (unit control agents). We believe that, to accommodate the distributed potential such as DG units and demand response, a relaxed centralized cooperation strategy with decentralized control functions will be most useful. Such a multi-agent based hierarchical hybrid control architecture is presented in [84].

6 Summary and Future Prospects

6.1 Summary

Existing static ratings, which are based on worst-case weather and pre-load conditions, are significantly conservative. The highly variable loading condition, prevalent in active distribution networks, requires efficient and economical utilization of the physical infrastructure. The RTTR system avails the true real-time capacities of components following the variability in local weather conditions. Nevertheless, given that margins will be reduced, the parameterization used in RTTR should err on the conservative side. It should also be noted that thermo-mechanical failure mechanisms will be exacerbated in this new paradigm, both due to the reduction in margins, and the more stochastic load flows in components.

Dynamic thermal models with physically validated convection and radiation heat transfer components are essential for the real-time thermal rating of distribution network components. Therefore, the inclusion of realistic installation conditions in formulating real-time convection correlations constitutes an improvement. This thesis proposed and validated dynamic thermal models for underground cables inside unfilled conduit by using installation-dependent convection correlations. The Raithby and Hollands correlation employed for horizontal concentric cylinders is less conservative due to its inclusion of natural convection phenomena.

Furthermore, in this thesis, a clear and expandable first principle approach was used to quantify heat transfer through ventilation openings of a prefabricated secondary substation. A scale model of a prefabricated substation was examined to draft a numerical solution, which is based on stack ventilation principles. Measurements from actual cabins and 3-D finite element method simulations were used to validate the numerical model. The proposed model showed good agreement with measurements in a controlled environment.

Due to the emerging customer level DR services and DG installations, distribution network operators have to deal with the stochasticity coming with relatively low number of households aggregated at secondary and primary substations to forecast and understand their load profile. As a second major contribution, this dissertation has demonstrated that classified class models based on AMR measurements can be used for short time load

forecasting as well as for load monitoring closer to individual customers. The load aggregation method presented in this thesis can be implemented in an existing distribution network with limited coordination and non-readily accessible AMR measurements. In addition, this dissertation has demonstrated that a load flow analysis based on customer point smart meter measurements can be used to compute LV node voltage levels.

This thesis also proposed a framework for day-ahead hour-by-hour thermal state forecasting of distribution network components. The stochasticity in weather forecasting is translated to stochasticities in distributed generation and customer load forecasts, and consequently to the main distribution network components' thermal state forecasts. The results show that the thermal state of components can be forecast with the required prediction interval. For shorter time periods, such as 3 hours ahead, environmental variables and distributed generation can be forecasted with an acceptable prediction interval. Hence the implementation of dynamic thermal rating needs almost real time component temperatures and environmental variable measurements. Provided that weather variables are forecast to the utmost accuracies, the implementation of component thermal state forecasting enables day-ahead planning for more economical and efficient distribution systems operation. For the real-time active distribution network control, the time resolution needs to be small enough (in the order of few hundred milliseconds for fault management and tens of seconds for voltage control and line congestions) to cope with the fastest volatility of DG and long enough to be compatible with the need to estimate the electrical state of the grid. The hourly control frameworks presented in this thesis came from the wide availability of hourly measured AMR data. Hence, the method loses accuracy in following real-time DG output as well as unforeseen system states that may be encountered. This is the primary reason the presented methods focused on day ahead network operational planning. Nevertheless, the testing and evaluation of the RTTR system with lower time resolutions will be a significant improvement on the presented method.

As the third major contribution, the thesis has utilized previously developed dynamic thermal models and AMR based load forecasting methods to propose a real-time thermal rating technique for the operation of active distribution networks. This study further quantifies the benefits of real-time thermal rating in accommodating new DGs and utilizing installed ones. The benefits of an RTTR system were quantified with the simulation of a typical active distribution network supplying a variety of household types and with different scenarios of DG penetration level. The introduction of real-time thermal rating in an active distribution network management system enhanced the loading capacity significantly compared to static rating. This has been revealed through an increased utilization of installed DGs and through better integration potential for new DGs. The increment of distribution network loading capacity with RTTR can be achieved without compromising the aging of network components.

Finally, in this dissertation, the synergy between coordinated voltage control and real-time thermal rating was investigated for an increased utilization of DG reactive power potential. Beyond its foremost benefit, enhancing network capacity and efficient utilization of network components, real-time thermal rating has demonstrated its advantage for a coordinated voltage regulation involving DGs. The benefit of incorporating RTTR with CVC is two-pronged. On one hand, the generated DG active power can be utilized better owing to an increased distribution network component load carrying capacity. On the other hand, the required reactive power for voltage regulation can be transferred without violating network components' capacity limits if RTTR is applied in a real-time basis. In the analysis, the CVC formulation with a combined loss and voltage penalty function objective and real-time thermal rating method exhibited better results in both minimizing the network losses and keeping the voltage close to one per unit. When network losses are insignificant, such as in the test network in this paper, the voltage penalty function objective performs better, by bringing the voltage to a flat stable level close to one per unit. In addition, the incorporation of static rating or RTTR with a loss minimization objective brought down the network losses by about 29%, compared to the static or RTTR rating with only the voltage penalty function objective. Furthermore, when the voltage penalty function and loss minimization objectives are used together, the observed overall performance is superior.

In order to realize the benefits provided by the RTTR system, utilities need to document the thermal conditions, such as installation setups and parameters associated with backfill and local ground conditions, and also made them accessible to distribution management systems. The dynamic thermal models of various installation conditions need to be stored in the RTTR system. Utilities are required only to rate local bottlenecks along the route of overhead or underground feeders. In addition, weather condition measurements as close to the physical installations as possible would enhance the reliability of the RTTR system.

6.2 Future Prospects

At each stage of this dissertation, for every untangled topic, even more interesting research problems have been emerging.

- Along a route of MV underground cables different types of installation scenarios might be experienced. Thermally challenged sections may vary from season to season. Computationally efficient, comprehensive and accurate rating methods have to be developed.
- The smart meter measurement based load flow analysis method for active distribution networks has to be developed further to aggregate appliance level consumptions. This enables the realization of the effect of appliance level demand response programs and future appliance penetration levels on the loading of active distribution network components.

- The RTTR method needs further development to make use of the widely installed secondary substation transformer temperature measurements made available only in recent decades.
- The practice of modeling substation loads by aggregating clustered individual households can be improved significantly by applying more robust and efficient clustering techniques.
- The real-time thermal rating of active distribution network will subject the distribution system components to highly variable hotspot and conductor temperatures. The impact of the continual heating and cooling, associated with highly variable rating, on the mechanical integrity of network components requires in-depth investigation.
- The impact of errors introduced with the weather variables and load forecasting techniques on the proposed RTTR framework should be investigated in future work.
- The wind turbine and PV models utilized in this thesis are simple models. One can improve thermal state estimations and network operation planning in active distribution networks by deploying more accurate and robust models of DGs, load and network components

References

[1] R. C. Dugan and T. E. McDermott, "Operating Conflicts for Distributed Generation on Distribution Systems," *Proc. Rural Electric Power Conf.*, Little Rock, AR, USA, Apr. 29 – May 01, 2001, pp. A3/1 -A3/6.

[2] S.C.E. Jupe and P.C. Taylor, "Distributed Generation Output Control for Network Power Fow Management," *IET Renewable Power Generation 3*, vol. 3, no. 4, pp. 371–386, Dec. 2008.

[3] R. F. Arritt and R.C.Dugan, "Distribution System Analysis and the Future Smart Grid," *IEEE Transactions on Industry Applications 47*, vol. 47, no. 6, pp. 2343-2350, Sep. 2011.

[4] A. Neumann and P. Brinckerhoff, "Unlock Distribution Capacity Using Dynamic Thermal Ratings," *The independent power and energy journal of Southern Africa (energize)*, pp. 18-19, Nov. 2008.

[5] D.A. Douglass, D.C. Lawry, A.A. Edris, and E.C. Bascom, "Dynamic Thermal Ratings Realize Circuit Load Limits," *IEEE Computer Applications in Power*, vol. 13, no. 1, pp. 38-44, Jan. 2000.

[6] A. Michiorri and P. Taylor, "Forecasting Real-Time Ratings for Electricity Distribution Networks Using Weather Forecast Data," *Proceedings 20th International Conference on Electricity Distribution*, Prague, Czech Republic, Jun. 8-11, 2009, pp. 1-4.

[7] R. C. Dugan, T. E. McDermott, and G. J. Ball, "Planning for Distributed Generation," *IEEE Industry Application Magazine*, vol. 7, no. 2, pp. 80-88, Apr. 2001.

[8] R. A. Walling, R. Saint, R. C. Dugan, J. Burke, and L. A. Kojovic, "IEEE Summary of Distributed Resources Impact on Power Delivery Systems," *IEEE Transactions on Power Delivery*, vol. 23, no. 3, pp. 1636-1644, Jul. 2008.

[9] R.A.F. Currie, G.W. Ault, and J.R. McDonald, "Methodology for Determination of Economic Connection Capacity for Renewable Generator Connections to Distribution Networks Optimized by Active Power Flow Management," *IEE Proceedings Generation, Transmission and Distribution*, vol. 153, no. 4, pp. 456-462, Jul. 2006.

[10] A. Borghetti, M. Bosetti, S. Grillo, S. Massucco, C. A. Nucci, M. Paolone, and F. Silvestro, "Short-Term Scheduling and Control of Active Distribution Systems With High Penetration of Renewable Resources," *IEEE Systems Journal*, vol. 4, no. 3, pp. 313-322, Aug. 2010.

[11] H.T. Yip, C. An, G.J. Lloyd, and P. Taylor, "Dynamic Thermal Rating and Active Control for Improved Distribution Network Utilization," *Developments in Power System Protection (DPSP 2010), 10th IET International Conference on Managing the Change*, Manchester, UK, Mar. 29 – Apr. 1, 2010, pp. 1-5.

[12] C. D'Adamo, S. Jupe, and C. Abbey, "Global Survey on Planning and Operation of Active Distribution Networks-Update of CIGRE C6. 11 Working Group Activities," 20th International Conference on Electricity Distribution (CIRED 2009), 8-11 June 2009, Prague, Czech Republic.

[13] Deliverable 2.1: Specification of Active Distribution Network Concept, IDEAL GRID FOR ALL (IDE4L), 25 April 2014. Available: http://webhotel2.tut.fi/units/set/ide4l/d21.pdf

[14] O. Samuelsson, S. Repo, R. Jessler, J. Aho, M. Kärenlampi, and A. Mamquist, "Active Distribution Network -Demonstration Project ADINE," IEEE PES InnovativeSmart Grids Technologies Conf. Europe, Gothenburg,2010, pp. 11–13.

[15] R. S. Olsen, J. Holboll and U. S. Gudmundsdóttir, "Dynamic Temperature Estimation and Real Time Emergency Rating of Transmission Cables," *2012 IEEE Power and Energy Society General Meeting*, San Diego, CA, USA, 22 – 26 Jul. 2012, pp. 1-8.

[16] D. Douglass, W. Chisholm, G. Davidson, I. Grant, K. Lindsey, M. Lancaster, D. Lawry et al. "Real-Time Overhead Transmission Line Monitoring for Dynamic Rating*," IEEE Transactions on Power Delivery*, vol. pp, no. 99, pp. 1, Dec. 2014.

[17] IEEE Guide for Loading Mineral-Oil-Immersed Transformers and Step-Voltage Regulators, IEEE Std C57.91-2011.

[18] H. Brakelmann, and G. Anders, "Increasing Ampacity of Cables by an Application of Ventilated Pipes," *IEEE/ IAS 39th Annual Meeting*, vol. 4, Seattle, USA, 3 – 7 Oct. 2004, pp. 2288-2295.

[19] F.P. Incropera and D.P. DeWitt, "Fundamentals of Heat and Mass Transfer," fifth ed., John Wiley & Sons, Inc., New York, 2002.

[20] J. H. Neher and M. H. McGrath, "The Calculation or the Temperature Rise and Load Capability of Cable Systems," *Transactions of the American Institute of Electrical Engineers Part III Power Apparatus and Systems*, vol. 76, pp. 752–772, Oct. 1957.

[21] G. J. Anders, M. Chaaban, N. Bedard, and R. W. D. Ganton, "New Approach to Ampacity Evaluation of Cables in Ducts Using Finite Element Technique," *IEEE Power Engineering Review* , vol. PER-7, no. 10, pp. 30-31, Oct. 1987.

[22] J. A. Pilgrim, D. J. Swaffield, P.L. Lewin, S.T. Larsen, F. Waite, and D. Payne, "Rating Independent Cable Circuits in Forced-Ventilated Cable Tunnels," *IEEE Transactions on Power Delivery*, vol. 25, no. 4, pp. 2046-2053, Jul. 2010.

[23] Cigré WG08-SC21, "Calculation of Temperatures in Ventilated Cable Tunnels," Electra, vol. 143, pp. 38-59. Aug. 1992.

[24] G. D. Raithby and K. G. T. Hollands, "A General Method of Obtaining Approximate Solutions to Laminar and Turbulent Free Convection Problems," in Advances in Heat Transfer, T. F. Irvine and J. P. Hartnett, Eds. New York: Academic, 1975, vol. 11, pp. 265–315.

[25] G. D. Raithby and K. G. T. Hollands, "Analysis of Heat Transfer by Natural Convection (or film condensation) for Three-dimensional Flows," *in Proc. 6th Int. Heat Transfer Conf.*, Washington, DC, 1978, vol. 2, pp. 187–192.

[26] G. J. Anders, "Rating of Electric Power Cables," IEEE Press Power Engineering Series, New York, USA, McGraw-Hill Book Company, 1997.

[27] E. Dorison and G.J. Anders, "Current Rating of Cables Installed in Deep or Ventilated Tunnels*", 8th International Conference on Insulated Power Cables,* proceedings of the Jicable'11 conference, Versailles, France, 19 – 23 Jun. 2011.

[28] K.T. Andersen, "Theoretical Considerations on Natural Ventilation by Thermal Buoyancy," *ASHRAE Transactions*, vol. 101, no. 2, pp 1103–1117, 1995.

[29] COMSOL, "Heat Transfer Module," 2012. [online]. Available: http://www.comsol.fi

[30] R. J. Millar, "A Comprehensive Approach to Real-time Power Cable Temperature Prediction and Rating in Thermally Unstable Environments," Doctoral Dissertation, Helsinki University of Technology, Espoo, Finland, 2006. IBSN-13 978-951-22-8415-8423

[31] S.M. Sellers and W. Z. Black, "Refinements to the Neher-McGrath Model for Calculating the Ampacity of Underground Cables," *IEEE Transactions on Power Delivery*, vol. 11, no. 1, pp. 12-30, Jan. 1996.

[32] Calculation of the Continuous Current Rating of Cables (100% Load Factor), IEC Std. 60287 (1969, 1982, 1994), 1994–1995, 1st ed. 1969, 2nd ed. 1982, 3rd ed.

[33] S. Tenbohlen, T. Stirl, and M. Stach, "Assessment of Overload Capacity of Power Transformers by On-line Monitoring Systems," *IEEE Power Engineering Society Winter Meeting*, Columbus, Ohio, pp. 329-334, 28 Jan. – 01 Feb., 2001.

[34] A. Kalam and S. Corhodzic, "Performances of Distribution Transformers Installed in Metallic Enclosures—An Australian Experience," *IEEE Transactions on Power Delivery*, vol. 20, no. 3, pp. 1970-1975, Jul. 2005.

[35] D. Susa, "Dynamic Thermal Modeling of Power Transformer," Doctoral Dissertation, Helsinki University of Technology, Espoo, Finland, 2005. ISBN 951-22-7742-5

[36] R. Vilaithong, S. Tenbohlen, and T. Stirl, "Investigation of Different Top-oil Temperature Models for On-line Monitoring System of Power Transformer," *IEEE International Conference on Condition Monitoring and Diagnosis*, Changwon, South Korea, 02 – 05 Apr. 2006.

[37] J. A. Pilgrim , D. J. Swaffield, P. L. Lewin, and D. Payne, "Rating Methods for Cables Installed in Unventilated and Partially Ventilated Surface Troughs," *Electrical Insulation Conference*, Annapolis, Maryland, 5 - 8 Jun. 2011, pp. 74-78.

[38] T. S. Larsen, “Natural Ventilation Driven by Wind and Temperature Difference,” Doctoral Dissertation, Department of Civil Engineering, Aalborg University, Jun. 2006. ISSN 1901-7294

[39] Mathworks, “SimscapeTM User's Guide” 2012. [online]. Available: http://www.mathworks.se/help/physmod/simscape/.

[40] Mathworks, “Ordinary Differential Equations,” 2012. [online]. Available: https://www.mathworks.se/help/matlab/ordinary-differential-equations.html.

[41] A. Seppälä , “Load Research and Load Estimation in Electricity Distribution,” VTT Publications, vol. 289. VTT:Espoo; 137, 1996.

[42] A. Mutanen, M. Ruska, S. Repo, and P. Järventausta, “Customer Classification and Load Profiling Method for Distribution Systems,” Power Delivery, IEEE Transactions on, vol. 26, no. 3 , July 2011, pp. 1755-1763.

[43] F. McLoughlin, A. Duffy, and M. Conlon, “Evaluation of Time Series Techniques to Characterize Domestic Electricity Demand,” *Energy, Journal Elsevier*, vol. 50, pp. 120-130, Feb. 2013.

[44] M. Meldorf, T. Täht, M. Lehtonen, A. Seppälä, and M. Jalonen, “A Method for Assessing the Maximum Load Flows in Distribution Systems,” *13th Power Systems Computation Conference (PSCC),* Trondheim, Norway, Jun. 28 – Jul. 2, 1999.

[45] R. Singh, B. C. Pal, and R. A. Jabr, “Statistical Representation of Distribution System loads Using Gaussian Mixture Model,” *IEEE Transactions on Power Systems*, vol. 25, no. 1, pp. 29-37, Oct. 2009.

[46] A. Seppälä, “Statistical Distribution of Customer Load Profiles,” *International Conference on Energy Management and Power Delivery (EMPD)*, Westin Stamford, Singapore, 21-23 Nov. 1995, vol. 2, pp. 696-701.

[47] A. Ahmad, I. Azmira, S. Ahmad, N. Ilyana, and A. Apandi, “Statistical Distributions of Load Profiling Data,” *2012 IEEE International Power Engineering and Optimization Conference (PEDCO)*, Melaka, Malaysia, 6-7 Jun. 2012, pp. 199-203.

[48] R. F. Arritt, R. C. Dugan, R. W. Uluski, and T. F. Weaver, “Investigating Load Estimation Methods with the Use of AMI Metering for Distribution System Analysis,” *IEEE Rural Electric Power Conference (REPC)*, Knoxville, TN, USA, 15-17 Apr. 2012, pp. B3-1 - B3-9.

[49] F. M. Andersen, H.V. Larsen, and T.K. Boomsma, “Long-term Forecasting of Hourly Electricity Load: Identification of Consumption Profiles and Segmentation of Customers,” *Energy Conversion and Management*, vol. 68, pp. 244-252, Apr. 2013,

[50] W. H. Kersting and R. C. Dugan, “Recommended Practices for Distribution System Analysis,” *IEEE PES Power Systems Conference and Exposition (PSCE)*, Atlanta, GA, USA, Oct. 29 2006-Nov. 1 2006, pp. 499-504.

[51] W. Labeeuw and G. Deconinck, “Residential Electrical Load Model Based on Mixture Model Clustering and Markov Models,” *IEEE Transactions on Industrial Informatics*, vol. 9, no. 3, pp. 1561-1569, Aug. 2013.

[52] F. J. McLoughlin, A. Duffy, and M. Conlon, “The Generation of Domestic Electricity Load Profiles Through Markov Chain Modeling,” *Euro-Asian Journal of Sustainable Energy Development Policy*, vol. 3, Jan. - Dec. 2010.

[53] T. Räsänen, D. Voukantsis, H. Niska, K. Karatzas, and M. Kolehmainen, “Data-based Method for Creating Electricity Use Load Profiles Using Large Amount of Customer-specific Hourly Measured Electricity Use Data,” *Applied Energy*, vol. 87, no. 11, pp. 3538-3545, Nov. 2010.

[54] K. Ghosh, D. L. Lubkeman, and R. H. Jones, “Load Modeling for Distribution Circuit State Estimation,” *IEEE Transaction on Power Delivery*, vol. 12, n. 2, pp. 999-1005, Apr. 1997.

[55] M. Z. Degefa, “Energy Efficiency Analysis of Residential Electric End-Uses: Based on Statistical Survey and Hourly Metered Data,” Master's thesis. Aalto University School of Science and Technology, 2010. Available: https://aaltodoc.aalto.fi/handle/123456789/10787

[56] M. Koivisto, P. Heine, I. Mellin, M. Lehtonen, “Clustering of Connection Points and Load Modeling in Distribution Systems,” *Power Systems, IEEE Transactions on*, vol. *28 no.* 2, May 2013, pp: 1255-1265.

[57] G. Reikard, “Predicting Solar Radiation at High Resolutions: A Comparison of Time Series Forecasts,” *Solar Energy*, vol. 83, no. 3, pp. 342-349, Mar. 2009.

[58] J. L. Torres, A. Garcia, M. De Blas, and A. De Francisco, “Forecast of Hourly Average Wind Speed with ARMA Models in Navarre (Spain),” *Solar Energy*, vol. 79, no. 1, pp. 65-77, Jul. 2005.

[59] T. H. M. El-Fouly, E. F. El-Saadany, and M. M. A. Salama, “One Day-ahead Prediction of Wind Speed Using Annual Trends,” *IEEE Power Engineering Society General Meeting, Montreal*, Quebec, Canada, 18-22 Jun. 2006, pp. 7-12.

[60] FMI-Finnish Meteorological Institute, 2014. [online]. Available: http://en.ilmatieteenlaitos.fi/

[61] A.D. Jones and C.P. Underwood, “A Modeling Method for Building-integrated Photovoltaic Power Supply,” *Building Serv. Eng. Res. Technol.*, vol. 23, no. 3, pp. 167-177, Aug. 2002.

[62] Solar Energy Services for Professionals, 2014. [online]. Available: http://www.soda-is.com/eng/index.html

[63] IEEE Std. 738-2006. IEEE Standard for Calculating the Current - Temperature Relationship of Bare Overhead Conductors.

[64] R. J. Millar and M. Lehtonen, “A Robust Framework for Cable Rating and Temperature Monitoring,” *IEEE Transactions on Power Delivery*, vol. 21, no. 1, pp. 313-321, 2006.

[65] R. J. Millar and M. Lehtonen, "Real-time Transient Temperature Computation of Power Cables Including Moisture Migration Modelling," *15th Power Systems Computation Conference*, PSCC 2005, Liege, Belgium, August 22-26, 2005.

[66] R.J. Millar, S. Kazemi, M. Lehtonen, and E. Saarijärvi, "Impact of MV Connected Microgrids on MV Distribution Planning," *IEEE Transactions on Smart Grid*, vol. 3, issue 4, 2012, pp 2100 - 2108.

[67] S. Kazemi, "Reliability Evaluation of Smart Distribution Grids," Ph.D. Dissertation, Depts. Elec. Eng., Sharif University of Technology and Aalto University, 2011. [online]. Available: http://lib.tkk.fi/Diss/2011/isbn9789526042411/

[68] M. E. Elkhatib, R. El-Shatshat, and M. M. A. Salama, "Novel Coordinated Voltage Control for Smart Distribution Networks with DG," *IEEE Trans. Smart Grid*, vol. 2, no. 4, pp. 598–605, Dec. 2011.

[69] A. Samadi, R. Eriksson, L. Soder, B.G. Rawn, and J.C. Boemer, "Coordinated Active Power-Dependent Voltage Regulation in Distribution Grids With PV Systems," *IEEE Trans. Power Del.*, vol. 29, no. 3, June 2014

[70] S. Engelhardt, I. Erlich, C. Feltes, J. Kretschmann, and F. Shewarega, " Reactive Power Capability of Wind Turbines Based on Doubly Fed Induction Generators," *IEEE Trans. Energy Convers.*, vol. 26, vo. 1, pp: 364-372, Oct. 2010.

[71] Kulmala, Anna. "Active Voltage Control in Distribution Networks Including Distributed Energy Resources." Tampereen teknillinen yliopisto. Julkaisu-Tampere University of Technology. Publication; 1203 (2014).

[72] A. Kulmala, S. Repo, and P. Järventausta, "Using Statistical Distribution Network Planning for Voltage Control Method Selection," *IET Conf. Proc. on Renewable Power Generation*, Edinburgh, UK, 6-8 Sept. 2011.

[73] N. Daratha, B. Das, and J. Sharma, "Coordination Between OLTC and SVC for Voltage Regulation in Unbalanced Distribution System Distributed Generation," *IEEE Trans. Power Syst.*, vol. 29, no. 1, Jan. 2014

[74] A. Kulmala, K. Maki, S. Repo, and P. Jarventausta, "Including Active Voltage Level Management in Planning of Distribution Networks with Distributed Generation," *Proc. IEEE PowerTech*, pp. 1-6, Bucharest, Jun. 2009.

[75] T. Sansawatt, L. F. Ochoa, and G. P. Harrison, "Smart Decentralized Control of DG for Voltage and Thermal Constraint Management," *Power Systems, IEEE Transactions on*, vol. *27, no. 3*, pp. 1637-1645, Mar. 2012.

[76] I. Bilibin and F. Capitanescu, "Contributions to Thermal Constraints Management in Radial Active Distribution Systems," *Electric Power Systems Research*, vol. *111*, pp. 169-176, Jun. 2014.

[77] T. J. T. Hashim, A. Mohamed, and H. Shareef, "A Review on Voltage Control Methods for Active Distribution Networks," *Prz. Elektrotech*., vol. 88, pp. 304–312, Jun. 2012.

[78] K. Turitsyn, S. Petr, B. Scott, and C. Michael, “Options for Control of Reactive Power by Distributed Photovoltaic Generators,” *Proc. of the IEEE*, vol. 99, no. 6, pp. 1063-1073, Jun. 2011.

[79] W. Zhang, F. Li, and L. M. Tolbert, “Review of Reactive Power Planning: Objectives, Constraints, and Algorithms,” *IEEE Trans. Power Syst.*, vol. 22, no. 4, pp. 2177-2186, Nov. 2007.

[80] E. R. Sichard, “GAMS, A User’s Guide, Tutorial,” GAMS Development Corporation, Washington, Mar. 2014.

[81] J. Z. Hansen, “Failure in MV joints (XLPE cable) in Heavy Loaded Cable Systems Connecting Large Windmills to the Distribution System,” *10th Nordic Conference on Electricity Distribution System Management and Development (NORDAC)*, Espoo, Finland, 10-11 Sep. 2012 .

[82] G. Celli, E. Ghiani, F. Pilo, and G. G. Soma, “Reliability Assessment in Smart Distribution Networks,” *Electric Power Systems Research*, vol. 104, pp.164-175, 2013.

[83] H. L. Willis, “Power Distribution Planning Reference Book,” second ed., Marcel Dekker, Inc., New York, 2004.

[84] C. X. Dou and B. Liu, “Multi-agent Based Hierarchical Hybrid Control for Smart Microgrid,” IEEE transactions on smart grid, vol. 4, no. 2, pp. 771-778, Jun. 2013.

Appendix- NTK#2 data

Table A1. *The 147 bus active distribution test network specifications (40MVA base 20kV MV system)*

No.	From	To	r(pu)	x(pu)	No.	From	To	r(pu)	x(pu)
1	16	2	0.008	0.006	*74*	77	75	0.037	0.046
2	32	3	0.005	0.004	*75*	97	76	0.017	0.021
3	20	4	0.010	0.008	*76*	48	77	0.019	0.023
4	13	5	0.005	0.004	*77*	81	78	0.042	0.052
5	1	6	0.003	0.003	*78*	78	79	0.037	0.046
6	38	7	0.004	0.003	*79*	86	80	0.021	0.026
7	2	8	0.013	0.010	*80*	80	81	0.020	0.025
8	41	9	0.019	0.015	*81*	46	82	0.036	0.044
9	2	10	0.006	0.005	*82*	79	83	0.027	0.034
10	1	11	0.053	0.042	*83*	76	84	0.043	0.053
11	30	12	0.006	0.005	*84*	47	85	0.028	0.035
12	14	13	0.006	0.005	*85*	94	86	0.032	0.039
13	1	14	0.007	0.006	*86*	79	87	0.037	0.046
14	3	15	0.005	0.004	*87*	89	88	0.024	0.029
15	22	16	0.010	0.008	*88*	90	89	0.020	0.016
16	33	17	0.021	0.026	*89*	27	90	0.285	0.351
17	28	18	0.014	0.011	*90*	90	91	0.036	0.044
18	21	19	0.005	0.004	*91*	55	92	0.082	0.102
19	29	20	0.005	0.004	*92*	49	93	0.053	0.065
20	1	21	0.017	0.014	*93*	70	94	0.020	0.016
21	1	22	0.018	0.014	*94*	74	95	0.047	0.058
22	4	23	0.017	0.014	*95*	69	96	0.029	0.036
23	8	24	0.027	0.021	*96*	48	97	0.027	0.033
24	10	25	0.006	0.005	*97*	73	98	0.050	0.062
25	35	26	0.004	0.003	*98*	134	99	0.130	0.161
26	37	27	0.022	0.027	*99*	99	100	0.026	0.032
27	9	28	0.013	0.010	*100*	100	101	0.058	0.071
28	12	29	0.005	0.004	*101*	101	102	0.051	0.063
29	6	30	0.003	0.002	*102*	113	103	0.047	0.058
30	1	31	0.022	0.018	*103*	103	104	0.029	0.036
31	7	32	0.004	0.003	*104*	104	105	0.066	0.082
32	18	33	0.033	0.040	*105*	107	106	0.064	0.078
33	30	34	0.002	0.002	*106*	108	107	0.104	0.128
34	40	35	0.007	0.006	*107*	56	108	0.256	0.315
35	41	36	0.005	0.004	*108*	64	109	0.022	0.028
36	17	37	0.011	0.013	*109*	111	110	0.077	0.095
37	1	38	0.002	0.002	*110*	125	111	0.032	0.039
38	5	39	0.006	0.005	*111*	110	112	0.019	0.023
39	23	40	0.005	0.004	*112*	100	113	0.023	0.018
40	31	41	0.024	0.019	*113*	104	114	0.086	0.105
41	24	42	0.035	0.043	*114*	123	115	0.024	0.029
42	49	43	0.035	0.043	*115*	126	116	0.040	0.050
43	19	44	0.018	0.015	*116*	110	117	0.028	0.035
44	78	45	0.018	0.023	*117*	116	118	0.028	0.035
45	72	46	0.011	0.008	*118*	128	119	0.028	0.035
46	82	47	0.013	0.017	*119*	135	120	0.032	0.039
47	72	48	0.032	0.039	*120*	140	121	0.028	0.035
48	84	49	0.035	0.043	*121*	138	122	0.027	0.034
49	68	50	0.046	0.057	*122*	122	123	0.041	0.051
50	63	51	0.113	0.139	*123*	115	124	0.055	0.068
51	43	52	0.027	0.033	*124*	11	125	0.040	0.032
52	52	53	0.066	0.082	*125*	119	126	0.015	0.018
53	58	54	0.027	0.033	*126*	112	127	0.062	0.076
54	62	55	0.047	0.058	*127*	146	128	0.029	0.035
55	55	56	0.098	0.121	*128*	143	129	0.019	0.023
56	52	57	0.018	0.023	*129*	142	130	0.060	0.074
57	71	58	0.024	0.030	*130*	130	131	0.016	0.020
58	54	59	0.026	0.032	*131*	127	132	0.031	0.039
59	61	60	0.071	0.087	*132*	141	133	0.072	0.089
60	59	61	0.074	0.091	*133*	133	134	0.021	0.026
61	61	62	0.050	0.061	*134*	129	135	0.097	0.120
62	50	63	0.088	0.109	*135*	137	136	0.055	0.068

63	45	64	0.020	0.025	***136***	127	137	0.068	0.084
64	51	65	0.011	0.008	***137***	139	138	0.072	0.089
65	65	66	0.013	0.016	***138***	140	139	0.026	0.032
66	43	67	0.019	0.023	***139***	136	140	0.039	0.048
67	96	68	0.032	0.040	***140***	124	141	0.032	0.039
68	84	69	0.049	0.061	***141***	129	142	0.046	0.056
69	44	70	0.018	0.014	***142***	145	143	0.027	0.033
70	98	71	0.048	0.060	***143***	124	144	0.048	0.059
71	109	72	0.029	0.035	***144***	119	145	0.021	0.026
72	74	73	0.021	0.026	***145***	147	146	0.042	0.051
73	88	74	0.138	0.170	***146***	42	147	0.133	0.165

Branches with shaded cells are underground cables and all others are overhead lines.

Table A2. *DG, SVC and OLTC connections*

	Type	***Node***	***DG Rating and Number***	
DG	WIND	102	50kW x 2 Turbines	
		108	50kW x 3 Turbines	
		92	50kW x 2 Turbines	
		66	50kW x 3 Turbines	
	PV	28	215Wp x 8 Panels	
		83	215Wp x 32 Panels	
		117	215Wp x 16 Panels	
SVC (0.5/opp.)	***Node***		***Max (MVA)***	***Min (MVA)***
	85		15	0
	121		30	0
OLTC (0.0125/opp.)	***Place***		***Max tap***	***Min tap***
	Primary Substation		1.11	0.91

Appendix- Publications I-VII

The implementation of price and network based demand response programs, the pervasiveness of electric vehicles, the increasing installation of DGs, the rising customer load base of urban areas and other emerging factors are creating a distribution network loading curve which is stochastic in nature and previously unseen in shape. This thesis unravels the real-time dependencies among active distribution network component thermal states, customer loads and distributed generation on their common environmental variables such as wind speed and solar irradiation. Through the dynamic thermal modeling of network components, the work has unlocked their real-time capacities. The introduction of real-time thermal rating in an active distribution network management system enhances the loading capacity significantly compared to static rating. This has been revealed through an increased utilization of installed DGs and through better integration potential of additional DGs.

Aalto-DD 104/2015

ISBN 978-952-60-6307-2 (printed)
ISBN 978-952-60-6308-9 (pdf)
ISSN-L 1799-4934
ISSN 1799-4934 (printed)
ISSN 1799-4942 (pdf)

Aalto University
School of Electrical Engineering
Department of Electrical Engineering and Automation
www.aalto.fi

BUSINESS + ECONOMY

ART + DESIGN + ARCHITECTURE

SCIENCE + TECHNOLOGY

CROSSOVER

DOCTORAL DISSERTATIONS